

**FOREIGN
BROADCAST
INFORMATION
SERVICE**

FBIS Report —

Science & Technology

Central Eurasia

This report may contain copyrighted material. Copying and dissemination is prohibited without permission of the copyright owners.

Science & Technology

Central Eurasia

FBIS-UST-95-051

CONTENTS

18 December 1995

SCIENCE AND TECHNOLOGY POLICY

Russian 'Scientific School' System Explained [Yu. Tretyakov, I. Melikhov; Moscow POISK No 44 (338), 28 Oct 95-3 Nov 95]	1
Creation of S&T Lobby Urged [I. Goryunov; Moscow POISK No 45(339), 4-10 Nov 95]	3
Russian State Science Centers Form Lobbying Association [M. Kalashnikova; Moscow NEZAVISIMAYA GAZETA 11 Nov 95]	4

SPACE SCIENCE AND ENGINEERING

Space Closed Gas Turbine Power Plants [V. Samsonov; Moscow VESTNIK MOSKOVSKOGO GOSUDARSTVENNOGO TEKHNIЧЕСКОГО UNIVERSITETA: SERIYA MASHINOSTROYENIYE No 1, Jan-Feb 95]	7
Gas Turbine and Steam Power Plants With Ceramic Modules [A. Kulandin, V. Dubershteyn, et al.; Moscow VESTNIK MOSKOVSKOGO GOSUDARSTVENNOGO TEKHNIЧЕСКОГО UNIVERSITETA: SERIYA MASHINOSTROYENIYE No 1, Jan-Feb 95]	13
Method for Nonlinear Correction of Dynamic Characteristics of Rudder Drive of Spaceplane Using Standard Model [A. Borovkov, I. Misyuk, et al.; Moscow VESTNIK MOSKOVSKOGO GOSUDARSTVENNOGO TEKHNIЧЕСКОГО UNIVERSITETA: SERIYA PRIBOROSTROYENIYE No 1, Jan-Mar 95]	17
Gyrocompasses Based on Gyrotachometers. Part I [S. Shestov, V. Bauman; Moscow VESTNIK MOSKOVSKOGO GOSUDARSTVENNOGO TEKHNIЧЕСКОГО UNIVERSITETA: SERIYA PRIBOROSTROYENIYE No 1, Jan-Mar 95]	22
Requirements on Navigational Support for Experiments From Lunar Polar Satellite Orbit [Ye. Aleksashin, Yu. Timofeyev, et al.; Moscow GEODEZIYA I KARTOGRAFIYA No 4, Apr 95]	31
Modeling a Plasma-Tuned Satellite Antenna [L. Kurina, G. Markov, et al.; Nizhniy Novgorod IZVESTIYA VYSSHIKH UCHEBNYKH ZAVEDENIY. RADIOFIZIKA Vol 37 No 6, Jun 95]	42
Comparative Analysis of Multiply Reusable Space Transport Systems [G. Lozino-Lozinskiy, E. Dudar; Moscow PROBLEMY MASHINOSTROYENIYA I NADEZHNOСТИ MASHIN No 4, Jul-Aug 95]	47
Determining Structure of Meteor Streams From Radar Observations [S. Kolomiyets, I. Milyutchenko; Moscow ASTRONOMICHSKIY VESTNIK Vol 29 No 4, Jul-Aug 95]	55
Optimum Synthesis of Multiray Optical Interferometer For Making Observations Through Inhomogeneous Atmosphere [L. Kopilovich; Kiev KINEMATIKA I FIZIKA NEBESNYKH TEL Vol 11 No 5, Sep-Oct 95]	61
Eko-Psi-95 Experiment in Mir Complex Described [V. Gritsenko; Moscow SEGODNYA 2 Nov 95]	67
Mir Leak Described [M. Chernyshov; Moscow SEGODNYA 2 Nov 95]	68
Russian Space Industry Described [S. Zhiltsov; Moscow KRASNAYA ZVEZDA 11 Nov 95]	68
Russian Engines for American Rockets [Moscow KOMMERSANT DAILY No 183, 4 Oct 95]	70

PHYSICS

Degradation of the Interphase Si-SiO ₂ Boundary Under Field and Radiation Effects [I. Klimov, Yu. Listopadov, et al.; St. Petersburg PISMA V ZHURNAL TEKHNIЧЕСКОY FIZIKI Vol 21 No 10, 26 May 95]	71
Growth of 3D Polytype 4H and 6H Silicon Carbide Crystals [A. Maksimov, A. Maltsev, et al.; St. Petersburg PISMA V ZHURNAL TEKHNIЧЕСКОY FIZIKI Vol 21 No 10, 26 May 95]	71
Diffusion Waveguides in Polycarbonate [A. Tomov; St. Petersburg PISMA V ZHURNAL TEKHNIЧЕСКОY FIZIKI Vol 21 No 10, 26 May 95]	72
Effective Heating of Electrons and Ions by Low Hybrid Waves in an FT-2 Tokamak [V. Budnikov, V. Dyachenko, et al.; St. Petersburg PISMA V ZHURNAL TEKHNIЧЕСКОY FIZIKI Vol 21 No 10, 26 May 95]	72
Possibility of Establishing the Neutron Generation Mechanism in the Mechanical Effect on Deuterated Matter [Ye. Fateyev; St. Petersburg PISMA V ZHURNAL TEKHNIЧЕСКОY FIZIKI Vol 21 No 10, 26 May 95]	72

- High-Temperature Superconducting Compound YBa₂Cu₃Se₂ with T_c = 371 K [V. Shabetnik, S. Butuzov, et al.; St. Petersburg PISMA V ZHURNAL TEKHNIЧЕСКОY FIZIKI Vol 21 No 10, 26 May 95] 73
- Electric Conductivity of Heated Superdense Plasma [V. Pogosov, I. Yakubov; St. Petersburg PISMA V ZHURNAL TEKHNIЧЕСКОY FIZIKI Vol 21 No 10, 26 May 95] 73

CHEMISTRY

- Estimation of the Thermodynamic Nonideality of the Detonation of an Emulsion Explosive [V. Odintsov, V. Pepekin, et al.; Moscow KHIMICHESKAYA FIZIKA Vol 13 No 11, Nov 94] 74
- Generation Mechanism of a Photodissociative Laser Based on the Electron Transition of the Fine Structure of a Chlorine Atom $^2P_{1/2} \rightarrow ^2P_{3/2}$ [A. Nadkhin, Ye. Gordon; Moscow KHIMICHESKAYA FIZIKA Vol 13 No 12, Dec 94] 81
- Using the Electrical Response of a Semiconductor Compound To Record the Chemical Transformation Behind the Front of a Shock Wave [S. Nabatov, A. Lebedev; Moscow KHIMICHESKAYA FIZIKA Vol 13 No 12, Dec 94] 89
- Estimating the Parameters of a New Class of Detonation of Emulsion Explosives [V. Odintsov, V. Pepekin, et al.; Moscow KHIMICHESKAYA FIZIKA Vol 13 No 12, Dec 94] 89

EARTH SCIENCES

- New Hypothesis on the Role and Importance of the Electric Field in Oceans [E. Alftan; Khabarovsk TIKHOKEANSKAYA GEOLOGIYA Vol 14 No 1, May-Jun 95] 98
- Shares Sold in Seven New Oil Companies [O. Gorokhova; Moscow KOMMERSANT DAILY 2 Nov 95] 101

Russian 'Scientific School' System Explained

964D0133A Moscow POISK in Russian
No 44 (338), 28 Oct 95-3 Nov 95 p 3

[Article by Yuriy Tretyakov, academician, Russian Academy of Sciences, and Igor Melikhov, academician, Russian Federation Academy of Natural Sciences under the "Portrait of the Problem" rubric: "We Are Not Saving That in Which We Take Pride"]

[FBIS Translated Text] In a recent issue of our newspaper (POISK No. 41), we published the Russian Federation governmental decree "Concerning Governmental Support of the Russian Federation's Leading Scientific Schools." The program approved in that decree calls for the distribution of special grants among the country's leading scientists on a competitive basis. Obviously, the measure will not solve all the pressing problems that have developed. The authors of the article that we are publishing today have analyzed the paths of development of Russia's scientific schools and presented their own versions of supporting them.

Modern science may be represented as a system of two types of scientific teams, namely, basic research laboratories and base laboratories. Basic research laboratories are geared toward short-term study of individual manifestations of natural and social processes and are the most important type of laboratory at the present time. Base laboratories, on the other hand, are tailored to multiyear systematic study of natural phenomena. Base laboratories are generally assembled into groups, with each using approaches, ideas, and methods developed by one of the scientific schools.

A scientific school is a team of very highly trained researchers that works on solving a large-scale problem and that during the course of its work, trains scientific workers in the art of research. The problem is generally of so large a scale that it requires the efforts of several generations of scientists and is solved on the basis of original ideas and methodologies developed by the main school. Schools are generally organized in the form of an institute or department or in the form of individual base laboratories or informal associations.

Scientific schools are an important factor in society's development. It is precisely schools that determine how necessary it is to obtain new information and the pace and quality with which information must be obtained. It is schools that make expert evaluations of the information obtained in basic research and base laboratories. Without the official stamp of scientific schools, new information would be denied entry into mankind's store of knowledge. By interacting with one

another, the schools compare information from different branches of science. We owe our harmonious world outlook to scientific schools. Were it not for the schools, our understanding of nature would be as far from the truth as a heap of stones is from the Taj Mahal. Furthermore, each school is a source of creative impulse and all that is generally referred to as spirituality.

By our estimates, the world now has approximately 5,000 natural science schools encompassing all directions of scientific exploration.

In the nineties, Russia has had about 500 functioning natural science schools that have been responsible for the country's big scientific and technical achievements. Many of these schools have by and large shaped their times. Natural science is now literally being transformed as a result of comprehension of the role of nonlinear processes and self-organization in nature. "Nonlinear thinking" has become a new paradigm for researchers. Indeed, the schools of L. Mandelshtam and A. Andronov analyzed the role of nonlinearity both in general and in detail back in the forties to the extent that little can be added to their analysis today. And N. Kurnakov's school gave science a methodology of physicochemical analysis that has long dictated chemistry's success in the investigation of complex natural systems.

Russian's scientific schools have worked so effectively that they have created the impression that Russian science as a whole is in a state of well-being. In actual fact, Russian science began lagging behind Western science back in the seventies. In the eighties, the development of Western science accelerated sharply while Russian science continued advancing at its previous pace. From 1980 through 1990, the Russian scientist's labor productivity increased by a factor of 3-4 while that of scientists in the United States increased by a factor of 20. By 1990 our laboratories' equipment and methods were four to six times worse than those in the United States. New ideas appeared with increasing rarity. Our laboratories' cognitive abilities became significantly lower than those in the West. Russian science could not supply the information support required for the pace of economic development required of leading countries. The financial support of science had to be increased. But the reverse occurred: In recent years investments in science have been cut by two-thirds. As a result, updating of laboratories' instrument park ceased, until by 1994 the "average age" of most (60 percent) measuring instruments was in excess of 15 years versus less than 5 years in the United States and Japan. Existing instruments began malfunctioning because of a lack of spare parts. Scientific associates' wages fell catastrophically. Some researchers left for abroad. Others entered different spheres of activity. Researchers do not duplicate one

another's work in schools; each has his own inimitable task. For that reason, each researcher's departure is a blow to his school. And most sciences have lost more than a third of their researchers. The influx of youth into the schools has stopped, and directors have learned to hide their tears when talented individuals leave for commerce.

The amount of available scientific literature has been reduced, which has inevitably resulted in a decrease in schools' intellectual potential. The intensity of research has decreased by a factor of two to eight. The quality of scientific production has decreased as well: Obsolete and worn-out equipment no longer provides the measurement precision that practice requires. Over the past 5 years virtually all Russia's schools have degraded at one pace or another. Some have even demonstrated brilliant achievements. Against the background of general collapse, however, such achievements were perceived as miracles.

Five years is an enormous period in the life of a scientific school. In science, the measure of time is the time during which the volume of information doubles. In the natural sciences the said period is between 5 and 15 years long. In chemistry in particular it is 8.3 years. This means that 75 percent of the knowledge on which chemistry will be based in 16.6 years is not yet known today. New knowledge will lead chemists to think in a new manner. Chemistry will be transformed into a science unknown to us today, and schools that have lagged behind scientific progress will not find a place in it. Although a 1- to 2-year delay in a school's development is correctable in the future, a shutdown for 8 to 10 years is lethal: the school cannot be reborn regardless of the amount of financial investment. Those politicians at various levels who talk and write so much about science obviously do not agree with this statement. As a rule, they express guarded optimism and certainty that Russian scientists will be able to endure everything and quickly forget these trying times. In this case, however, optimism is unjustified. If the situation does not change radically within the next 2 or 3 years, some scientists may perhaps endure but there will be no schools.

Without a system of scientific schools, Russia cannot be independent, much less a great power. A country's independence and greatness is, along with everything else, determined by its information potential, which is in turn directly linked to the activity of its schools. Therefore, if the schools are destroyed, they will have to be created anew, which is a very complicated matter. After having analyzed the history of the development of the world's largest schools, one can conclude that each school develops in three stages. In the first stage, the

potential head of the school develops hypotheses and methodological approaches to solving a problem. Next, the research methods are assimilated and personnel are trained. In other words, the school is established. In the second stage, very simple model systems are studied and particular laws are established. In the third stage, complex systems are studied and general laws of their behavior are deduced. In the said process, the information output from the school is insignificant until the middle of the second stage, after which it snowballs. A school amasses most of its knowledge in the third stage. The first stage lasts between 2 and 5 years, whereas the second stage lasts between 5 and 10 years. Consequently, during the course of that time, a school produces virtually no information but rather simply absorbs resources that may later be recouped many times over. If, for one reason or another, a school collapses before the end of the second stage, the total yield from its work will turn out to be low. The incubation period in a school's development is an objective inevitability. The creation of a system of scientific schools therefore requires uncompensated expenditures for many years. Obviously, those expenditures will be many times greater than what is needed to keep schools from collapsing. Only the extreme impoverishment of a country can justify the collapse of its scientific schools. Russia, which imports more expensive automobiles from abroad than any other country throughout the world, can hardly be considered impoverished. In Russia, the development of science is obviously considered a secondary task whose financing can be indefinitely suspended in this difficult period. But that view is erroneous. Limiting the financing of science for 8 to 10 years is equivalent to killing it.

A rational amount of financing of scientific schools can be estimated by proceeding from the expenditures on science in the United States. Russia does not have her own experience in determining the reasonableness of expenditures, whereas in the United States science is financed very economically. According to published statistics, approximately \$19 billion was spent on basic research in the United States in 1990. Fifty-four percent of that amount went to universities and research centers where scientific schools are concentrated. In the United States, approximately 300,000 individuals were involved in basic research, and the material and information support of their work (not counting their wages) averaged approximately \$10,000 per individual researcher per year. In Russia, an average of five base laboratories belongs to each school. If it is assumed that each of our 500 natural science laboratories has an average of 20 individuals, that means that approximately 50,000 individuals are involved [in basic research]. Given the same yearly funding to support the research of one individual (excluding his wages) as in the United States,

this would mean the equivalent of \$450 million each year. We are certain that that level of expenditure is objectively necessary to provide the currently required intensity and quality of scientific investigation. If that level is not reached, the effectiveness of the investigation falls sharply and the work becomes uncompetitive or even useless. The optimum level of expenditure does not depend on the will of some legislator or civil servant but is instead determined by the level of development of world science.

Basic research must be financed by the government because knowledge is not a commodity and the likelihood that the accumulation of knowledge be financed by market structures is low. In the United States, for example, firms contribute no more than 21 percent to the financing of basic science. Calling upon base laboratories to earn their own money by filling orders from market structures is therefore the equivalent of calling for a shift from basic research to applied research. Many scientific schools are now being forced to fill such orders, and the disastrous effects of the practice on the solution of basic problems are already clear.

Financing of scientific schools should be a priority. As a rule, schools have postgraduate students and doctoral candidates, organize conferences and seminars, create knowledge bases and expert systems, and publish monographs and textbooks. One such example is G. Devyatyy's school, which not only developed the theory of deep purification and many methods of obtaining high-purity materials but which also trained 90 candidates and 15 doctors of sciences, published several monographs and textbooks, conducted a university lecture course, created a data bank and exhibition/collection of high-purity materials, organized an all-union conference, and worked on the publication of a special journal. All that required a great deal of funding over and above the amount provided by its research work.

Because schools conduct lengthy scientific investigations, their financing should be predetermined 5 to 8 years in advance. A governmental program for developing national schools that would reflect all directions of investigation for which Russia assumes responsibility before the world community may become the form of long-range financial planning. It is widely believed that a system of long-range financial planning that nearly excludes competition among researchers cannot provide the necessary pace of work and is therefore inferior to a system of short-term financial support on a competitive basis (a grant system). The fact that most scientific funds throughout the world use the grant system is confirmation of the grant system's superiority. It is clear, however, that the nature of financing must correspond to the nature of the research being financed. If 5

to 8 years is required to solve a research problem, financing of the research work should be planned for the same time period. The grant system is suitable for basic research laboratories and for those base laboratories whose problems may be broken down into subproblems effective enough to win a competition. The system is not suitable for scientific schools conducting long-term, front-line scientific exploration. Of course, any school can artificially single out an effective chain of tasks from its problems; however, this generally destroys the logic of their work. Both the pace and quality of long-term scientific investigation should also be regulated by a scientometric analysis of laboratories' activity.

Such analysis makes it possible to identify scientific schools, determine which base laboratories are incapable of providing the required pace of work, and rank projects from the standpoint of the amount of financing. A general method of scientometric analysis has recently been developed. Once it has been adapted for the respective branches of science, it may be used to estimate the capabilities of all the country's teams. Given the country's strained material resources, this type of "inventory" of laboratories seems necessary. After a base laboratory has received long-term financial support, it must be subjected to monitoring by independent experts who evaluate the pace and quality of its work annually. An expert evaluation should be conducted by many experts so that it can be objective. It is therefore a good idea to combine expert evaluations conducted by individuals with expert evaluations conducted by groups, specifically an evaluation that involves discussion of works at seminars and conferences. The said discussion may be conducted analogously to a dissertation defense, which is to say by using a secret ballot procedure. Seminars and conferences will then become stimuli for accelerating works with the most democratic form of monitoring of their course. We suggest that centralized financing of scientific schools within the framework of a governmental program with democratic monitoring of the course of the research based on a scientometric analysis of laboratories' work will result in a pace of development of basic science consistent with Russia's place among the world's countries.

Creation of S&T Lobby Urged

964D0131A Moscow POISK in Russian
No 45(339), 4-10 Nov 95 p 1

[Article by Igor Goryunov: "Where Are You, the Party of Science?"]

[FBIS Translated Text] Russian science, as a result of conducting market reforms, has become a demilitarized, "deideologized" and open world. So stated Minister

Boris Saltykov, speaking in the Palace of Scientists at a meeting dedicated to formulation of the strategy and tactics of the scientific community on the eve of the parliamentary elections. But in the opinion of Lyudmila Vartazarova, chairman of the Socialist Party of Workers, the "deideologization" has led to a loss of "purposefulness," that is, a loss of clear guideposts in the scientific and technical policy of the state.

The threat which this carries was set forth in the "Manifesto in Defense of Culture," proclaimed at the meeting, which was signed by scientists and cultural workers of St. Petersburg.

The St. Petersburg specialists feel that the course being pursued by the state has led to the development of exceptionally dangerous trends. The breakdown of Russian science is taking place, morals are going downhill and cultural values are being lost.

The manifesto stated: "Specific measures for correcting the situation must be undertaken immediately." In the announced document it is emphasized that the authorities of today do not comprehend what is going on. Repeated appeals of scientists to higher legislative and executive agencies and to the president "have had a zero effect."

However, for a true scientist a negative result also is a result. The authors of such messages were convinced that the appeals of scientists, even the most meritorious, to the pertinent authorities will scarcely find any response. In the Soviet years one could count on a reaction from the authoritative bodies. Now no heed is given to a cry from the soul even from the most eminent persons in the country.

Accordingly, it is necessary to seek other methods for influencing organizations responsible for the fate of Russian science, education and culture. There must be a new concept of interrelationships between the scientific community and the authorities. Its principal provisions must be shared by scientists of the most different political persuasions: from the "Demvybor Rossii" to the Russian Federation Communist Party.

However, the problem is not only the formulation of such a concept. This is a necessary but by no means an adequate condition. It is necessary to organize a scientific lobby to exert an influence on the authorities and public opinion. The scientific community also must be concerned with its organization if it actually wishes to participate in the struggle for drawing up the budget and its expenditure, for an appropriate tax policy and science legislation.

Without a "brain center," working out a scientific ideology for the development of society, it will be

impossible for example, for an agrarian or masked "criminal" lobby to prevail.

But for the time being only some forms for conduct of the preelection struggle have been defined — it has been decided to organize work on finding candidates in single-mandate districts who could, regardless of their party affiliation, represent the interests of science in the State Duma and Federation Council. After a corresponding analysis a list of such candidates must be published in the press. And it only remains for the scientific community to vote for "their people."

At the meeting no preference was given to any one of the political currents. The essence of the position of scientists on this score was expressed by the adoption of a document calling on different political parties to assume specific obligations in formulating a state strategy in the scientific and technical sphere. The RF Communist Party, "Zhenshchiny Rossii," Demokraticeskaya partiya, "Demvybor Rossii" and "Kongress russkikh obshchin" are even now ready to sign this document.

In general the background against which the discussion of the position of the scientific community transpired on the eve of the elections was created by an address of the American president, received by Russian scientists via Internet and read from the podium. Bill Clinton expresses disagreement with the congress, planning to reduce expenditures on science "for the sake of financial stabilization." "The future does not have its voters. But we all at the same time are electors of the future. And we must resist limitations on investments in those spheres which will be crucial for economic growth of the country in the 21st century."

So it also is in Russia. Each of us makes his choice. But at the same time we are choosing the future of the country and its science.

Russian State Science Centers Form Lobbying Association

964D0131B Moscow NEZAVISIMAYA GAZETA
in Russian 11 Nov 95 p 2

[Article by Marina Kalashnikova: "A New Lobbyist Has Appeared in Russia. Russian Science For the Time Being Is Receiving Lip Service Rather Than Real Assistance"]

[FBIS Translated Text] Russian science is manifesting inventiveness in order to survive. On the eve of the elections it must push all possible buttons: state, private, public and emotional. An Association of State Science Centers (ASCC), whose introduction took place the other day at the All-Russian Aviation Materials Scientific Research Institute (VIAM), has been organized.

This is something like a Trade Union of Directors of State Science Centers (SSC) or a "volunteer fire company for rescuing children from a fire." The association intends to lobby in the State Duma, the Federation Council, ministries and departments capable of supplying money and affording advantages for saving the institutes which are the leaders of Russian science. Can a structure traditionally appealing to state institutes be effective under market conditions and a change in national priorities? Will it be capable of convincing the new holders of wealth and resources in Russia — the fuel-energy complex and the banks — to allocate a "chunk" for the support of science?

All of science cannot be saved if for no other reason than that Russia inherited it from the USSR in a greatly bloated condition. In 1993, by a presidential decree, and then by a resolution of the RF government, the interim status of State Scientific Center (SSC) was authorized for enterprises, scientific organizations and institutions of higher education. Those selected received the right to special forms of state support for a period of 2 years. The SSC designation was contended for by 400 scientific organizations among the 5,000 existing in Russia and 61 won this title. Regionally the leaders were Moscow and Moscow Oblast, where the SSC designation was awarded to 40 institutions; there were 12 in St. Petersburg, 3 in Novosibirsk, 2 in Kaluga Oblast and 1 each in Ulyanovo, Orlovo and Tomsk Oblasts and Stavropol Kray. Eleven SSC are located in 9 scientific cities — Zhukovskiy, Obninsk, Obolensk, Troitsk, Protvino, Mendeleyevo, Dmitrovgrad, Koltsovo and Nizhnyy Arkhyz. But for the time being there is no SSC in a single secret administrative-territorial formation.

For example, the Kurchatov Institute in Moscow and the All-Russian Scientific Research Institute of Grain-Legume and Groat Crops in Orlovo Oblast are included in the same list. The selection criteria did not provide for proportional representation for either regions or branches. According to the members of the selecting commission, the world rating of achievements was taken into account, but the principle of "who needs it more" dominated. For example, space scientific research institutes were not included because they were characterized by a relatively favorable situation and are enjoying funding under other state programs. The conferring of the SSC designation does not change the forms of ownership. According to Nikolay Gorbatenko, responsible for work with the SSC in the Minnauka (Ministry of Science and Technical Policy), this is something like the "boutonniere of the Legion of Honor," giving the right on an interim basis to enjoy the special favor of the state. The label is applied in front of the name of institution,

even if its name already contains such a word combination. For example, the Vektor Virology and Biotechnology Center in Koltsovo village in Novosibirsk Oblast carries a long title "twice SSC." But what will one not bear for the sake of one's own salvation!

However, for the time being such a granting of titles has brought no significant relief. Initially the SSC idea assumed full maintenance by the state. A presidential decree and a government resolution only provided for advantages. In actuality, however, great privileges were not received other than freeing from taxation on land and real property. But this does not solve the principal problem because 90 percent of the debts of the SSC — natural monopolists — are now primarily for energy, communication services, water supply and sewerage.

The idea of interbranch scientific and technical complexes, falling through in the late 1980's, again loomed behind the intention to award the SSC designation not only to one, but at the same time to several related institutions. At Zhukovskiy it was proposed that 5 organizations be combined under this title, but only two received it — the Flight Testing Institute and the Central Aerohydrodynamics Institute — and each separately. The Russian Academy of Sciences for a long time objected to the SSC idea, proposing its own versions. The opposition was dropped when the advantage of gaining access to state investments became evident. The key question — the mechanism by which the SSC relate to the state — remains unclear to any and all of the "dramatis personae" — the SSC directors, as well as the representatives of the Minnauka and the Department of Science and Higher Education of the RF government. While the Minnauka, Russian Academy of Sciences, State Committee for the Defense Industry, State Committee for Property and other departments have sought a compromise, the SSC have had their water, electricity, heating and communication cut off and 6 of them today are on the brink of bankruptcy.

Among the immediate undertakings, German Zagaynov, general director of the association, announced that during the period 14-23 November there would be an exhibition-report of SSC activity during the last 2 years, to be held at VIAM facilities. This will determine their right to be voted into the list of SSC for the next period; protection of the interests of the SSC before arbitration tribunals and lobbying in legislative institutions will be discussed. Our political parties and movements do not always reflect the interests of narrow and specialized groups. A lobby may possibly help.

The awarding of the SSC status, in the opinion of Andrey Kulagin, head of a Minnauka administration, "is more likely a tribute to past services than a policy for

determining future priorities." There also is a directly opposite opinion. German Zagaynov, ASSC general director, asserts that the choice of SSC must lay the foundation for a new state scientific and technical policy. For the time being it is being worked out, to use the expression of Mikhail Kirpichnikov, director of the Department of Science and Higher Education of the government, in a "Brownian movement" fashion. Today it is possibly easier to survive on one's own, betting on and playing up to some one of the natural monopolies or that narrow part of the military industrial complex which has already been able to find its way into the international market (space and the exportation of competitive weapons). In the changing situation the greatest influence and the money for which science must contend is not in the hands of the defense branch, but with the oil and gas interests and the banks. Their need for scientific and technological development work is incomparably less than was true for the former defense industry and even the present-day defense sector and they differ in structure from the traditional activity of Soviet science. They will not die from starvation who are able to propose a cheap method for finding oil more rapidly and more simply expelling it from a well. But right now it is difficult to find sponsors for a drug, invented by our science, which is capable of replacing an antibiotic. The importation of drugs will bring incomparably greater profits to those who control the pharmaceuticals market. Will the ASSC or the state be able to straighten this out?

In those matters within its competence, the ASSC has done plenty. Its initiative, in the persona of Mister Zagaynov, is vigorously penetrating many fields and offices. But there also are fears: how will the association distribute the money collected from one source or another for support of the SSC and will the activity of the association not diminish the attention of the Minnauka and other departments which now fund the SSC? Yevgeniy Fedosov, director of the SSC Institute of Aviation Systems, feels that the principal problem is support of the national experimental base. The Minnauka is in no position to assume this burden in its entirety. The State Committee for the Defense Industry for the most part is funding the development of specific technical systems. Scientists are receiving support from grants. Will the ASSC get the necessary funds for developing the experimental base?

At the NPO Aerodinamika there exists the bold idea of going farther than the ASSC and establishing a scientific exchange where the technical proposals of the science centers and the orders of enterprises will find one another. A databank will be accessible on a commercial basis to both Russian and foreign capital, opening the way to the international labor market. "An entire aircraft will not be ordered from us, it is far more likely that the order will be for some part for it, the development of which will be more perfect and advantageous," assures Vladimir Sidenko, the general designer at Aerodinamika. This will increase the chances for small business, which will be more flexible and inexpensive under market conditions. It is easier to close a small laboratory after it has performed its mission, whereas the giants are regenerated into a self-maintaining system and a burden to the budget. The high economic efficacy of such a scheme possibly would make investment in science more attractive for new Russian business and banks. And science also would turn out to be more profitable than when "in the grip" of the state. An exchange without fail must have its own development bank, from which without additional bureaucratic steps there would be funding for both basic and applied research. The exchange, bringing together the most diverse technical finds, will be able to become a place for smoothing out the relations between the science lobby and the branch interests, as well as a tool of political influence.

For the time being such projects sound utopian. But it is essential to support both them and the ASSC if science is ever to break away from its long-time practice of begging the state to "give" and energetically involve itself into the "Brownian movement" of politics on the same equal basis as its other numerous present-day participants. The ASSC, according to Mister Kirpichnikov, is a "great boon for the transition period, an attempt under new conditions to establish a new structure." In his opinion the Russian Academy of Sciences could not perform the function of a scientific lobby because "for too long a time it has occupied an almost suicidal position and has greatly discredited itself." In the Minnauka it is hoped that on the eve of the elections the ASSC will convince thinking people to keep Russian science in mind. Mister Kirpichnikov feels that "scientific specialists must again feel that they have a sound roof over their heads."

Space Closed Gas Turbine Power Plants

957A1110A Moscow VESTNIK MOSKOVSKOGO GOSUDARSTVENNOGO TEKHNIЧЕСКОГО UNIVERSITETA: SERIYA MASHINOSTROYENIYE in Russian No 1, Jan-Feb 95 (manuscript received 27 Aug 92) pp 25-32

[Article by Vladimir Leonidovich Samsonov, candidate of technical sciences, head, Section for Space Closed Gas Turbine Power Plants, EM Scientific Research Institute, Moscow State Technical University imeni N. E. Bauman; the first paragraph is an abstract; UDC 629.7.54]

[FBIS Translated Text] *The results of multiyear research and development work on space closed gas turbine power plants carried out at the Moscow State Technical University imeni N. E. Bauman under the direction of the author are presented. The fields of application in which such power plants are most advantageous are examined. The results of testing of experimental copies of the power plants, their principal assemblies and elements are given. Aspects of use of the developed power plants in conversion work are discussed.*

Space closed gas turbine power plants (CGTPP), which in the literature are often simply called power plants (PP), operating in a Brayton cycle, have a number of advantages. In contrast to a closed piston-driven PP, operating in a Stirling cycle, they are characterized by a higher specific power and a long continuous-operation useful life. In contrast to closed steam turbine PP, operating in a Rankine cycle, CGTPP are characterized by a high efficiency and high reliability, which is attributable to the use of a working medium in the form of a mixture of neutral gases having excellent compatibility with construction materials. The enumerated qualities result in a preference for space CGTPP among other PP of the generator class.

Due to the use of gas bearings in CGTPP turbogenerators there is virtually no wear in these critical units. These PP therefore have a long continuous-operation useful life attaining 30 or more years. As indicated by research, in the range 0.5...5,000 kW space CGTPP, not

yielding in reliability to PP based on solar cells, and also based on thermoelectric and thermoemission converters, considerably surpass them with respect to such indices as compactness, mass and economy.

Figure 1 shows the typical layout of a space CGTPP [1].

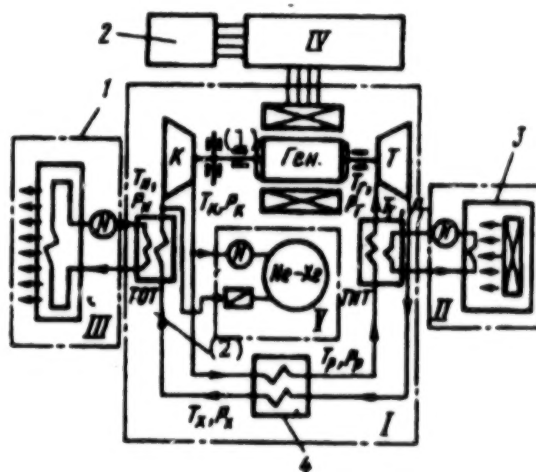


Fig. 1. Layout of space CGTPP: 1 — radiator; 2 — payload; 3 — heat source; 4 — recuperator.

Key: (1) Gen; (2) HRHE

The power conversion system I includes 4 units: turbogenerator-compressor unit (TGC), recuperator, source heat exchangers (SHE) and heat removal heat exchangers (HRHE). These units are connected by lines, thereby forming a closed gas circuit in which a helium-xenon mixture with a molecular weight optimum for the PP power level circulates. The principal unit of this system — the TGC unit — for increasing reliability has a single shaft with a common rotor resting on two supporting and one two-sided supporting gas-dynamical bearings.

In the heat source system it is possible to use a solar concentrator with a heat pickup, nuclear reactor or radioisotope chamber.

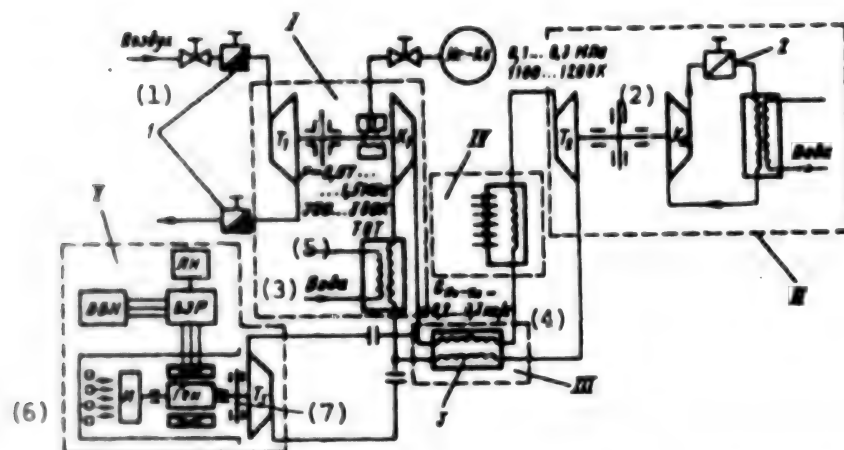


Fig. 2. Layout of stand for tests of CGTTP units: I — compressor unit; II — turbine part; III — recuperator part; IV — heater part; V — dynamic simulator of TGC and electric subsystem of CGTTP; 1 — vacuum valves; 2 — throttle; 3 — recuperator.

Key: (1) air; (2) MPa; (3) Water; (4) kg/s; (5) HRHE; (6) I; (7) Gen

The radiator of the heat dissipation system operates either by the direct release of heat from the helium-xenon mixture through the wall into space or with an intermediate liquid circuit, depending on the makeup of the CGTTP on the spacecraft. It is proposed that a droplet radiator with the direct radiation of heat into space by hot droplets of a liquid heat transfer agent circulating in the heat dissipation system [2] be used for high-power CGTTP, the area of whose radiator surface limits the possibility of their placement aboard spacecraft.

The electric system IV is used for conversion, rectification or distribution of the electric current produced by the generator of the TGC unit of the power conversion system, depending on the makeup of the spacecraft payload.

The gas regulation system V is intended for compensating for microleakage from the closed circuit of the power conversion system, as well as for regulating the quantity of gas in it when there are large power consumption changes.

Using such a system American specialists have constructed a surface CGTTP with a power $N_e = 2-15$ kW with an electric simulator of the heat source (prototype of a space power plant), in the course of the tests accumulating more than 50,000 hours of continuous fault-free operation without degradation of the output characteristics [3]. The efficiency of this plant exceeds 30 percent with an electric power of 7 kW. As a result, American specialists preferred a solar CGTTP over solar cells for new-generation orbital stations with a power

consumption 20-300 kW. According to their data, such a choice will make it possible to save 3-4 billion dollars during operation of the Freedom orbital station over the course of 30 years [4]. We obtained similar results in a study of the possibility of using a solar CGTTP for new-generation Mir orbital stations and a general-purpose space platform.

Due to high economy and reliability the use of space CGTTP with a power $N_e = 0.5-10$ kW with a radioisotope chamber as a heat source is extremely promising. The high efficiency of this plant (20-35 percent) not only reduces expenditures on loading ^{238}Pu into the radioisotope chamber by tens of millions of rubles (in comparison with the case of use of traditional thermoelectric generators), but also ensures good layout properties of the plant in the spacecraft. Such plants have no alternatives for spacecraft with high power consumption during flights to Mars, to distant planets and to outer space.

The combination of a CGTTP with a nuclear reactor for spacecraft with a high power consumption (more than 100 kW), as a result of the high efficiency of power conversion (up to 50 percent), provides substantial advantages over thermal emission PP with respect to size and weight characteristics. A high efficiency of the CGTTP can be attained by use of ceramic materials, as well as materials based on carbon fibers, which ensures a temperature increase at the entrance into the turbine up to 2,400 K.

Space CGTTP, in combination with a turbine gas expander, are extremely promising for producing a great quantity of cold at the cryogenic temperature level

necessary for the cooling of infrared transducers and containers for the storage of cryogenic fluids under orbital conditions. When using such solar plants it is possible to reduce the overall dimensions of the plant by 1-1.5 orders of magnitude in comparison with the dimensions of solar cells in combination with traditional piston-driven cooling plants. In this case the TGC unit in the CGTPP is replaced by a turbocompressor-gas expansion unit.

And finally, space CGTPP are without an alternative in a case when for the spacecraft payload there must be delivery not only of electric power, but also the pumping of a great quantity of gas through it. This applies, in particular, to such users as supersonic electroionization CO_2 and CO lasers, as well as a Cu vapor transonic laser, intended for power transmission in space [5].

It can therefore be concluded that CGTPP are some of the principal power sources for space vehicles used for different purposes.

The Moscow State Technical University imeni N. E. Bauman, with the support of the aerospace industry, has for a long time been investigating and developing space CGTPP in a broad range of electric powers. However, the experimental study was made of the PP as a whole and their assemblies for an electric power level 1...20 kW.

Due to the uniqueness of the gas-dynamical and heat exchange processes in the assemblies and elements of the centrifugal compressors, centripetal turbines, gas bearings of the TGC block rotors, recuperator, heat exchanger for heat dissipation, radiator, etc., transpiring at low Re numbers ($< 10^5$) and numbers $Pr = 0.2...0.5$, characteristic of helium-xenon mixtures, stand equipment was developed for their autonomous investigation and testing.

Figure 2 is a diagram of this stand. It consists of compressor, recuperator, heating and turbine parts, as well as the power plant electric system intended for investigation and testing of the supporting systems of the TGC unit rotors.

The basis for the compressor part of the stand is a single-shaft low-temperature turbocompressor which includes the centrifugal compressor K1 and the drive air turbine T1 to be tested. The unit rotor rests on gas bearings. The working medium of the tested centrifugal compressor (He- Xe, Kr, Ar and others) is separated from the air by means of a cutoff device.

When testing other CGTPP elements the compressor part of the stand serves as the source of the working medium.

In investigations and tests of the recuperator and centripetal turbine (CT) all the components of the stand shown in Fig. 2 were in operation. The turbine part of the stand is the most complex. Its basis is a single-shaft high-temperature turbocompressor with the CT to be tested, braking compressor and rotor on high-temperature gas-dynamical bearings.

The stand (part V) is used in investigating and testing the gas-dynamical support systems of the rotors for the CGTPP single-shaft TGC units. The tests are carried out using a dynamic simulator of the TGC unit with heating of its hot part by quartz lamps.

The hot assemblies and elements of assemblies of all parts of this stand are heat insulated. The electric heater of the heating part of the stand also is carefully heat insulated.

The stand was outfitted with thermocouples, pressure transducers, current eddy devices for measuring small movements in elements of the gas bearings and wheels of the CC and CT, flow meters, chromatographs, frequency meters, etc. Highly economical stages of the CC with an efficiency 80 percent, CT with an efficiency 90 percent, high-speed a-c generators ($n = 24,000...45$ rpm), supporting gas-dynamical systems of the TGC unit rotors in the electric power range 1...20 kW and compact recuperators with a degree of recuperation up to 96 percent were investigated and tested on this stand.

A surface prototype of a space CGTPP with a power $N_s = 3$ kW was constructed on the basis of the developed technology. Figure 3 is a diagram of this stand. The role of a space heat source (solar concentrator — heat pickup) is played by an electric heater, whereas the role of the radiator is simulated in the form of a liquid-water heat exchanger. The gas in the HRHE is cooled by a silicone fluid which is then cooled by water from the main network.

The specifications of the surface copy of the space power plant are as follows: nominal electric power 3.0 kW, current voltage 220 V, degree of increase in gas pressure in compressor 1.75, frequency 1,333 Hz, rotation of TGC unit rotor 40,000 rpm, degree of recuperation 95 percent, gas temperature at entrance into turbine 1,130 K, at entrance into compressor — 308 K, working medium — helium-xenon mixture with a molecular weight 83.8. The TGC is designed in the form of a single-shaft unit whose rotor rests on thin-film gas bearings of the hinged type. The outer diameter of the CC wheel is 90 mm, that of the CT wheel is 105 mm and that of the generator rotor is 55 mm.

The body of the generator stator is cooled by a silicone fluid. The temperature of the hottest point of the stator

of this quadrupole generator with a massive rotor does not exceed 200°C . The wheels of the turbodynamo were cast, the wheel of the CC was made from titanium alloy and the CT wheel was made from a heat-resistant alloy. The bimetallic generator rotor is fabricated by heat-diffusion welding. The working surface of the thin-film gas bearings has a polyamide coating. The mass of the TGC unit (Fig. 4) is 43 kg and the mass of its rotor is 4.2 kg; the overall dimensions of the unit are: maximum diameter (along the connecting pipes) 330 mm, length 580 mm.

The recuperator is a countercurrent lamellated-ribbed heat exchange unit with a matrix formed by heat exchange surfaces with short straight offset ribs. The construction material is corrosion-resistant steel. The thickness of the ribbed surface is 0.1 mm and that of the separation plates is 0.2 mm. The overall dimensions of the recuperator matrix are: length 500, width 300 and height 400 mm. The recuperator weight is 80 kg.

The HRHE is made in a stand variant. Its lamellated-ribbed construction is fabricated from aluminum alloys.

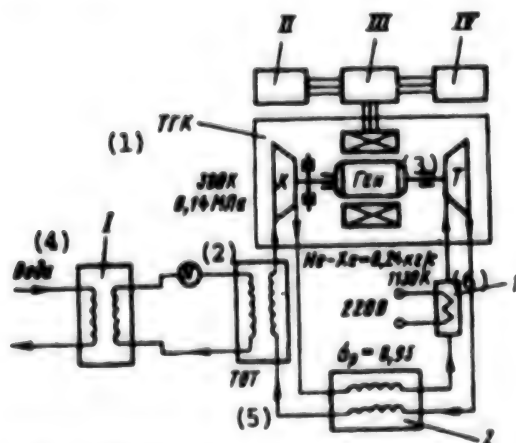


Fig. 3. Diagram of surface prototype of space CGTPP with power $N_e = 3$ kW. I — radiator simulator; II — ballast load; III — electric regulation unit; IV — payload; 1 — electric heater; 2 — recuperator.

Key: (1) TGC; (2) MPa; (3) Gen; (4) Water; (5) HRHE; (6) kg/s

The electric heater has Nichrome tubular heat-releasing elements. It is constructed in the dimensions of the solar pickup-accumulator for a CGTPP with a power $N_e = 20$ kW. The power plant is started up by means of a generator operating in a motor mode. The synchronous frequency of rotor rotation in the TGC unit is 24,000 rpm.

The total time which the power plant functioned exceeded 500 hours with 100 "start-stop" cycles. The results of the tests indicate a potential possibility of attaining a prolonged (years) continuous-operation useful life. The resulting plant efficiency attains 24 percent.

Detailed information on a surface prototype of a space CGTPP with $N_e = 3$ kW is given in [6].

Applicable to solar CGTPP of promising orbital stations and space platforms, the Moscow State Technical University imeni N. E. Bauman is investigating designs of a space solar pickup-accumulator (Fig. 5). In particular, experiments are being carried out for determining the operability of niobium capsules with LiF — the principal elements of such pickup-accumulators. In order to determine voids accompanying LiF hardening, one of the capsules making up this element was first subjected to tomographic examination with the simultaneous processing of the results on a computer after thermal cycling in vertical and horizontal positions. Information on these experiments was presented in [7].

Research on the conversion applications of space CGTPP indicated that they may play an important role in solving ecologic and resource-conserving problems on the Earth [8].

In particular, it seems promising to use low-power CGTPP operating on organic fuel for cathode protection of main gas pipelines, radio relay communication systems and small farms in inaccessible regions of the planet instead of low-efficiency organic-fuel steam turbine PP employed at the present time.

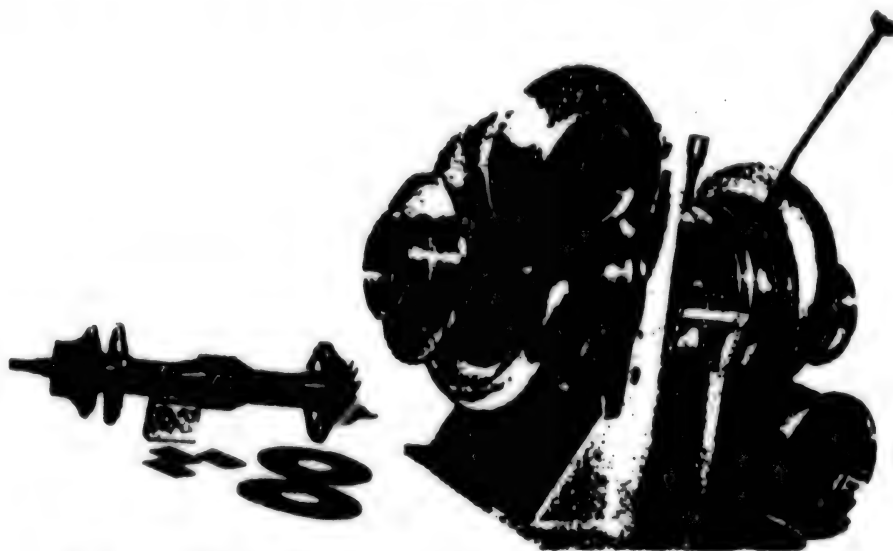


Fig. 4. TGC unit of surface prototype of space CGTPP with power $N_e = 3$ kW.

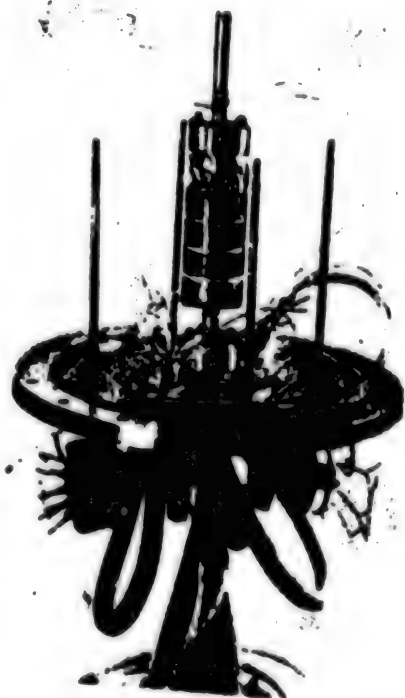


Fig. 5. Tubular element with niobium capsules filled with LIF of space solar pickup-accumulator.

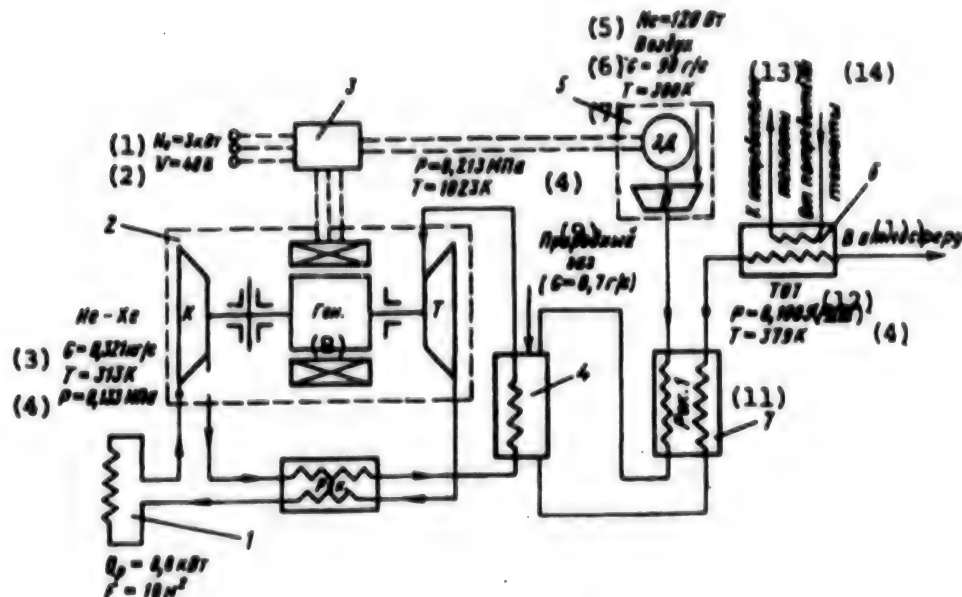


Fig. 6. Schematic diagram of CGTPP with power $N_g = 3$ kW operating on natural gas: 1 — radiator; 2 — TGC unit; 3 — electric regulation unit; 4 — gas heater; 5 — electric fan; 6 — final user of released heat; 7 — air recuperator.

Key: (1) kW; (2) V; (3) kg/s; (4) MPa; (5) W; (6) air; (7) g/s; (8) Generator; (9) Natural gas; (10) To atmosphere; (11) Recuperator; (12) HRHE; (13) To heat user; (14) From heat user

Figure 6 is a schematic diagram of a CGTPP with a power $N_g = 3$ kW operating on natural gas for line users on main gas pipelines. For making maximum heat use in the heat source system of this CGTPP there is an air recuperator and a terminal gas-fluid heat exchanger of a system for heating communication system equipment. Independent tests of this system with a total duration of 47 hours with more than 100 "on-off" cycles indicated its reliable and efficient operation [9]. Tests are now also being carried out of experimental copies of CGTPP with a power $N_g = 3$ kW operating on natural gas which include the proposed heat source system.

The conclusion can therefore be drawn that the use of low-power CGTPP both in space and on the ground is promising.

Bibliography

1. Podshivalov, S. A., Ivanov, E. I., Muratov, L. I., et al., *Energeticheskiye ustanovki kosmicheskikh apparatov* (Power Plants for Space Vehicles), Moscow, Energoizdat, 1981.
2. Konopka, W., Calia, V. and Brown, R., Liquid droplet radiator passive collector testing, in: Proc. of the 20th IECEC, No 859400, pp 1430-1438.
3. McCormick, J. E. and Dunn, J. H., NASA 30,000-hour test demonstration of closed Brayton cycle reliability, Paper AIAA, No 77-499.
4. Secunde, R., Labus, T. and Lovely, R., Solar dynamic power module design, Proc. of the 24th IECEC, No 899408, pp 299-308.
5. Samsonov, V. L., Advantages of Brayton cycle applications for a satellite power system, in: Second International Symposium SPS-91 "Power From Space", Paris/Gif-Sur-Yvette, 27-30 Aug. 1991.
6. Bragin, A. N., Vasilyev, A. N., Golubev, S. V., et al., Experimental copy of space closed gas turbine power plant with electric power 1...3.5 kW, in: Tez. dokl. Vsesoyuznoy mezhvuz. konferentsii "Gazoturbinnyye i kombinirovannyye ustanovki," Moskva, 19-21 noyabrya 1991 (Summaries of Reports at All-Union Intercollege Conference "Gas Turbine and Combined Power Plants," Moscow, 19-21 November 1991), Moscow, p 32, 1991.
7. Sokolov, V. F., Experimental study of behavior of lithium fluoride in capsules of solar receiver-accumulator of space solar closed gas turbine power plant, IBID., p 104.

8. Voronin, V. G., Samsonov, V. A. and Shmidt, K. A., Conversion uses of closed gas turbine power plants operating on organic fuel, IBID., p 37.

9. Voronin, V. G., Golubev, S. V., Dyumin, Yu. V., et al., Closed gas turbine power plants with an electric power 3 kW operating on natural gas for line users on main gas pipelines, IBID., p 38.

Gas Turbine and Steam Power Plants With Ceramic Modules

957A1111A Moscow VESTNIK MOSKOVSKOGO GOSUDARSTVENNOGO TEKHNIЧЕСKOGO UNIVEKSIТETA: SERIYA MASHINOSTROYENIYE in Russian

No 1, Jan-Feb 95 (manuscript received 25 Aug 92) pp 45-51

[Article by A. A. Kulandin, doctor of technical sciences, professor, academician, Russian Academy of Transportation, V. Kh. Dubershteyn and A. V. Sudarev; the first paragraph is an abstract; UDC 621.438]

[FBIS Translated Text] A study was made of the application of ceramic construction materials (CCM) for the high-temperature uncooled feed-through parts of gas turbine power plants (GTPP) in the case of their autonomous operation and in combination with a recovery unit. The characteristics of a thermodynamic analysis are given with optimization of the unit-modular approach to the finalization of design schemes for GTPP and the desirability of using a cycle with intermediate air cooling in the compression process is pointed out. The possibility of increasing the efficiency of thermal electric power plants by 15-18 percent is established.

In the technical-economic assessment of thermal electric power plants the most important factors taken into account are the thermal economy or total efficiency, determining the specific expenditures of fuel and the specific thermal load on ecologic conditions in the location region, as well as the specific (per unit of produced electric power) discharge of harmful substances (NO_x , CO and others). Among the different types of stationary thermal power equipment it is gas-vapor power plants with a recovery unit (GVPP/RU) which have the highest indices.

The total efficiency (η_t) of GVPP/RU is dependent primarily on the efficiency of the gas turbine (GTPP) and steam turbine (STPP) plants (η_g and η_s), the degree of binarity of the thermodynamic cycle (η_k and the recovery unit (η_r). With an accuracy to 2-3 percent the efficiency of the GVPP/RU is defined by the equation

$$\eta_t = 1 - (1 - \eta_g \eta_k) (1 - \eta_s \eta_r) (1)$$

Naturally, it is desirable that all the components entering into this equation be as high as possible. But they are

interrelated (an increase in some results in a decrease in others) and these relationships determine optimization of the parameters of the working process and the GVPP/RU cycle with respect to ensuring a maximum total efficiency. There is no need for optimizing solely the maximum temperature cycle (T_{∞} [cc = closed cycle], which must be as high as possible when using any GTPP cycles. As indicated by an analysis, an increase in T_{∞} for the GVPP/RU has a greater value than for an autonomous GTPP.

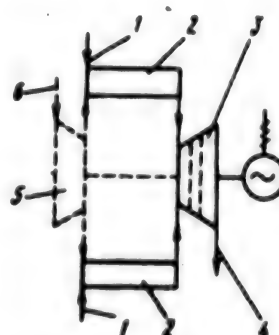


Fig. 1. Schematic diagram of GTPP with ceramic modules: 1) air entry into modules with ceramic turbines; 2) modules with ceramic turbines; 3) metal power turbine; 4) exhaust; 5) variant of common low-pressure compressor; 6) air entry into common low-pressure compressor.

In the traditional embodiment of elements of the feed-through part of a metal turbine the T_{∞} increase is limited by both the increase in expenditures of compressed air for cooling and the uniqueness of the employed materials and coatings. A complication of the technology results in a sharp increase in the cost of the items. The traditional materials for GTPP turbines are heat-resistant alloys, those close to the limit of reserves with respect to an increase in the maximum cycle temperature

The use of ceramic construction materials (CCM) for the fabrication of high-temperature uncooled elements of the feed-through parts of a GTPP makes possible a substantial increase in efficiency of both an autonomous GTPP, but especially a GVPP/RU. With an increase in T_{∞} in this case there is assurance of a continuous increase in η_g , it becomes feasible to realize a GVPP/RU with $\eta_k = 1$ with a simultaneous increase in η_g and η_r . Thus, all four coefficients entering into equation (1), on which the total efficiency η_t is dependent, increase

However, taking into account existing technologies, a number of restrictions are imposed on items made of

CCM: the mean mass temperature $T_{\eta_{cc}}$ must not exceed $1,300^{\circ}\text{C}$; the size of the loaded parts is limited (the height of the blades of the axial turbines must not be greater than 50-60 mm, the outer diameter of the working wheel of the axiradial turbines must not be greater than 180-200 mm); the turbine disks, considering strength requirements, must be solid, which gives rise to definite design and technologic difficulties in connecting the shaft to the disk, and also makes impossible the successive placement of several turbine stages on the same shaft; an increased negative influence of heat cycling with high levels of the time temperature derivative $d/b\tau$ predetermines use of a GVPP/RU primarily for bearing base loads.

The mechanical properties of the CCM exert a significant influence both on the design-layout solutions and on the specifics of a thermodynamic analysis for optimizing the GTPP heat circuits and cycles.

The need for obtaining a high unit power of a GTPP as part of a GVPP/RU with a restricted discharge of the working medium through sections of the CCM feed-through parts leads to a unit-modular solution for a gas generator (Fig. 1). The working medium is directed from several modules with ceramic turbines (CTM) into a single metal pressure turbine (PT). In this case variants are possible either with a free PT (solid lines in Fig. 1) or with a general low-pressure compressor (LPC), driven by the necessary number of PT stages, which depending on the required frequencies of rotation may have either a common or different shafts with stages of the free PT (dashed lines in Fig. 1).

In turn, the structural layout of the CTM is two- or three-shaft with individual shafts for each turbine stage. The number of CTM shafts is determined by the admissible gas temperature before the PT, with an increase in which the number of shafts is reduced, but the design and technology of the PT blade crowns is more complicated. Thus, a simplification of one structural unit results in a complication of another.

In a thermodynamic analysis a study was made of four GTPP cycles: Brayton (B), regenerative with final regeneration (FR) with intermediate regeneration (IR) and with intermediate air cooling in the compression process (IC). In contrast to the traditional thermodynamic analysis of cycles, where as efficiency indices use is made of the efficiency η_a and the disposable work l_a , when

using the CTM it is necessary to replace l_a by the CTM disposable unit power N_{ap} . This is attributable to the fact that it is impossible to ensure the stipulated CTM power by the necessary discharge of working medium, as is possible in ordinary GTPP. Accordingly, cycles which without a loss of efficiency have higher values of the product of the degree of pressure increase and work l_a are advantageous. In a comparison of the thermodynamic efficiency of the cycles the unit power N_{ap} must be regarded as conditional, since in its determination use is made of some maximum admissible area of the critical section, which is determined after detailed design work.

The dependencies $\eta_a = f(N_{ap})$, derived with the participation of S. L. Yegorov, are illustrated in Fig. 2 for the cycles illustrated in the figure. When $T_{cc} = \text{const}$ the indices of the B cycle are dependent on only a single parameter: the degree of pressure increase π_{an} . The FR and IR cycles are dependent not only on π_{an} , but also on the degree of regeneration, assumed to be 0.85. The IR cycle is shown for the case of the most feasible positioning of regenerative bleeding on the distribution line between the last stage of the ceramic turbine and the PT.

The indices of the IC cycle are dependent on two parameters of the working process — the total degree of pressure increase π_c and its distribution in the compression process in the LPC and in the high-pressure compressor (HPC) (π_{LPC} and π_{HPC}). For each π_c level on the lines $\eta_a = f(N_{ap})$ there are two characteristic points corresponding to such relations between π_{LPC} and π_{HPC} with which in one case $\eta_{a, \text{max}}$ is attained, and in the other case — $N_{ap, \text{max}}$ is observed.

The principal advantage of a cycle with FR is a high efficiency. But with relatively low π_{an} values about 6-8 in the region $\eta_{a, \text{max}}$ a low CTM unit power ($N_{ap} = 0.5 \text{ MW}$) is obtained, which increases their number. Thus, the advantage of the FR cycle and a GTPP with a metal feed-through part (small π_{an} is transformed into an inadequacy for a GTPP with ceramic turbines as part of the GVPP/RU. A cycle with IR has a considerably lesser maximum efficiency than a cycle with FR, but higher levels of reasonable degrees of pressure increase ($\pi_{an} = 14-18$), which substantially increases N_{ap} with $\eta_{a, \text{max}}$ in both cycles.

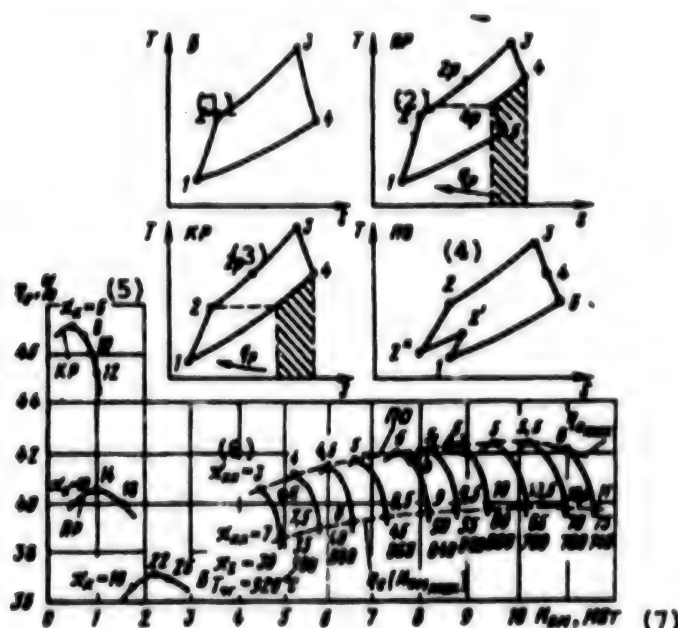


Fig. 2. Dependencies $\eta = f(N_p)$ of GTPP with $T_{cc} = 1,300^\circ\text{C}$ applicable for Brayton cycles (B) with final regeneration (FR), intermediate regeneration (IR) and with intermediate air cooling (IC).

Key: (1) B; (2) IR; (3) FR; (4) AC; (5) π_{in} ; (6) π_{LP} ; (7) MW

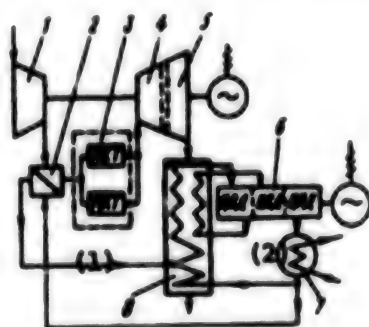


Fig. 3

Cycle B is used in gas turbine construction both autonomously and as part of a GVPP/RU. In a design with CTM, due to an absence of losses in cooling at $T = 1,300^\circ\text{C}$, there is an appreciable increase in efficiency (up to 36.5-37 percent) in comparison with the best modern GTPP. GTPP with CTM operating in cycle B as part of a GVPP/RU make it possible to achieve an efficiency of 54-55 percent.

A cycle with AC for GTPP with CTM is most attractive both in an autonomous variant and as part of GVPP/RU units with different thermal and design schemes. The principal advantages of this cycle are: a high efficiency (41-42 percent), high degrees of pressure increase, which realistically may attain 35-50, which reduces the required number of CTM; a low-temperature heat exchanger for intermediate AC is far simpler to construct than high-temperature heat exchangers for FR and IR.

When using a "classical" scheme (Fig. 3) in the makeup of the GVPP/RU a moderate π_{in} value was adopted (point a in Fig. 2) with degrees of pressure increase in centrifugal LPC, IPC and HPC equal to 3.7, 3.5 and 2.5 respectively. The moderate value $\pi_{in} = 32$ with $T_{cc} = 1,300^\circ\text{C}$ was governed by the need to have an acceptably high gas temperature at the entrance to the recovery unit for steam generation. The gas temperature in the exhaust is 515°C and the temperature of the live steam is $460-480^\circ\text{C}$.

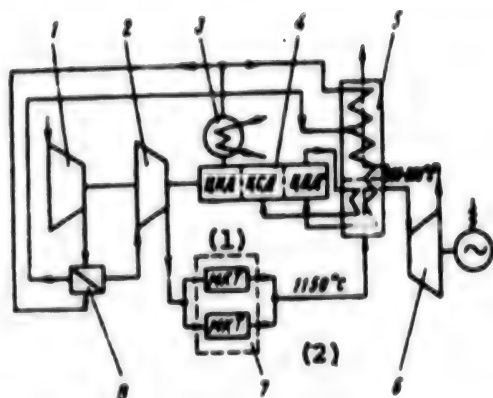


Fig. 4. Thermal scheme of GVPP/RU with AC, with LPC and IPC drive by steam turbine: 1) LPC; 2) IPC; 3) condenser; 4) steam turbine with intermediate steam heating; 5) recovery unit; 6) metal PT; 7) two-shaft CTM unit; 8) intermediate air cooler.

Key: (1) LPC, IPC, HPC (left to right); (2) CTM

We emphasize that the use of a GTPP with intermediate AC in the GVPP/RU is possible only with a high gas temperature beyond the combustion chamber. Otherwise the temperature of the live steam will be low, which evidently requires additional conveyance of heat at the input into the recovery unit, a decrease in the degree of binarity ($\eta_b < 1$) and an efficiency η_e in accordance with equation (1). In the case of autonomous use, in order to increase π_e , there are no restrictions on reduction of exhaust temperature. Accordingly, even when $T_e = 1,300^\circ\text{C}$ it is possible to achieve $\pi_e = 50$ (for example, $\pi_{LPC} = 5.8-6.0$ in the common axial compressor, $\pi_{HPC} = 3.5$ and $\pi_{IPC} = 2.5$ in the IPC and HPC of a two-shaft CTM). The temperature before the common metal turbine is entirely acceptable and is about $1,040^\circ\text{C}$. In this case a quite high efficiency will be attained $\eta_e = 41.8$ percent (point c in Fig. 2).

We note some peculiarities of the GVPP/RU heat system shown in Fig. 3.

A steam turbine with intermediate steam heating, but without regenerative takeoffs; with a temperature of the combustion products at the PT output 515°C , η_e about 0.37-0.38.

The flow of cold feed water at the condenser output is divided into two parts. Part of the discharge is directed into an air cooler, from which after heating it is directed to a corresponding heat exchange section of the recovery unit; another part is directed to the cold output (in the direction of gas movement) heat exchange section with

ceramic heat exchange surfaces not subjected to low-temperature corrosion.

The diagram shows a recovery unit of the feed-through type (the boiler also may of the drum type).

The total efficiency of the GVPP/RU, designed in accordance with the diagram in Fig. 3, is $\eta_e = 0.6$, but the power of a gas turbine with intermediate AC is more than double the power of the steam turbine. The latter makes possible some modification of this scheme by using the PT not for the generation of electric power, but for driving the LPC. The output electric power and the efficiency in this case do not change, but there is an increase in the power of the GTPP PT by a factor of almost 1.5. A merit of the modified scheme is the installation of only one generator, but a shortcoming is that autonomous GTPP operation is impossible.

The following goals are pursued in another of the considered GVPP/RU heat systems (Fig. 4):

Simplification of design by a changeover to a single-shaft CTM scheme, for which the gas from the ceramic turbine stage enters at a temperature about $1,150^\circ\text{C}$ into the high-temperature section of the RU.

Reduce the temperature of the gas before the metal power turbine to $800-850^\circ\text{C}$.

Increase the temperature of the live steam upon entry into the GTPP to that adopted in modern condensation SPP — a temperature $540-560^\circ\text{C}$. This increases the efficiency η_e (without regenerative takeoffs) from 37-38 to 40-41 percent, and also SPP power.

In Fig. 4 the heat system is shown in a variant of a LPC and IPC drive by a steam turbine, although it also can be designed in a variant similar to that shown in Fig. 3, that is, with a drive of the compressors (or one of them) by a gas turbine and drive of the electric generator proper by a steam turbine.

A problem for thermal engineering equally important as an increase in the efficiency of the power units is, as noted above, the problem of reducing the specific discharge of harmful substances into the atmosphere (NO_x , CO). Although there are no fundamental differences in measures for reducing the content of NO_x and CO in exhaust gases in high-temperature GTPP with ceramic feed-through parts in comparison with ordinary GTPP and SPP, this question requires independent detailed analysis.

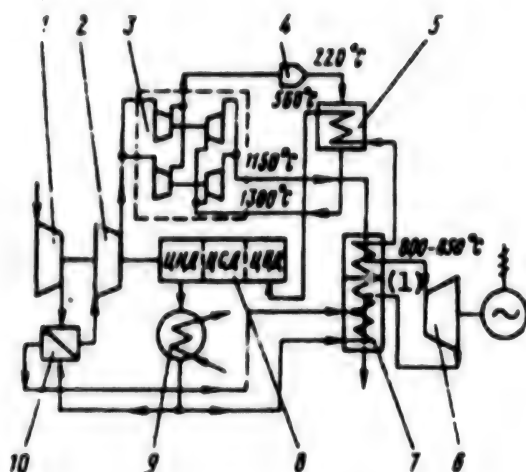


Fig. 5. Heat system for GVPP/RU with stoichiometric fuel combustion: 1) LPC; 2) IPC; 3) two-shaft CTM unit; 4) combustion chamber; 5) steam heater; 6) metal PT; 7) recovery unit; 8) steam turbine; 9) condenser; 10) intermediate air cooler.

Key: (1) LPS, IPC, HPC (left to right)

We note only that there is basis for expecting a possibility of reducing the content of harmful impurities by a specific organization of the combustion process in chambers constructed of CCM in comparison with ordinary metal chambers.

It is possible to use heat systems in which there is stoichiometric combustion in the absence (or with a low content) of oxygen in the combustion products (Fig. 5). This also makes it possible to use "dry" purification methods, including conversion to inexpensive catalytic devices not requiring use of precious metals.

Conclusions:

1. The use of CCM for the fabrication of high-temperature uncooled elements of the feed-through parts of a GTPP will make possible a substantial increase in the efficiency of thermal electric power plants (by 15-18 percent), both on the basis of autonomous GTPP and especially in GTPP/RU.

2. Due to known technologic restrictions on the size of loaded parts fabricated from CCM it is desirable to employ a block-modular approach to organization of the feed-through part of a GTPP. These restrictions also lead to a specific approach when optimizing the parameters of the working process of the thermodynamic cycles and heating schemes.

3. For GTPP it is desirable to use a thermodynamic cycle with intermediate air cooling in the compression process.

4. GTPP/RU heating schemes with the stoichiometric combustion of fuel and using catalytic purification devices for exhaust gases, applying the conversion principle, are of interest but require further research.

Method for Nonlinear Correction of Dynamic Characteristics of Rudder Drive of Spaceplane Using Standard Model

957A1132A Moscow VESTNIK MOSKOVSKOGO GOSUDARSTVENNOGO TEKHNIЧЕСКОГО УНИВЕРСИТЕТА: SERIYA PRIBOROSTROYENIYE in Russian No 1, Jan-Mar 95 pp 38-44

[Article by A. G. Borovkov, candidate of technical sciences, assistant professor, I. V. Misyuk, graduate student, A. G. Kalashnikov and M. N. Demenkov, Automatic Control Systems Department, Moscow State Technical University imeni N. E. Bauman; the first paragraph is an abstract; UDC 62-82-585.2+62-52.001.5]

[FBIS Translated Text] The efficiency of correction of the dynamic characteristics of a rudder drive are examined using information on the rate of the pressure drop in the pressure cylinder working cavities and a refined model of the drive load is presented.

It is proposed that the frequency characteristic of the rudder drive of a space vehicle be corrected, and specifically that the resonance peak at frequencies corresponding to the frequency of fluid oscillations in the fuel tanks be reduced. Clearly expressed resonance phenomena arise as a result of the weak characteristic damping of the rudder drive (RD), as well as the low damping constant of the kinematic circuit in the neighborhood of the characteristic frequency of the elastic circuit. The presence of low-frequency resonance in the rudder channel is inadmissible because in this case the characteristic frequencies of oscillations of the elastic contour and the elastic oscillations of the rocket body converge.

A special feature of the dynamics of a rudder drive for a class of flightcraft, control of whose thrust vector is accomplished by means of the jet engine drive, is the great moment of inertia of the rotating engine; limited rigidity of kinematic circuit elements; low damping constant; nonlinearity of the friction characteristics.

Accordingly, for stable RD operation it is necessary, on the one hand, to ensure a stipulated phase lag which is attained for the most part by an increase in the drive quality factor, and on the other hand, to ensure suppression of resonance at the frequency of the elastic

circuit, which is amplified with an increase in the quality factor. It follows from an analysis of the mentioned requirements that without additional correction devices the simultaneous satisfaction of these requirements is impossible.

One of the methods for solving this problem is the introduction of a correcting feedback in the rudder drive scheme for the derivative of the pressure drop in the cavities of the rudder drive pressure cylinder — hydromechanical correction (HMC) [1]. The essence of HMC is based on passage of the working fluid from the pressure cylinder high-pressure cavity into the low-pressure cavity at the time of appearance of oscillatory processes. For a digital RD with a mechanical feedback the use of HMC makes it possible to use the positive properties of the analog internal feedback for correction of the RD-load circuit. A shortcoming of hydromechanical devices of such a type is their operation in the LF range of the amplitude-phase-frequency characteristic, an increase in structural mass and size.

The formulation of the problem involves solving the problem of correcting the rudder drive-motor elastic circuit by digital correction (DC) devices. A special feature of this system (Fig. 1,a) is the absence, due to design complexities, of a technical possibility for measuring the load coordinate, that is, the angle of

rotation of the longitudinal axis of the engine jet relative to the rocket body. In the formation of the DC signal use is made of information on the intermediate variables of state of the system, on the pressure drop in the pressure cylinder cavities and movement of the pressure cylinder rod (Gray code).

There are different methods for solving problems of this class. A method for organizing correction by use of a standard model, taking into account the action of dissipative forces in the kinematic scheme and the influence of the nonlinear segment of the characteristic curves of frictional forces in the bearings, was proposed in [2]. The use of a standard model makes it possible to discriminate load information criteria. An algorithm for control of the system on the basis of the output coordinate was described in [3], where the necessary accuracy was attained by curve fitting of the control algorithm coefficients. On the basis of the collected information an algorithm was written for digital correction of the rudder drive and this produces the correcting signal fed to a 12-digit summator, thus performing system signal correction.

Mathematical model of loaded RD with digital correction. Figure 1 is schematic diagram of the RD-load elastic system. The rudder drive is a digital electrohydraulic tracking drive with three amplification stages.

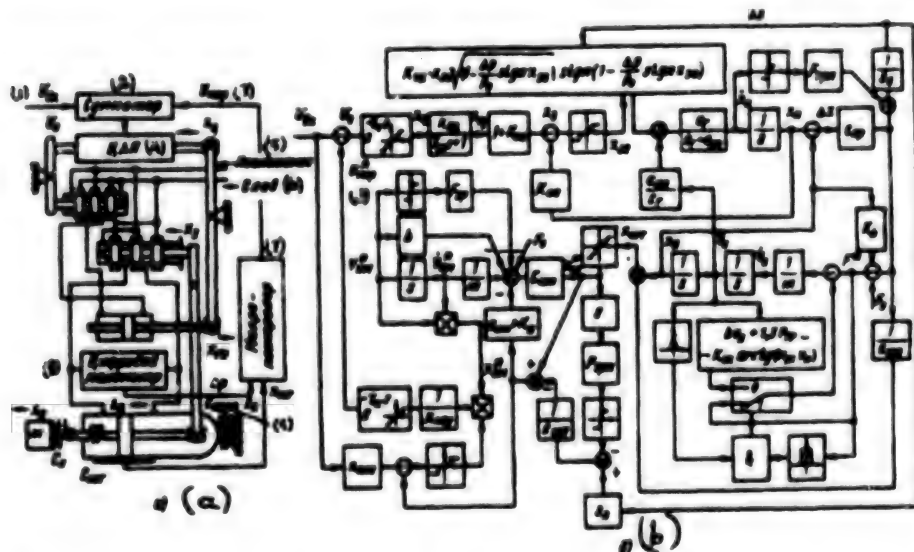


Fig. 1. Schematic (a) and structural (b) diagrams of rudder drive with correction.

Key: 1. U_m ; 2. summator; 3. U_{cm} ; 4. DAC; 5. Injection; 6. Discharge; 7. Microcontroller; 8. Digital manometer; 9. x_{mip}

A 12-digit digital-to-analog converter (DAC) is used as the first amplification stage; a 7-digit binary code (the lowest 5 digits are used for correction) is fed to the DAC input and the mechanical movement of the working rod is read from the DAC output. The next two amplification stages are represented by a slide valve hydrodistributor, in each case with a rigid mechanical coupling.

Information on movement is read from the pressure cylinder rod by means of a system of digital sensors of linear movements and together with information on the pressure drop in the pressure cylinder cavities, received from a digital manometer, is fed to a computer which constructs a mathematical model of the load, on the basis of which a nonlinear feedback signal is shaped which is proportional to the power gradient, which is fed to the DAC input.

The dynamics of the considered system is described by differential equations of motion with the following assumptions: the DAC is a net lag component with a time constant $\tau_{cyt} = 0.015$ s; the injection and discharge pressure is constant; the elastic modulus (hydraulic stiffness) and viscosity of the working fluid are constant and are not dependent on number and temperature; hydrodynamic forces in the second and third amplification stages are not taken into account; the masses of the slide valves, pistons and pressure cylinders are neglected due to their smallness in comparison with the mass of the

load; RD operation in the neighborhood of the cavitation modes and the phenomenon of stipulated rod position drift are not described.

With allowance for these assumptions we write the DAC equation $X_{cyt} = 1/[1 - \tau_{cyt}]T_{hyps}(U_s/\Delta_{cyt})\Delta_{cyt}$, where τ_{cyt} is the lag time constant; Δ_{cyt} is DAC quantization — DAC rod movement in response to the sending of a single control signal; T_{hyps} is a function for discarding a fractional part; the equation describing the second amplification stage is

$x_{amp} = X_{cyt} - K_{fb,1}x_{amp})K_{v,1}$ or $T_{amp}x_{amp}^* + x_{amp} = K_{in}x_{cyt}$, where $K_{v,1}$ is the amplification factor for the speed of stage 2; $K_{fb,1}$ is the kinematic feedback factor; $T_{amp} = 1/K_{v,1}K_{fb,1}$; $K_{in} = 1/K_{fb,1}$ [here and in the text which follows the asterisk indicates that the preceding letter is surmounted by a dot and two asterisks represent two dots]; the equation for the kinematic circuit relating the coordinates of the piston and load is

$C_{nd}\Delta x = S_p\Delta p - F_{hy} \text{ sign}(x_p^*)$, where $\Delta x = x_p - x_{load}$; S_p is the area of the pressure cylinder piston; Δp is the pressure drop in the pressure cylinder cavities; F_{hy} is the dry friction force on the rod and piston seals; C_{nd} is the reduced stiffness of the working piston.

In turn,

$$C_{np} = \begin{cases} (1/C_k + 1/C_{kopn} + 1/C_{mt} + 1/C_p + 1/C_H)^{-1}; & x_3 \leq \Delta_3 \\ (1/C_k + 1/C_{kopn} + 1/C_{mt} + 1/C_H)^{-1}; & x_3 > \Delta_3 \end{cases}$$

Note: The following subscripts and superscripts recur in the Russian formulae which follow. Their rendition in the English translation is indicated:
cy = amp; k = cyl; oc = fb; ix = in; wp = rod; n = p; mty = fr/f;
kopn = body; mt = rod; H = load; K = att; j = valve; ty = fr; X = fl;
CX = dry; KOP = cor; CMC = sys. The meaning of these and other abbreviations is evident from the text.

here C_{at} , C_{load} are the rigidities of attachment of the RD to the support and the load; C_{body} , C_{rod} , C_{hy} are the rigidities of the RD body, loaded part of the rod and the hydraulic spring, governed by the compressibility of the working fluid in the cavities of the RD pressure cylinder; x_{val} is the coordinate of the valve of the third amplification stage; Δ_{val} is the positive valve coverage of the principal hydroamplifier.

The equation of motion of the load $m x_{load}^{**} = F^* - F_{fr/f}(F^*, x_{load}^*)$; $F^* = C_{nd}\Delta x = K_{pos}x_{load} - F_0$, where C_{nd} is the reduced rigidity of the RD; K_{pos} is the position force coefficient; F_0 is static force; $F_{fr/f}$ is a nonlinear function describing the dependence of the dry and viscous friction levels on the total (external, elastic and static) force F^* imparted to the load and the velocity of load movement.

$$F_{\text{нтр}} = \begin{cases} F^*, F^* < 1.3 F_{\text{тр}} & \text{и } \dot{x}_n = 0; \\ b \dot{x}_n + 1.3 F_{\text{тр}} - K_{\text{сх}} \operatorname{arctg}(K_{\text{ж}} x_n). \end{cases}$$

$K_{\text{ж}}$ is a coefficient characterizing the dependence of dry friction on the velocity of load movement.

The velocity equation for the RD third amplification stage is written in the form

Here b is the viscous friction damping factor; $F_{\text{н}}$ is dry friction force; $F_{\text{dry}} = (2/\pi)0.3F_{\text{н}}$ is the dry friction factor;

$$\dot{x}_n = x_{30} K_v \sqrt{1 - \frac{\Delta p}{p_0} \operatorname{sign}(x_{30})} \operatorname{sign}\left(1 - \frac{\Delta p}{p_0} \operatorname{sign}(x_{30})\right) - \frac{s_n}{C_r} \Delta p^0.$$

where K_v is the RD velocity amplification factor; p_0 is the injection-discharge pressure difference; x_{valve} is the effective coordinate of the third amplification stage valve.

Using the equations for RD-load kinematic coupling, it is possible to transform this equation. Since

$$\Delta p = \frac{C_{\text{np}}}{s_n} \Delta x + \frac{F_{\text{rpn}}}{s_n} \operatorname{sign}(\dot{x}_n), \quad \text{то}$$

and neglecting the derivative of the second term, we obtain $\Delta p^* = (c_{\text{red}}/s_p) \Delta x^*$. Then

$$\dot{x}_n = \frac{C_r}{C_r + C_{\text{np}}} K_v x_{30} \sqrt{1 - \frac{\Delta p}{p_0} \operatorname{sign}(x_{30})} \operatorname{sign}\left[\left(1 - \frac{\Delta p}{p_0} \operatorname{sign}(x_{30})\right) + \frac{C_{\text{np}}}{C_r + C_{\text{np}}} v_n\right].$$

where v_{load} is the velocity of load movement.

The following restrictions are imposed on the coordinate x_{valve} :

$$x_{30} = \begin{cases} 0, |x_3| \leq \Delta_3; \\ x_3 - \Delta_3 \operatorname{sign}(x_3), \Delta_3 < |x_3| < x_{3\text{max}}; \\ (x_{3\text{max}} - \Delta_3) \operatorname{sign}(x_3), |x_3| \geq x_{3\text{max}}. \end{cases}$$

Here $x_{\text{valve max}}$ is maximum valve motion.

The equation for the third stage feedback has the form $x_{\text{valve}} = (1 + K_{\text{ph}}) x_{\text{arip}} - K_{\text{ph}} x_p$. The x_{rod} coordinate can be found from the x_p coordinate: $x_{\text{rod}} = (c_{\text{red}}/c_{\text{sh}}) \Delta x + x_{\text{load}}$, where $c_{\text{sh}} = (1/c_{\text{rod}} + 1/c_{\text{load}})^{-1}$.

The system of sensors of linear movements is described by the equation $x_{\text{rod}} = T_{\text{hys}} (x_{\text{rod}}/\Delta_s) \Delta_s$, where Δ_s is sensor discreteness.

In the mathematical model the load will be described by a simplified differential equation

$$m \ddot{x}_{HM} + b \dot{x}_{HM} + K_H x_{HM} + F_0 + F_{TP} \operatorname{sign}(\dot{x}_{HM}) = c_{HM} (\dot{x}_{HT} - \dot{x}_{HM}).$$

[In the above equation HM = simulated load]

Jumplike deviations of the x_{HM} coordinate, having a random character, may be observed under the influence of aerodynamic perturbations and nonuniform fuel combustion. It is therefore desirable to obtain this coordinate not by mathematical simulation, but directly from the system. This problem can be solved by installing a digital manometer connected to both pressure cylinder cavities. Then

$$\dot{x}_{HM} = \dot{x}_{HT} - \frac{\Delta p_{H2} - F_{TPH} \operatorname{sign}(\dot{x}_{HT})}{c_{HM}},$$

where Δp is information on the pressure drop in the pressure cylinder cavities, read from the digital manometer.

It must be noted that in this case there is no need to determine the velocity of the rod — only its direction need be determined. Since we will obtain \dot{x}_{HM} directly from the system in real time, the order of the mathematical model equation will be reduced to 1, and this reduces its integration time in the correction process. The equation for the principal correcting relationship has the form

$$U_c = U_{H2} - U_{KOP}; \quad U_{KOP}^* = T_{KUC} (U_{KOP} / \Delta_{H2}) \Delta_{H2} [t - \tau_k],$$

where τ_{cor} is the lag constant for the correcting device (integration time of the mathematical model equations);

$$U_{KOP} = \begin{cases} 0, & |K_{CHC} U_{H2} - \dot{x}_{HM}| > \Delta_{H2}; \\ \left(\dot{x}_{HM} - \dot{x}_{HM} \right) \operatorname{sign} \left(K_{CHC} U_{H2} - \dot{x}_{HM} \right) / K_{KOP}; \end{cases}$$

here Δ_{in} is the magnitude of the insensitivity zone within which no correction is made, K_{sys} is the static system transfer factor, K_{cor} is the feedback coefficient. Figure 1.b is a block diagram.

Study of the equations of motion using digital correcting device. The system of equations was studied by its integration by the fourth- fifth order Runge-Kutta method using a computer with the following RD-load system parameters:

$$\begin{aligned} m &= 579 \text{ H} \cdot \text{c}^2 \cdot \text{cm}^{-1}; \quad b = 260 \text{ H} \cdot \text{c} \cdot \text{cm}^{-1}; \quad F_0 = 0; \quad K_H = 1890 \text{ H} \cdot \text{c} \cdot \text{cm}^{-1}; \\ K_{oc1} &= 0.5; \quad K_{oc} = 0.166; \quad K_{v1} = 475 \text{ c}^{-1}; \quad p_0 = 2100 \text{ H} \cdot \text{cm}^{-2}; \\ K_v &= 81.3 \text{ c}^{-1}; \quad \Delta_3 = 0.005 \text{ cm}; \quad x_{3max} = 0.154 \text{ cm}; \quad K_{\Sigma} = 500; \\ F_{TP} &= 2600 \text{ H}; \quad c_H = 18 \cdot 10^5 \text{ H} \cdot \text{cm}^{-1}; \quad c_H = 11 \cdot 10^5 \text{ H} \cdot \text{cm}^{-1}; \\ c_{HT} &= 40 \cdot 10^5 \text{ H} \cdot \text{cm}^{-1}; \quad c_T = 25 \cdot 10^5 \text{ H} \cdot \text{cm}^{-1}; \quad c_{KOPH} = 44 \cdot 10^5 \text{ H} \cdot \text{cm}^{-1}; \\ F_{TPH} &= 2260 \text{ H}; \quad S_H = 157.6 \text{ cm}^2; \quad \Delta_{H2} = 0.000625 \text{ cm}; \quad \tau_k = 0.015 \text{ c} \end{aligned}$$

and the digital correction unit parameters: $\Delta_{cy1} = 0.0001 \text{ cm}$; $K_{sw} = 50,000$; $\tau_{sw} = 0.02 \text{ s}$; $\Delta_{ind} = 0.01 \text{ cm}$.

The equation for the load model was integrated with the interval τ_{cor} and the remaining equations with the interval $\tau \leq \tau_{cor}$.

The system was studied with the sending of a command signal in the form of a step constituting 4 percent of the maximum rod stroke (0.05 cm), which corresponds to the amplitude of the command signal during in-flight rocket stabilization.

Figure 2 shows the transient process of the RD-load system with correction "on" and "off." The presence of a scatter of steady values between the corrected and uncorrected system is attributable to the existence of a high level of dry friction, which gives rise to an insensitivity zone. Figure 2 also shows a corrected command signal with allowance for lag of the DAC and correcting device. The graph shows that the control is in antiphase with the oscillations of the uncorrected system and has some lead relative to it.

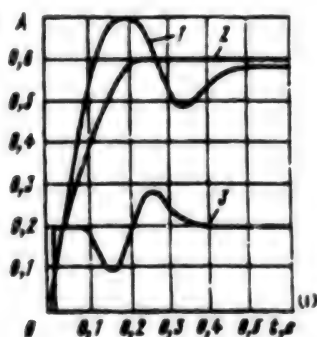


Fig. 2. Time dependence of velocity v_{load} with correction (2) and without correction (1); (3) shape of correction signal.

Key: 1) s

It must be noted that with the sending of sinusoidal command signals to the input this correction exerts a weak influence on the phase and amplitude of the output signal up to 1.5 Hz and therefore there will be assurance of the phase lag necessary for stable rocket motion at the frequencies of oscillations of the fuel components in the tanks (0.5...1.5 Hz).

Possible field of applicability of correction. The proposed correction variant can be regarded as an alternative when correcting the drive of the Energiya booster described in [1].

Nonlinear correction with a feedback, proportional to the rate of change in kinetic energy, can be used in both digital and analog forms and makes it possible to solve problems in the dynamics of actuating systems with allowance for requirements on the smoothness of motion of the controlled object when there is a lag in the direct circuit.

Bibliography

1. Bayda, S. P. and Beletskiy, D. S., Nonlinear correlation of dynamic characteristics of rudder drives of second stage of Energiya booster, *TEKHNICHESKAYA KIBERNETIKA* (Technical Cybernetics), No 4, pp 128-135, 1990.
2. Borovkov, A. G. and Misyuk, I. V., Comparative analysis of methods for compensating for frictional autooscillations in tracking systems, *IZV. VUZov, ser: MASHINOSTROYENIYE* (News of Institutions of Higher Education. Series on Machine Building), No 12, pp 76-78, 1992.
3. Bortsov, Yu. A. and Yunger, I. B., *Avtomaticheskkiye sistemy s razryvnym upravleniyem* (Automatic Systems With Discontinuous Control), Leningrad, Energiyashizdat, 1986, 165 pages.

Gyrocompasses Based on Gyrotachometers. Part I

957A1132B Moscow VESTNIK MOSKOVSKOGO GOSUDARSTVENNOGO TEKHNICHESKOGO UNIVERSITETA: SERIYA PRIBOROSTROYENIYE in Russian No 1, Jan-Mar 95 (manuscript received 15 Nov 94) pp 119-127

[Article by S. A. Shestov, doctor of technical sciences, professor, and V. A. Bauman, candidate of technical sciences, docent, Gyroscopic Instruments and Orientation, Navigation and Stabilization Systems Department, Moscow State Technical University imeni N. E. Bauman; the second part of the article will be published in a later number of the journal; the first paragraph is an abstract; UDC 621.395.664]

[FBIS Translated Text] *Designs, equations of motion and an analysis of errors, speed and noise immunity parameters are proposed for surface gyrocompasses constructed on the basis of gyrotachometers, finding wide use in systems for azimuthal orientation of surface objects employed in many branches of the economy.*

The modern development of technology raises problems in the development of systems for the azimuthal orientation of surface objects (SO) for both defense (armored and reconnaissance vehicles, "mobile" missiles, etc.) and civilian (tunneling equipment for shafts and tunnels, bottom work, objects situated within geophysical, oil and gas wells, etc.) purposes. The solution of such problems requires gyrocompasses (GC) having a quite high accuracy and requiring only a short time for seeking the meridian (up to 8 minutes), small volume (up to 3 dm³ and a low mass, labor input and cost. These requirements are not met by the gyrocompasses used on seagoing vessels and spacecraft and the azimuthal orientation systems employed in aviation [1]. Accordingly, work has been undertaken in proposing, analyzing and developing other methods for gyrocompass orientation based, for example, on measurement of apparent

deviations of gyroplatforms and free gyroscopes, measurement of information signals from the channels for

horizontal reduction of platforms and gyroverticals and use of gyrotachometers (GT) [2].

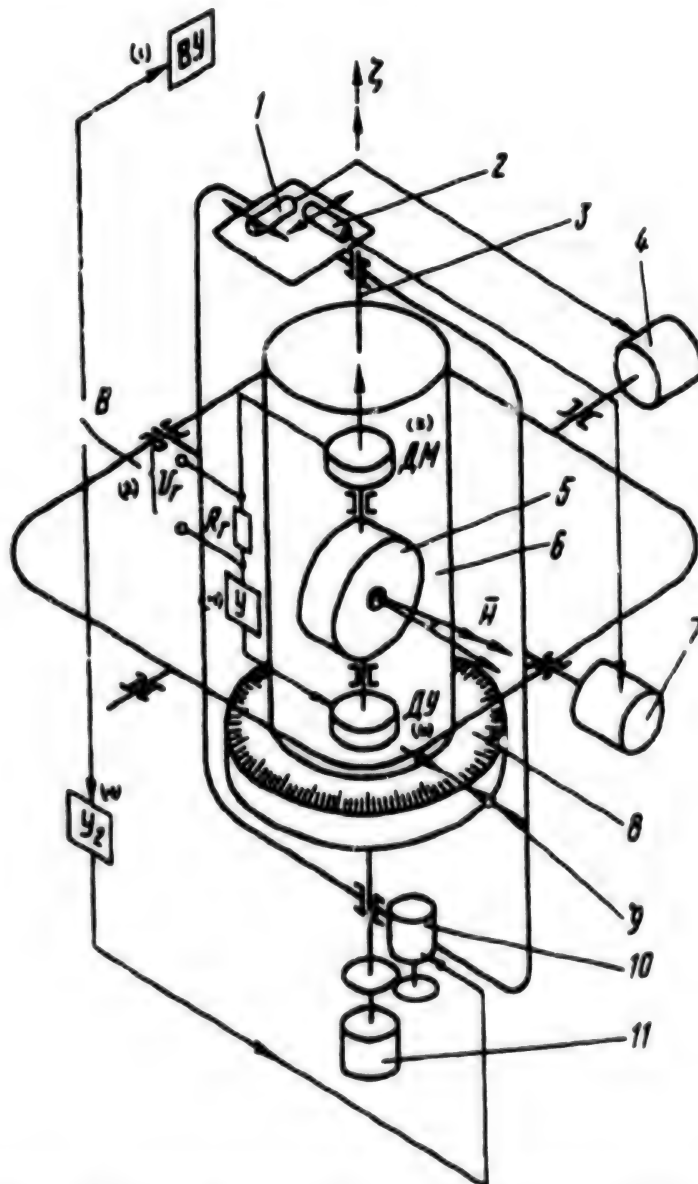


Diagram of gyrocompass on a horizontal platform: A — 1, 2) accelerometers; 3) axis of azimuthal rotation of platform with GT; 4,7) actuating motors of system; 5) moving GT component; 6) GT body; 8, 9) mechanical device for reading course angles; 10) actuating motor with tachogenerator of system for azimuthal rotation of platform; 11) electromechanical device for reading course angles; B — switch of gyrocompass orientation signals: (at bottom — geometric, at top — analytic).

Key: 1. computer; 2. V_a ; 3. V_a ; 4. A; 5. moment sensor; 6. angle sensor

Systems for azimuthal orientation of SO constructed on the basis of GT have proven to be the most universal. We will examine them in greater detail because information published on them is of a fragmentary character [3, 4].

In order to be specific, by the term GT we will mean a precision gyrounit (GU) with two degrees of freedom whose moving component has a feedback. Such a GT, installed on a base fixed relative to the Earth, strives to match the vector of its kinetic moment (virtually coinciding with the rotor axis (RA) of the gyromotor) with the vector of the horizontal component of the velocity of the Earth's rotation, lying in the plane of the meridian. Theoretically, the GT also may use any other type of gyroscopic device for measuring the angular velocity (laser gyroscope, dynamically tunable gyroscope, etc.).

The functional-kinematic layout of a GC constructed on the basis of a GT for the most part is determined by two methods: use of information read from the GT or minimizing of the GC error caused by nonhorizontality of the GT input axis. This error is generated by the vertical component of the velocity of the Earth's rotation and is already known from the theory of a Foucault GC as the inclination error. The figure illustrates an example of the functional-kinematic layout of a GC constructed on the basis of a GT.

With respect to the method for using information, GC schemes are divided into geometric and analytic. In geometric schemes the GT output signal is used in reducing the GT RA to the plane of the meridian, after which the RA, like a magnetic needle, indicates the direction to the north. In analytic schemes the GT output signal is fed to the input of a computer, which using some algorithm computes the SO course angle.

The inclination error also can be minimized geometrically and analytically. In geometric minimization the GT input index is reduced to the plane of the horizon and thereafter is held there. This can be realized by mounting the GT either on a platform which is held in the horizontal plane by means of tracking systems whose sensing elements are accelerometers or on a physical pendulum. In analytic minimizing of inclination error a platform or pendulum is not required, but the GT body is attached directly to the SO body and accordingly duplicates all its inclinations. In this case the GC has large inclination errors. In order to lessen them, accelerometers are mounted on the GT body. The signals of these accelerometers, containing information on the angles of

SO inclination, are used for compensating for the inclination errors. We note that the attachment of the GT body to the SO body, simplifying GC design, reduces the noise immunity of GC readings because the GT also senses the oscillations and vibration of the body.

The examined GC schemes can be constructed using standard-produced precision GU, accelerometers and computers, which is a substantial merit of such GC.

The principal operating characteristics of GC constructed using a GT are as follows: time required for reaching a working mode, that is, the time expended on performing servicing operations; time required for determining the course angle; error in determining the course angle; noise immunity of GC readings.

The time required for reaching a working mode is determined for the most part by the setting of the nominal GT thermal mode. Computations and tests of a GC constructed using a GT indicated that with a negative ambient temperature the power of the built-in system for thermostating a precision GU is inadequate for bringing the GT to a nominal thermal mode. Accordingly, it is necessary either to develop an additional system for thermal protection of the GT or a system for algorithmic compensation of GC temperature errors. The problems arising in this case were examined in [5].

The remaining operational characteristics are determined on the basis of a GC mathematical model. We will construct such a model for the GC scheme illustrated in the figure on the assumption that the GT input axis is geometrically held in the plane of the horizon, the GT has reached a nominal thermal mode and the dynamic processes in the electric circuits and electronic units can be neglected in comparison with mechanical systems.

We introduce into the examination a base system of geographic coordinates (CS) $O\xi\eta\zeta$ referenced to the Earth and right-handed CS $Oxyz$, referenced to the body of the SO, GC body, platform, GT body and GT moving component. We stipulate the relative angular position of these CS as a result of angular movement of the first kind, that is, Euler-Krylov angles are used.

Using the introduced CS, we obtain (with allowance for quantities only of the first infinitesimal order) the following projections of the absolute angular velocity onto the axis of the GT moving component and onto the platform z-axis:

$$\begin{aligned}\omega_x^r &= \omega_n \sin(\psi + \gamma_n) + (\omega_z + \dot{\psi})(\alpha_n \sin \gamma_n - \beta_n \cos \gamma_n - \beta_n - \beta_r) + \\ &+ \omega_n \cos(\psi + \gamma_n)(\gamma_{xn} + \gamma_{nn} + \gamma_x + \gamma_r) + (\dot{\psi})(\cos \gamma_n - (\gamma_{xn} + \gamma_{nn} + \gamma_x + \\ &+ \gamma_r) \sin \gamma_n) + \kappa(\sin \gamma_n + (\gamma_{xn} + \gamma_{nn} + \gamma_x + \gamma_r) \cos \gamma_n) + \dot{\alpha}_n + (\gamma_x + \gamma_r) \beta_n - \\ &- (\beta_x + \beta_r) \dot{\gamma}_n + \dot{\alpha}_r; \\ \omega_y^r &= \omega_n \cos(\psi + \gamma_n) + (\omega_z + \dot{\psi})(\beta_n \sin \gamma_n + \alpha_n \cos \gamma_n + \alpha_x + \alpha_r) - \omega_n(\gamma_{xn} + \\ &+ \gamma_x + \gamma_{nn} + \gamma_r) \sin(\psi + \gamma_n) - \dot{\psi}(\sin \gamma_n + (\gamma_{xn} + \gamma_{nn} + \gamma_x + \gamma_r) \cos \gamma_n) + (1) \\ &+ \kappa(\cos \gamma_n - (\gamma_{xn} + \gamma_{nn} + \gamma_x + \gamma_r) \sin \gamma_n) - (\gamma_x + \gamma_r) \dot{\alpha}_n + \dot{\beta}_n + (\alpha_x + \alpha_r) \dot{\gamma}_n + \beta_r; \\ \omega_z^r &= \omega_n[(\beta_x + \beta_r) \sin(\psi + \gamma_n) - (\alpha_x + \alpha_r) \cos(\psi + \gamma_n) + \beta_n \sin \psi - \alpha_n \cos \psi] + \\ &+ \omega_z + \dot{\psi} + \dot{\psi}[(\beta_x + \beta_r) \cos \gamma_n + (\alpha_x + \alpha_r) \sin \gamma_n - (\kappa - \beta_n)] + \kappa[(\beta_x + \\ &+ \beta_r) \sin \gamma_n - (\alpha_x + \alpha_r) \cos \gamma_n + (\dot{\psi} - \alpha_n)] + (\beta_x + \beta_r) \dot{\alpha}_n - (\alpha_x + \alpha_r) \dot{\beta}_n + \dot{\gamma}_n + \dot{\gamma}_r; \\ \omega_z^n &= \omega_n(\beta_n \sin \psi - \alpha_n \cos \psi) + \dot{\psi}(\beta_n - \kappa) + \kappa(\dot{\psi} - \alpha_n) + \omega_z + \dot{\psi} + \gamma_n.\end{aligned}$$

Note: The following subscripts and superscripts recur in the Russian formulas which follow. Their rendition in the English translation is indicated:

$r = g$; $\pi = pl$; $K = c$; $K\pi = \text{fin pl}$; $M\pi = \text{in pl}$; $\Delta M = m$; $\Delta y = a$; $\Delta = m$; $B = \text{per}$; $T\Gamma = TG$; $M = I$; $pH = \text{in d}$; $H = \text{in}$. The meaning of these and other abbreviations is evident from the text.

where

$$\omega_n = U \cos \phi, \quad \omega_z = U \sin \phi$$

are the projections of the velocity U of the Earth's rotation onto the axes of the geographic CS; ϕ is the latitudinal position of the GC; δ, κ, ψ are SO pitching, banking and course angles; α, β are the angles of deviation of the GC units (to which the CS are referenced) from the plane of the horizon and γ — in the plane of the horizon; $\delta^*, \kappa^*, \psi^*$ are the angular

velocities of the SO body caused by force impacts acting upon it (wind loads, ground tremors, ground subsidence, etc.) [here and elsewhere in the text the asterisk indicates that each of these Greek letters is surmounted by a dot]; $\alpha^*, \beta^*, \gamma^*, \alpha^*, \beta^*, \gamma^*$ are the angular velocities of the platform and the GT moving component caused by external and internal force impacts acting upon them.

The GC mathematical model includes three groups of equations.

The equation for the GT moving component (with allowance only for quantities of the first infinitesimal order) is

$$\begin{aligned}-J_x \ddot{\omega}_x^r - D_r \dot{\gamma}_r + K_{AM} i - H \omega_x^r - \gamma_r H \omega_y^r + (J_y^x - J_x^x)(\omega_y^r)^2 \gamma_r - (\omega_x^r)^2 \gamma_r + \\ + \omega_y^r \omega_x^r + M_x^r = 0;\end{aligned}\quad (2)$$

where J_x, J_y, J_z are the axial and equatorial moments of inertia of the moving GT component; D_r is the damping coefficient of the GT moving component; K_{AM} is the GT moment sensor transfer coefficient; i is current strength

in the GT feedback circuit; H is the kinetic moment of the gyromotor; M_x^r is the total perturbing moment operative around the GT output axis.

The equations for the GC electric circuits are

$$\begin{aligned} U_{AY} &= U_{AY}^A - K_{AY} \gamma_r; U_{Y1} = U_{Y1}^A + K_{Y1} U_{AY}; I = U_{Y1} R_Z^{-1}; R_Z = R_r + R_{AM}; \\ U_r &= IR_r; U_{Y2} = U_{Y2}^A - K_{Y2} (U_r + U_{oc}); U_{oc} = K_p U_{\pi}; U_{\pi} = U_{\pi}^A + \\ &+ K_{\pi n} \gamma_n. \end{aligned} \quad (3)$$

where

$$U_{AY}, U_{Y1}, U_r, U_{Y2}, U_{oc}, U_{\pi}, U_{AY}^A, U_{Y1}^A, U_{Y2}^A, U_{\pi}^A$$

are the output and spurious signals of the angle sensor, amplifiers A1 and A2, gyrotachometer and tachogener-

ator; $K_m, K_{A1}, K_{A2}, K_{ng}, K_{TG}$ are the transfer coefficients for the angle sensor, amplifiers, strength of the feedback regulator for platform reduction and tachogenerator; R_r, R_{AM} are active electric resistances of the GT output resistor and the control winding of the moment sensor; n is the reducer transmission ratio.

The equation of motion for a platform with a GT is:

$$-J_n \ddot{\omega}_n^R + nM_A - M_n = 0; S_A n \gamma_n + M_A = K_A U_{Y2}. \quad (4)$$

where J_n is the moment of platform inertia with allowance for the reduced moment of inertia of the motor rotor; ω_n^R is the absolute angular acceleration of the platform; M_n is the moment created by the motor; M_A is the moment of resistance of platform supports;

S_m is the motor rotor damping factor; K_m is the motor transfer coefficient.

Differentiating expression (1) in time for ω_n^R and ω_n^s , we obtain

$$\begin{aligned} \ddot{\omega}_n^R &= \ddot{\psi} + \ddot{\gamma}_n + \ddot{\theta}(\beta_n - \kappa) + \ddot{\kappa}(\theta - \alpha_n) + \ddot{\theta}(\beta_n - \kappa) + \\ &+ \ddot{\kappa}(\theta - \alpha_n) + \omega_n[(\beta_n + \alpha_n)\dot{\psi} \sin \psi - (\dot{\alpha}_n - \dot{\beta}_n)\dot{\psi} \cos \psi] \\ \ddot{\omega}_n^s &= \ddot{\psi} + \ddot{\gamma}_n + \ddot{\gamma}_r + \ddot{\theta}[(\beta_n + \beta_r) \cos \gamma_n + (\alpha_n + \alpha_r) \sin \gamma_n - (\kappa - \beta_n)] + \\ &+ \ddot{\kappa}[(\beta_n + \beta_r) \sin \gamma_n - (\alpha_n + \alpha_r) \cos \gamma_n + (\theta - \alpha_n)] + \ddot{\alpha}_n(\beta_n + \beta_r) - \\ &- \ddot{\beta}_n(\alpha_n + \alpha_r) + \ddot{\theta}(\dot{\alpha}_r \sin \gamma_n + \dot{\beta}_r \cos \gamma_n - (\kappa - \dot{\beta}_n)) + \dot{\gamma}_n[(\alpha_n + \alpha_r) \cos \gamma_n - \\ &- (\beta_n + \beta_r) \sin \gamma_n] + \ddot{\kappa}(\dot{\beta}_r \sin \gamma_n - \dot{\alpha}_r \cos \gamma_n + (\theta - \dot{\alpha}_n)) + \dot{\gamma}_n[(\alpha_n + \alpha_r) \times \\ &\times \sin \gamma_n + (\beta_n + \beta_r) \cos \gamma_n] + \dot{\alpha}_n \dot{\beta}_n - \dot{\beta}_n \dot{\alpha}_r + \omega_n(\dot{\beta}_r \sin(\psi + \gamma_n) - \\ &- \dot{\alpha}_r \cos(\psi + \gamma_n)) + (\dot{\psi} + \dot{\gamma}_n)(\beta_n + \beta_r) \cos(\psi + \gamma_n) + (\alpha_n + \\ &+ \alpha_r) \sin(\psi + \gamma_n)] + \dot{\psi}(\alpha_n \sin \psi + \beta_n \cos \psi) + \dot{\beta}_n \sin \psi - \dot{\alpha}_n \cos \psi. \end{aligned} \quad (5)$$

$$\quad (6)$$

Substituting expressions (1), (5) and (6) into (2) and (4) and excluding the intermediate variables in equations

(2)-(4), we obtain the equation of motion for the GC platform:

$$(J_n + K_{AM}^{-1} n K_A K_{Y2} R_T J_r) \ddot{\gamma}_n + [(S_A + K_A K_{Y2} K_P K_{TT}) n^2 - K_{AM}^{-1} n K_A K_{Y2} \times \\ \times R_T H (\beta_n + \beta_r)] \dot{\gamma}_n + K_{AM}^{-1} n K_A K_{Y2} R_T H \omega_n \sin(\psi + \gamma_n) = M_n, \quad (7)$$

where M_n is the perturbing moment.

In a general case the analytic expression for M_n is unwieldy because it is written on the basis of the unwieldy expressions (1), (5), (6). We will examine the principal special cases.

Ideal case when $M_n = 0$. Then for a steady platform position we have

$$\sin(\psi + \gamma_n) = 0. \quad (8)$$

Equation (8) has two solutions

$$\psi + \gamma_n = 0; \quad \psi_1 = -\gamma_n; \quad (9)$$

$$\psi + \gamma_n = 180^\circ; \quad \psi_2 = 180^\circ - \gamma_n. \quad (10)$$

Solution (9) corresponds to a stable equilibrium of the platform and solution (10) corresponds to an unstable equilibrium ("spurious zero"). In GC schemes with continuous platform reduction the spurious zero problem is not pertinent because the slightest perturbation of the GT moving component (as is always observed in practical work) causes a triggering of the tracking system and platform reduction to a position of stable equilibrium.

An analysis of the coefficient on γ_n^* shows that depending on the value and signs on the random angles β_n and β_r it may be both positive and negative. In the latter case the motion of the platform will be unstable. The reason for this is the possible angle of deviation $\beta_n + \beta_r$ of the GT output axis from the platform axis

of rotation. In this case the component of angular velocity of platform reduction $(\beta_n + \beta_r) \gamma_n^*$ is projected onto the GT input axis. As a result the GT reacts not only to the useful angular velocity ω_n , but also to the perturbation $(\beta_n + \beta_r) \gamma_n^*$. The nature of platform motion is dependent on the ratio of the values ω_n and $(\beta_n + \beta_r) \gamma_n^*$.

In experimental studies of GC an unstable platform motion was detected in the form of increasing amplitudes of platform oscillation about the plane of the meridian, passing into continuous platform rotation with an increasing velocity. This phenomenon has been called "gyroscope capture."

The coefficient on γ_n^* , and therefore also the nature of platform motion, may change during the time of GC operation due to a change in the latitude ϕ of GC position and change in the angle $\beta_n + \beta_r$. A differentiating link must be introduced in order to ensure the stability and quality of platform reduction system operation. A DG-1 actuating motor-generator was used as such in the constructed GC variants.

On the basis of solution of the nonlinear differential equation (7), found, for example, by the so-called "alinement" method, it is possible to find the time required for platform reduction to the plane of the meridian with large initial angles $\phi + \gamma_n < 180^\circ$, that is, the time required for determining the course angle. The minimum experimental time for determining the course angle with an initial angle of deviation of the platform from the plane of the meridian by 179° was about 3 minutes.

In the first approximation we find the error in determining the course angle. For this purpose we will assume that the GC is in a steady position (that is, $\alpha_n^* = \beta_n^* = \gamma_n^* = \alpha_r^* = \beta_r^* = \gamma_r^* = 0$), but tremors of the SO body are absent (that is, $\delta = \kappa = \psi^* = 0$). Under these conditions the expression for M_n is simplified and on the basis of equations (1)-(4) we obtain

$$\sin(\psi + \gamma_n) = \psi + \gamma_n = \frac{1}{H \omega_n} (M_n^r - \frac{K_{AM} M_n}{n K_A K_{Y2} R_T} - \frac{K_{AM} U_{Y2}^A}{K_{Y2} R_T} - \frac{K_{AM} K_P U_{TT}^A}{K_{Y2} R_T}) + \\ + (\beta_n + \beta_r - \alpha_n \sin \gamma_n + \beta_n \cos \gamma_n) \operatorname{tg} \varphi - (\gamma_{nn} + \gamma_{nr} + \gamma_n + \gamma_r) \cos(\psi + \gamma_n). \quad (11)$$

An analysis of expression (11) reveals that a GC with continuous platform reduction has no methodical errors: all the error components are instrumental and have a quite clear physical sense. We note that the error is dependent on the latitude of the place of GC operation and increases with an increase in latitude.

The GC readings are read when its platform is reduced with a small error (11) to the plane of the meridian. In this position the directional gyroscopic moment $H\omega_\gamma(\phi + \gamma_\mu)$ is small. As a result, even weak perturbing effects drive the movable GT component from a position of

equilibrium and a controlling signal is sent platform reduction system, which begins to perform damping oscillations relative to the plane of the meridian. The sending of readings from the GC is interrupted. This is the essence of the poor noise immunity of readings of GC constructed using geometric schemes.

We will find analytic expressions for possible perturbing influences on the GC at the time when readings are sent from it. For this we obtain an expression for M_{per} on the assumption that the GC is ideally constructed

$$U_{\gamma_2}^* = U_{\pi}^* = 0, \alpha_r = \beta_r = \gamma_r = \alpha_k = \beta_k = \gamma_k = \gamma_{nn} = \gamma_{kn} = 0, (M_n = M_k = 0).$$

the platform is in the plane of the horizon ($\alpha_\mu = \beta_\mu = 0$) and that the banking angles κ and pitching angles δ of the SO are equal to zero.

With allowance for these conditions we find $\omega_\gamma^{\mu}, \omega_\gamma^k, \omega_\gamma^s$ and we substitute them into equations (2) and (4). As a result, we obtain

$$\begin{aligned} J_n \ddot{\gamma}_n + (S_A n^2 + n^2 K_A K_{\gamma 2} K_p K_{\pi}) \dot{\gamma}_n + K_{\gamma n} n K_A K_{\gamma 2} R_T H \alpha_\gamma (\psi + \gamma_\mu) = \\ = -J_n [\ddot{\psi} + \dot{\theta}(\beta_n - \kappa) + \kappa(\dot{\theta} - \dot{\alpha}_n) + \omega_\gamma(\beta_n \sin \psi - \dot{\alpha}_n \cos \psi)] - K_{\gamma n} n K_A \times \\ \times K_{\gamma 2} R_T (J_r [\ddot{\psi} + \dot{\gamma}_n + \dot{\gamma}_r + \dot{\theta}(\dot{\alpha}_r \sin \gamma_n + \beta_r \cos \gamma_n - \kappa + \dot{\beta}_n) + \kappa(\beta_r \sin \gamma_n - \\ - \dot{\alpha}_r \cos \gamma_n + \dot{\theta} - \dot{\alpha}_n) + \dot{\alpha}_n \beta_r - \dot{\alpha}_r \dot{\beta}_n - \omega_\gamma(\alpha_r - \beta_n \sin \psi + \\ + \dot{\alpha}_n \cos \psi)] + D_r \dot{\gamma}_r + H(\dot{\theta} \cos \gamma_n + \kappa \sin \gamma_n + \dot{\alpha}_n + \dot{\alpha}_r) - \\ - (J_\gamma^k - J_\gamma^s)(\dot{\theta} \cos \gamma_n + \kappa \sin \gamma_n + \dot{\alpha}_n + \dot{\alpha}_r)(\kappa \cos \gamma_n - \dot{\theta} \sin \gamma_n + \dot{\beta}_n + \dot{\beta}_r)). \end{aligned} \quad (12)$$

The right-hand side of equation (12) characterizes the perturbing influences, each of which may drive the GC platform from a stable position, and shows that the perturbing influences on the GT and the platform were caused by the angular acceleration of any of the moving GC components ($\gamma^{**}, \gamma^{**}, \gamma^{**}$) and SO angular acceleration (ψ^{**}), as well as virtually any combination of SO angular accelerations (δ^*, κ^*) and moving GC components ($\alpha^{**}, \beta^{**}, \alpha^{**}, \beta^{**}$ [here the two asterisks indicate that two dots surmount the accompanying Greek letter]).

The impact of high-frequency harmonic effects can be reduced somewhat by careful choice of parameters for the GT feedback and platform reduction system, but it is virtually impossible to lessen the influence of low-frequency and pulsed perturbing influences.

GC schemes with time separation of GT signal measurement and platform reduction processes were proposed and studied for the purpose of lessening the shortcomings characteristic for GC schemes with continuous plat-

form (P) reduction. We will examine one of these as an example. The GC scheme shown in the figure will be supplemented by an integrator (I) and controlling unit whose purpose is setting of the time intervals and performing switching of the electric circuits. The cyclogram of GC operation contains three subcycles (SC). The first subcycle is a pause necessary for the damping of all transient processes in the GC systems. In the second SC the GT output is connected to the I input, the GT output signal "is accumulated" at the I output, no controlling signal is fed to the actuating motor and the platform is fixed in position; the second SC ends upon the elapsing of the time T_1 of the second SC. Then begins the third SC — the GT-I connection is broken, the I output is connected to the control winding of the actuating motor, I is discharged and the actuating motor rotates the platform, bringing it close to the plane of the meridian. The third SC continues for the duration of one cycle. Then the cycles are repeated, as a result of which the platform is discontinuously reduced to the plane of the meridian.

The motion of the GC platform in one of the cycles is described by the system of equations:

$$\begin{aligned} -J_n \ddot{\gamma}_n + nM_A - M_n &= 0; \quad S_A n \dot{\gamma}_n + M_A = K_A U_{\gamma 2}; \quad U_{\gamma 2} = \\ &= K_{\gamma 2} U_n^p + U_{\gamma 2}^A; \quad U_n^p = U_n^{pm} e^{-t/T_n^p}; \quad U_n^{pm} = U_n^A + K_n \int_0^T U_r dt, \end{aligned} \quad (13)$$

where U_1^A , U_1^p , U_1^{pm} are the initial, current and spurious discharge voltages; T_1^p is the discharge time constant; K_1 is the transfer coefficient.

We find the GT- U_n output signal by using expressions (2) and (3) and in the final expression retaining only terms of the first infinitesimal order:

$$J_r \frac{R_r}{K_{Ay} K_{\gamma 1}} \ddot{\gamma}_r + D_r \frac{R_r}{K_{Ay} K_{\gamma 1}} \dot{\gamma}_r + K_{Ay} U_r = R_r [H \omega_n \sin(\psi + \gamma_n) + N_n]. \quad (14)$$

where N_n is the deflecting moment operative around the GT output axis and in a general case containing dynamic perturbations (gyroscopic and inertial moments) and quasistatic perturbations of the weighting moments type (M_n).

Assuming that $N_n = 0$, using formulas (13) and (14) we obtain the equation of motion for the platform in one cycle:

$$J_n \ddot{\gamma}_n + n^2 S_A \dot{\gamma}_n = nK_A K_{\gamma 2} U_n^{pm} e^{-t/T_n^p} - M_n. \quad (15)$$

By solving equation (15) we find the angle and the time required for reducing the platform in one cycle:

$$\dot{\gamma}_n = \frac{K_A K_{\gamma 2} U_n^{pm} T_n^p}{n^2 S_A} \left(1 - e^{-t/T_n^p} \right) - \frac{M_n}{n^2 S_A} t_A; \quad (16)$$

$$t_A = T_n^p \ln \frac{nK_A K_{\gamma 2} U_n^{pm}}{M_n} \quad (17)$$

Using expressions (16) and (17) we will construct a graph of platform motion from which it is possible to judge the stability of GC operation and the time for determining the course angle.

We find the error in determining the course angle on the assumption that the platform has reached a steady position ($\gamma^{**} = 0$, $\gamma_n^* = 0$). Then from equation (15) we have:

$$nK_A K_{\gamma 2} U_n^{pm} e^{-t^*/T_n^p} - M_n = 0. \quad (18)$$

where t^* is the specific moment in time for onset of the equality (18).

Expanding equality (18) with allowance for expressions (13) and (14), we obtain

$$\psi + \gamma_n = \frac{1}{H\omega_n} \left(\frac{K_{\Delta n} M_n}{n K_A K_{\gamma 2} K_n R_r T_n} e^{i' / T_n^0} - \frac{K_{\Delta n} U_n^{\Delta}}{K_n R_r T_n} + M_n^r \right) + (\beta_n + \beta_r - \alpha_n \sin \gamma_n + \beta_n \cos \gamma_n) \operatorname{tg} \varphi - (\gamma_{nn} + \gamma_{nn} + \gamma_n + \gamma_r) \cos(\psi + \gamma_n). \quad (19)$$

It follows from a comparison of formulas (19) and (11) that with a correct choice of the parameters K_1 and T_1 the error in GC schemes with the separation of processes is somewhat less than in GC schemes with continuous platform reduction.

Schemes with discontinuous platform (P) reduction make possible a considerable increase in the noise immunity of GC readings. The interference signal accumulated at the I output is not always capable of causing the triggering of the platform reduction circuit. We will show this for the case of a pulsed impact on the moving GT component, most probable in actual practice. The solution of equation (14) in the case of a pulsed impact has the form

$$U_r^n = U_r^n e^{-t/T_r} \sin(\omega t + \varphi_r). \quad (20)$$

$$U_n^n = K_n \int_0^T U_r^n dt = \frac{K_n U_r^n \omega}{T_r^{-2} + \omega^2} \left[1 - e^{-T_n/T_r} \left(\frac{1}{\omega T_r} \sin \omega T_n + \cos \omega T_n \right) \right].$$

In a correctly designed GC $T_1 \gg T_r$, $\omega \gg 1/T_r$, then

$$U_n^n = (K_n / \omega) U_r^n. \quad (21)$$

Expression (21) shows that with proper choice of the K_1 and ω quantities the noise signal at the I output can be considerably reduced, and accordingly, the GC noise immunity is increased.

In addition, the GC schemes with discontinuous P reduction give a specific possibility in these schemes for cutting off the P reduction system at the end of this cycle when the I output signal is equal to zero. In this case P does not have a possibility for moving relative to the SO body and its noise immunity is virtually ideal.

where U_n^{cur} , U_n^{in} are the current and initial levels of the GT interference signal caused by pulsed influences; ω is the frequency of the characteristic oscillations of the GT moving component; ϕ_0 is the initial phase of these oscillations; T_1 is the time constant of the interference signal damping exponent.

The U_n^{cur} signal is fed to the input of I, at whose output we will have a spurious controlling signal U_1^{cur} . Assuming that $U_1^{\text{cur}} = 0$, $\phi_1 = 0$, we obtain

However, when the reduction system is cut off errors may arise in the GC readings due to both to rotation of the SO body in the azimuthal plane and a random compensation for useful signal interference at the I output. Fundamental solutions for the detection of these errors and their elimination are simple.

Among the shortcomings of GC schemes with discontinuous P reduction it is necessary to include an increase in the time for determining the course angle due to "down time" of P in the course of the "pause" and "signal accumulation" SC. In order to lessen this shortcoming it is proposed that prior to the onset of standard discontinuous P reduction the platform be rotated in the direction of approach to the plane of the meridian by 90° . This procedure gives a decrease in the maximum time for determining the meridian by approximately half because even in the worse case standard P reduction begins with

the initial angle of RA deviation from the plane of the meridian by 90° , not 180° .

Analytic GC schemes are used for the purpose of reducing the time required for determining the course angle and simplifying the GC design. However, their realization has its special features and difficulties.

Analytic GC schemes will be examined in Part II of the article.

Bibliography

1. Andreyev, V. D., et al. (editors), *Razvitiye mekhaniki giroskopicheskikh i inertialnykh sistem* (Development of Mechanics of Gyroscopic and Inertial Systems), Moscow, Nauka, 1973.
2. Nazarov, B. I. and Khlebnikov, G. A., *Girostabilizatory raket* (Rocket Gyrostabilizers), Moscow, VIMO SSSR, 1975, 216 pages.
3. Voronkov, N. V., Kuttyrev, V. V. and Ashimov, N. M., *Giroskopicheskoye oriyentirovaniye* (Gyroscopic Orientation), Moscow, Nedra, 1980, 296 pages.
4. Kargu, A. I., *Izmeritelnyye ustroystva letatelnykh apparatov* (Flightcraft Measuring Devices), Moscow, Mashinostroyeniye, 1988, 219 pages.
5. Shestov, S. A., *Teplovyye raschety giroskopicheskikh ustroystv: Uchebnoye posobiye* (Thermal Computations of Gyroscopic Devices: Study Aid), Moscow, Izd-vo MG TU, 1992, 128 pages.
6. Ishlinskiy, A. Yu., *Oriyentatsiya, giroskopy i inertialnaya navigatsiya* (Orientation, Gyroscopes and Inertial Navigation), Moscow, Nauka, 1976, 670 pages.

Requirements on Navigational Support for Experiments From Lunar Polar Satellite Orbit

957A1117A Moscow GEODEZIYA I KARTOGRAFIYA in Russian Apr 95 No 4, pp 10-20

[Article by Yevgeniy Pavlovich Aleksashin, doctor of technical sciences, professor, Yuriy Sergeyevich Timofeyev, candidate of technical sciences, senior scientific specialist, and Aleksandr Mikhaylovich Shirenin, candidate of technical sciences, senior scientific specialist, Moscow State Administration for Geodesy and Cartography; UDC 528.715:629.78]

[FBIS Translated Text] The most rigorous requirements on navigational support for the operation of satellite-borne instrumentation are imposed by researchers who are engaged in on-line and postflight processing of the results of an orbital survey of the surface for the purpose of constructing a reference coordinate system and mapping, with determination of the parameters of the outer gravity field and study of the dynamics of the

translational-rotational motion of a celestial body [2, 8, 11]. As a rule, if these experiments are supported by adequately precise navigational data, no problems arise in their use for coordinate-time referencing and processing of the results of other experiments. Accordingly, in examining the problems involved in navigational support of the instruments carried aboard a lunar polar satellite (LPS) we will first of all start from the requirements which are imposed on the above-mentioned experiments.

The coordinate-time referencing problem is formulated in the following way: in a coordinate system rigorously referenced to the moon it is necessary to determine the vectors of the positions

$$\bar{R}_T^{-T} = [X_T, Y_T, Z_T]$$

of points on the physical surface of the moon on the basis of the coordinates of their images measured in the coordinate system of the satellite-borne instrument and corresponding to two or more moments in time. A special case of this problem is determination at the moments of observation of the spherical coordinates of the traces of the principal axes of the instruments on the physical surface of the moon or a celestial body. We will use a dynamic selenocentric system, as it was defined in [3], as the coordinate system rigorously coupled to the moon. For computing R_T^* [Note: Here and in the text which follows an asterisk following a letter indicates that in the original text the letter has an overline; two asterisks — the letter has an overline with a caret above the overline; three asterisks — the letter carries a caret; four asterisks — the letter carries a tilde] we will use an algorithm realizing direct orbital intersection based on a search for the mean-weighted position of a physical point on the segment of the minimum distance of the intersecting projecting rays which correspond to the images of this point obtained at two moments in time. This algorithm is described by the formulas:

$$\begin{aligned} \bar{R}_{22} &= \bar{R}_{21} - \bar{R}_2; \quad \bar{A}_1 = M_1 \bar{r}_1; \quad \bar{A}_2 = M_2 \bar{r}_2; \\ \rho_1^1 &= \bar{A}_1^T \bar{A}_1; \quad \rho_2^1 = \bar{A}_2^T \bar{A}_2; \quad \rho_{12} = \bar{A}_1^T \bar{A}_2; \\ \alpha &= \rho_{12}^1 - \rho_1^1 \rho_2^1; \quad a_1 = \bar{A}_1 \bar{R}_{22}; \quad a_2 = \bar{A}_2 \bar{R}_{22}; \\ k_1 &= 1/(a_1 \rho_{12} - a_2 \rho_1^1); \quad k_2 = 1/(a_2 \rho_{12} - a_1 \rho_2^1); \\ \bar{R}_T &= 0.5(k_1 \bar{A}_1 + k_2 \bar{A}_2). \end{aligned} \quad (1)$$

where

$$\bar{R}_t^T = [X_t, Y_t, Z_t], \quad \bar{R}_{t+1}^T = [X_{t+1}, Y_{t+1}, Z_{t+1}]$$

are the position vectors of the LPS at the times $t, t+1$ in the system rigorously referenced to the moon;

$$\bar{r}_t^T = [x_t, y_t, -f], \quad \bar{r}_{t+1}^T = [x_{t+1}, y_{t+1}, -f]$$

are the position vectors of the image of the very same physical point, stipulated in the coordinate system of a videoinstrument with the focal length f at the times $t, t+1$;

$$M_t = (l_{1t}, l_{2t}, l_{3t}), \quad M_{t+1} = (l_{1(t+1)}, l_{2(t+1)}, l_{3(t+1)})$$

are the matrices for transformation from the instrument system to the system rigorously referenced to the moon, stipulated at the times $t, t+1$ and being functions of the orientation parameters

$$\bar{M}_t^T = (l_{1t}, l_{2t}, l_{3t}), \quad \bar{M}_{t+1}^T = (l_{1(t+1)}, l_{2(t+1)}, l_{3(t+1)})$$

It follows from (1) that the vectors R_t^* of the sought-for point is the vector function

$$\bar{R}_t = \bar{F}_R(\bar{P})$$

of the 17-dimensional vector of the P^* parameters

$$P^T = [x_t, y_t, X_t, Y_t, Z_t, l_{1t}, l_{2t}, l_{3t}, x_{t+1}, y_{t+1}, X_{t+1}, Y_{t+1}, Z_{t+1}, l_{1(t+1)}, l_{2(t+1)}, l_{3(t+1)}, f]. \quad (2)$$

Thus, the components of the P^* vector (2) must be accessible at the time of the experiment for the coordinate-time referencing of the results of on-board experiments from a LPS orbit. They are obtained in the form of evaluations together with the covariation matrices of errors from the results of making and processing navigational measurements containing random errors. The components of the subvectors r^* and the covariation matrices of their errors K_r are computed on the basis of measurements of the coordinates x, y of the images of physical points in the instrument system. The components of the subvectors R_t^* and covariation matrices K_{R_t} of their errors are obtained on the basis of trajectory measurements, components of the subvectors λ^* and covariation matrices of their errors K_λ on the basis of measurements of the LPS orientation parameters [1].

Assume that P^{**} is the vector of evaluations of the parameters and that K_p is the covariation matrix of errors of the P^{**} vector. The coordinate-time referencing problem essentially involves computation of evaluations of the position vectors R_t^{**} of physical points and the covariation matrices $K_{R_t}^{**}$ of their errors. We have

$$\hat{R}_t = \bar{F}_R(\hat{P}); \quad \hat{K}_{R_t} = G_t^T \hat{K}_P G_t, \quad (3)$$

where

$$G_t = [\bar{V}_t \bar{F}_R^T]$$

is a gradient 17×3 matrix of the vector-function \bar{F}_R for the P parameters;

$$\bar{V}_t^T = [\partial/\partial x_t, \dots, \partial/\partial f]$$

is a 17-dimensional vectorial differentiation operator for the P^* components.

The components of the sought-for vectors R^{**}_T and the covariation matrices K^{**}_{RT} by virtue of (1) and (3) are essentially dependent on the programs, makeup and accuracy of the navigational measurements used for determining the components of the vector of the P^{**} parameters, as well as on the processing algorithms defining the rules for computing the P^{**} evaluations from the vector sample of measurements.

The principal objective of this study was therefore the construction of mathematical models of the processes transpiring on the real flight of a LPS and directly related to the collection of data necessary for the coordinate-time referencing of the results of operation of the onboard instruments. The constructed models were used in numerical computer experiments for determining the a priori accuracy characteristics of the refer-

encing results. Some recommendations have been formulated on planning the LPS orbit, selecting the type, makeup and programs for navigational measurements for ensuring the necessary accuracy in the referencing of experiments.

We will proceed on the assumption that the LPS carries instrumentation which can be used in navigational measurements: a frequency generator which fixes the time scale aboard the satellite and a device for registering the moments of events transpiring on this scale; devices ensuring the conducting of surface radiotechnical measurements for determining the LPS orbit; gyroscopic system for working out and maintaining the stipulated LPS orientation modes; topographic and sidereal videoinstruments; altimeter.

Table 1

Experiment	H, km	T	revolutions/day	IDL_1^0	b_{in}^0	P(%)
I	100	1 ^h 58 ^m	12	-1.1	1.45	0.3(21)
II	200	2 08	12	-1.2	2.97	0.7(23)
III	300	2 18	10	-1.3	4.45	0.5(12)

With respect to performance of the scientific missions of the LPS flight and supporting experiments with the required navigational information the parameters of the working orbit from which these experiments will be made are not a matter of indifference. In particular, the conditions of solar illumination of the surveyed surface and the geometry of its coverage by the scanning swaths of the topographic camera are of considerable importance for the problems which we examined. The LPS orbit must be planned in order to meet these or other illumination and coverage requirements. The usual set of parameters for the planning of orbits is: a — semiaxis major, e — eccentricity, i — angle of inclination of the orbital plane to the selenoequator, ω — distance of the pericenter from the orbit ascending node, α_0 — selenocentric right ascension of ascending node, τ — time of transit through the pericenter. In surface surveys preference is given to images of an approximately identical scale, which predetermines the choice of an orbit with an eccentricity equal to zero, that is, a circular orbit. Since all points in such an orbit are located at identical distances from the surface, it is unimportant which of them, instead of the pericenter, is taken as the reference point. Thus the parameters ω and τ become free. Naturally, for maintaining the status of a

polar orbit the angle i must be close to 90° . It therefore follows that when planning a LPS orbit it is possible to vary only two parameters: α_0 and a .

Assume that α_s, δ_s are the selenocentric right ascension and declination of the sun at the time t . Under the term "illumination conditions" of some point on the lunar surface at the time t we will understand the angle of solar elevation γ_{TS} above the local horizon. If α_T, δ_T are the selenocentric right ascension and declination of a given point on the lunar surface, then

$$\gamma_{TC} = \arcsin(\sin \delta_T \sin \delta_C + \cos \delta_T \cos \delta_C \cos (\alpha_T - \alpha_C)) \quad (4)$$

It follows from (4) that for a stipulated moment in time α_s, δ_s and a stipulated declination of the point δ_T the angle γ_{TS} is dependent only on the difference $\alpha_T - \alpha_s$. If the point belongs to the trace of the ascending branch of an orbit with $i = 90^\circ$ on the selenocentric celestial sphere, then $\alpha_T = \alpha_0$, that is, the illumination in the circle of declinations δ_T in this case is dependent only on

the difference $\Delta\alpha_{ns}$ of the selenocentric right ascensions of the node α_n and sun α_s . By stipulating the maximum admissible γ_{ns} in the selected circle of declinations δ_T from (4), we obtain the values

$$\Delta\alpha_{ns}^+, \Delta\alpha_{ns}^-$$

corresponding to the "morning" and "evening" angles of elevation γ_{ns} .

Now from the relation $\Delta\alpha_{ns} = \alpha_n - \alpha_s$ we determine α_n , ensuring the stipulated illumination conditions. The realization of the required α_n is accomplished by proper choice of the moment of transfer of the LPS from a standby orbit to a working orbit. Due to the orbital motions of the Earth relative to the sun and moon α_s increases as time passes, whereas α_n for $i = 90^\circ$ remains unchanged. In order to ensure the required illumination

conditions as long as possible it is necessary that the difference $\Delta\alpha_{ns}$ correspond to the "morning" case, that is, be positive. In addition, it makes sense to change somewhat the LPS orbital angle of inclination i somewhat in order that due to precession the orbital node be displaced away from the sun. Node precession is determined using the formula [4]

$$\Delta\alpha_n = \frac{3C_{20M}(R_M/a)^2\sqrt{\mu}}{2(1-e)^{3/2}a\sqrt{a}} \cos i(t-t_0), \quad (5)$$

$$\pi = \pi$$

where $C_{20M} = -0.206 \times 10^{-3}$ is the zonal harmonic in expansion of the force function of lunar attraction; $R_M = 1,738$ km is the mean radius of the moon; $\mu = 4,902.90$ km³/s² is the lunar gravitational parameter.

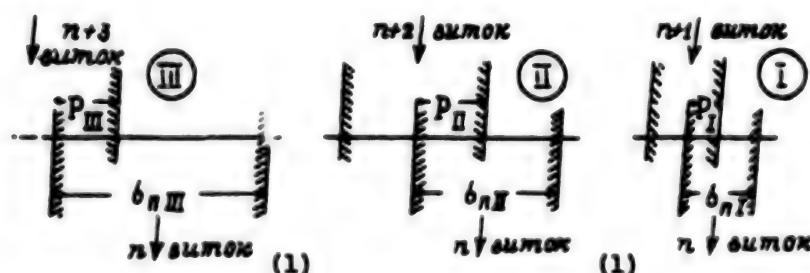


Fig. 1. Geometry of coverage of lunar equator by satellite transits as function of spacecraft altitude, scanning swaths and end laps.

1. Satellite transit

It follows from (5) that $\Delta\alpha_n > 0$ when $\cos i < 0$, that is, when $90^\circ < i < 180^\circ$. In order to retain the possibility of observing the pole from orbit it is admissible that the camera axis be deflected from the local vertical in a range 5° , that is, the status of the polar satellite will be conserved if $i = 95^\circ$.

The LPS orbit semiaxis major a entering into (5) is the most significant parameter determining the geometry of coverage of the lunar surface by topographic camera scanning swaths. The change ΔL_n of the selenographic longitude of the LPS orbit ascending node during a satellite transit (transit interval) is governed by two effects: by the precession $\Delta\alpha_{ns}$ during the LPS revolution period $T = t - t_0$ and the displacement of the node during the time T due to lunar rotation, that is,

$$\Delta L_n = \Delta\alpha_n - \omega_M T, \quad (6)$$

where $\omega_M = 0.2661699489 \times 10^{-3}$ rad/s is the angular velocity of lunar rotation;

$$T = 2\pi a\sqrt{a}/\sqrt{\mu}$$

is the period of LPS revolution.

Using (5) and (6) and varying the a parameter, it is possible to obtain different $\Delta L_n(a)$. However, for the considered problems there is interest only in those

$\Delta L_{11}(a)$ which are found in a definite relation to the width of the topographic videocamera scanning swath

$$b_s = 2 \left[\arcsin \left(\frac{R_n + H}{R_n} \sin \left(\arctg \frac{l}{2f} \right) \right) - \arctg \frac{l}{2f} \right] \cdot \pi = \pi \quad (7)$$

where l is the length of the frame edge; f is the videocamera focal length; H is LPS flight altitude.

Figure 1 shows the geometry of coverage of the selenoequator by satellite transits as a function of the altitude of the circular orbit $H_{\text{trans}} = a - R_{\text{moon}}$. For a camera with the parameters $l = 180$ mm, $f = 400$ mm the figure also shows the scanning swaths (7) and their end laps. Table 1 gives the periods of revolution T , the number of rotations per terrestrial day and interval of satellite transit ΔL_{11} . If the survey scale is limited to not less than 1:800,000 and a minimum side lap P , as follows from Fig. 1 and Table 1 the optimum orbit (in the sense of coverage geometry) will be an orbit with an altitude $H_{\text{trans}} = 300$ km, $a = 2,038$ km.

In Fig. 2, in a projection onto a selenocentric celestial sphere with the radius R_m , are plotted a spot of illumination of the moon by the sun with isolines of angles of equal solar elevation γ_s and 10-day traces of the LPS orbit showing the relative change in the positions of the orbital traces in the solar spot as a function of time. The initial position of the ascending orbital node relative to the sun, that is, the positive ("morning") difference lygDla_{11} at the initial moment was selected under the condition that at the point of the trace $\delta_1 = 40^\circ$ the solar angle of elevation is $\gamma_s = 30^\circ$. In Fig. 2 it is possible to trace the change in illumination conditions both along the flight trajectory and as a function of the change in the difference of the selenocentric right ascensions of the ascending node of the LPS and the sun. The convergence of the node and sun after 10 days is about 9° , that is, $\Delta \alpha_{11}$ during each 10 days of flight changes by about 9° .

It also is of interest to ascertain the required number of days for continuous mapping of the moon from the selected orbit by a topographic videocamera ($f = 400$ m, $l = 180$ mm). Figure 1 and Table 1 show that when working with a side lap of 23 percent the program for camera activation on the ascending revolution must be

structured in such a way that a survey is made after two transits on the third, that is, on the $n+3$, $n+6$, etc. transits. The displacement of the survey transits over the physical surface of the moon due to its rotation and precession of the orbital node using formulas (5) and (6) even in this case is $\Delta L_{11} = -3.9^\circ$.

The time between survey transits is 0.2875^d ($24,840^s = 6.9^h$). Proceeding on the basis of ΔL_{11} it is necessary to have 92 such transits in order to cover the selenoequator completely by scanning swaths with an overlap 23 percent. Hence the required number of days for a continuous lunar survey is 26.45^d . During this time the difference $\Delta \alpha_{11}$ changes by -23.8° . In the middle of the survey period it is desirable that $\Delta \alpha_{11} = 0^\circ$. Then it is necessary to make the initial $\Delta \alpha_{11}$ equal to $+11.9^\circ$. Figure 2 shows the initial and final positions of the survey transits in the solar spot.

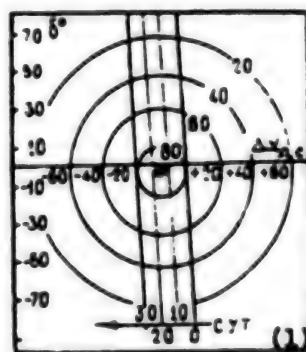


Fig. 2. Relative change in positions of traces of LPS orbit in solar spot on the moon as a function of time.

1. Days

Thus, a LPS orbit with the following parameters was selected for numerical modeling: — circular orbit ($e = 0$, $\omega = 0$, $a = 2,038$ km, $H = 300$ km); — inclination angle $i = 95^\circ$; — initial difference $\Delta \alpha_{11}$ of the selenocentric right ascensions of the ascending orbital node and the sun $+11.9^\circ$, that is $\alpha_{11} = \alpha_s + 11.9^\circ$; — the initial time τ of transit of the node is equal to the time during which α_s is computed.

For a comparative assessment of different sources of navigational information when determining the vector P^* a computer was used in making experiments simulating the real processes of navigational determinations

of the orbit and orientation of the LPS and in computing the selenocentric coordinate vectors R_T^* of the observed points. The referencing efficiency criterion used was the Euclidean norms of the traces of the covariation matrices K_{RT} of the errors of the vectors R_T^*

$$\sigma_{RT} = (\sigma_x + \sigma_y + \sigma_z)^{1/2},$$

where $\sigma_x, \sigma_y, \sigma_z$ are the dispersions of the errors of the components of the vectors R_T^* standing on the diagonal of the matrix K_{RT} , determined from expression (3).

A LPS orbit, selected by the method described above, was adopted as the reference orbit for all experiments, whereas the orbital orientation mode in which the +z axis of the topographic camera was directed along the LPS radius-vector, the +x axis was directed along the transversal in the direction of motion and the +y axis was directed along the vector of the kinetic moment was used as the nominal mode of LPS orientation. Coaxially with the topographic camera system there also is the coordinate system of the sidereal camera, but their optical axes are directed in opposite directions (-z and +z respectively).

A system of first-order nonlinear differential equations [2] was used for predicting the orbital motion of the LPS relative to the physical surface of the moon.

$$\begin{aligned} \dot{\bar{R}}_j &= \bar{V}_j; \\ \dot{\bar{V}}_j &= \frac{-\mu \bar{R}_j}{R_j^3} + \bar{g}_{j, \lambda, c} - 2(\bar{\omega}_\lambda \times \bar{V}_j) - \\ &\quad - \bar{\omega}_\lambda \times (\bar{\omega}_\lambda \times \bar{R}_j) + \bar{F}_v, \end{aligned} \quad (8)$$

where $g_{j, \lambda, c}^*$ is the vector of the total perturbations from the acentrality of the lunar gravitational field and the attraction of the Earth and sun; ω_λ^* is the vector of angular velocity of the moon; F_v^* is the random vector of unsimulated accelerations with the mathematical expectation $E[y^*]_{v_1=0}$ and the stipulated covariation matrix

$$K_{Fv} = E\{\bar{F}_v \bar{F}_v^T\}$$

Since the components of the vectors R_j^*, V_j^* are determined on the basis of trajectory measurements, they are known with errors. Accordingly, it also is necessary to predict the covariation matrix of errors of the vectors R_j^* along the trajectory. We introduce the LPS vector

$$\bar{q}_j^T = [\bar{R}_j^T, \bar{V}_j^T]$$

and its covariation matrix of errors K_{qj} . Then, in accordance with the linear theory of stochastic processes [5], the covariation matrix K_{qj} satisfies the Riccati linear differential equation

$$\dot{K}_{qj} = G_{qj}^T K_{qj} + (G_{qj}^T K_{qj})^T + K_{Fv} \quad (9)$$

where G_{qj} is the gradient matrix of the right-hand sides of equations (8) for the q_j^* components. This equation also was used in the simulation for predicting K_{qj} along the orbit.

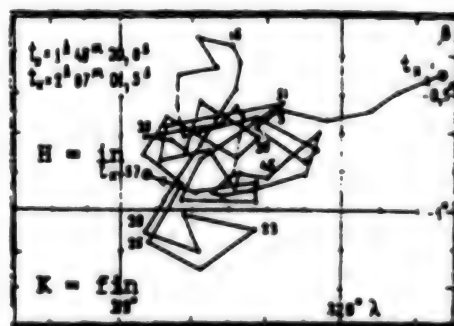


Fig. 3. Trace of optical axis of Zond-8 spacecraft camera on celestial sphere in inertial orientation mode during lunar survey.

The LPS phase vector q^* , and the covariation matrix K_{q^*} at the time of measurements are evaluated using a Kalman filter [5] employing the following algorithm

$$\begin{aligned} (G_s^T \bar{K}_{q^*} G_s + \bar{K}_d) W &= I; U = \hat{K}_s^T G_s W; \\ \hat{q}_s^* &= \bar{q}^* + U \left[(\bar{d} - d) - G_s^T (\bar{q}_s^* - \hat{q}_s^*) \right]; (10) \\ \hat{K}_{q^*} &= (I - U G_s^T) \hat{K}_{q^*} (I - U G_s^T)^T + U \bar{K}_d U^T, \end{aligned}$$

where G_s is the gradient matrix of the measured functions of the components of the phase vector q^* ; $K^{***}_{q^*}$ is the covariation matrix of errors of the vector $q^{**}_{q^*}$, predicted on the basis of equations (9) at the time of measurements; $K^{****}_{q^*}$ is the covariation matrix of the measurement errors; $q^{**}_{q^*}$ is the LPS phase vector predicted using equations (8) at the time of measurements; $q^{**}_{q^*}$ is the evaluation of the LPS phase vector obtained after processing of the measurements; d^{**} is the vector sample of measurements; $K^{****}_{d^{**}}$ is the covariation matrix of errors of the vector $q^{**}_{q^*}$, obtained after processing of measurements; d^* is the computed value of the vector sample of measurements; $q^{**}_{q^*}$ is the value of the vector $q^{**}_{q^*}$ when performing an iteration with the number v ; I is a unit matrix.

Two approaches were used in simulating the process of determining LPS orientation.

In the first it was assumed that the LPS is in an orbital orientation mode, supported by gyroscopic systems within the limits of the accuracy level admissible for them. An analysis of operation of actual orientation systems in such a mode shows that the deviations of the spacecraft axes from a stipulated position within the limits of the threshold of response of the gyroscopes are unpredictable.

The space vehicle control system maintains a stipulated orientation in a pulsed mode and the motion of the optical axis of the camera resembles Brownian motion (Fig. 3) [2, 7, 8]. Accordingly, in this study when using the first approach the orbital orientation mode is simulated by the uniform rotation of the LPS relative to the y-axis in such a way that the -z axis traces the lunar center of mass. This rotation is perturbed by random (in the form of white noise) moments relative to each axis.

In the second approach the model of LPS rotation is not stipulated and the actual orientation at the time of the experiment is determined from sidereal camera data. The measurement information is formed from star images determined in the camera coordinate system, x , y and the corresponding equatorial coordinates α^{****} , δ^{****} of stars selected from the onboard computer

catalogue. In this case the following iteration algorithm [1] was used for determining the LPS orientation parameters λ^* and covariation matrices K_{λ^*} of their errors:

$$\begin{aligned} \bar{\Delta \lambda} &= \bar{\lambda}_i - \hat{\lambda}_i; \bar{\Delta d} = \bar{d} - \hat{d}; \\ c &= K_{\lambda^*} A^T; D = \bar{K}_{d^{**}} B^T; H = I_n \\ S &= B D + A c; \bar{b} = -(\bar{F} + A \bar{\Delta \lambda} + B \bar{\Delta d}); (11) \\ S \bar{L} &= \bar{b}; \\ \bar{\delta \lambda} &= c \bar{L} + \bar{\Delta \lambda}; \bar{\delta d} = D \bar{L} + \bar{\Delta d}; \\ \hat{\lambda}_i &= \hat{\lambda}_i + \bar{\delta \lambda}; \\ \hat{K}_{\lambda^*} &= K_{\lambda^*} - c S^{-1} c^T, \end{aligned}$$

where λ^{**} are the a priori orientation parameters; λ^{*}_{01} , d^{**}_{01} is the vector sample of the measurements;

$$\bar{d}^T = \{x_i, y_i, x_i^*, y_i^*, z_i^*\}$$

x^{****}_i, y^{****}_i are the coordinates of the image of the i -th star, measured in the instrument coordinate system;

$$x_i^*, y_i^*, z_i^*$$

are the components of the unit vector of the star from the catalogue corresponding to it; d^* is the vector of the computed measurement values; $K^{****}_{\lambda^*}$ is the a priori covariation matrix of errors λ^{**} ; A is a gradient matrix consisting of the partial derivatives of the limitations F^* for the λ^* components; $K^{****}_{d^{**}}$ is the covariation matrix of measurement errors; B is a gradient matrix consisting of the partial derivatives of the limitations F^* for the d^* components; F^* is a vector function of the limitations.

In this problem for the i -th star the limitations are written in the form

$$\bar{F}_i = \bar{R}_i - K_{\lambda^*} M_{\lambda^*} (\bar{\lambda}) \bar{r}_{c_{q^*}} = \text{inst in}$$

where

$$(\hat{R}_i)^T = [X_i^*, Y_i^*, Z_i^*]; \hat{r}_i = [x_i, y_i, z_i]$$

K_i is a proportionality factor; $\lambda^{**}_{i\alpha}$, $K^{**}_{i\alpha\alpha}$ is the sought-for vector of the orientation parameters and the covariation matrix of its errors.

The evaluations $\lambda^{**}_{i\alpha}$ of the LPS orientation parameters computed using algorithm (11) describe its orientation in the star catalogue system, that is, in the geoequatorial system of the means of the equator and equinox of the epoch J 2000.0. However, for their use in the intersection formulas (1) they must describe LPS orientation in a system rigorously referenced to the moon. The parameters $\lambda^{**}_{i\alpha}$ and the matrix $K^{**}_{i\alpha\alpha}$ are scaled using the algorithm:

the $\lambda^{**}_{i\alpha}$ parameters are used at the measurement time t in forming the matrix $M_{i\alpha\alpha}(t, \lambda^{**}_{i\alpha})$ of the "instrument - inertial" conversion;

then the following are computed at the time t : $M(T_0, t)$ is the matrix for precession from $T_0 = J 2000.0$ to t and $M_e(t)$ is the "equator-ecliptic" conversion matrix [3]; $M_m(t)$ is the "ecliptic-system rigorously coupled to the moon" conversion matrix [10];

the "instrument-rigorously coupled to the moon" conversion matrix is computed at the moment in time t

$$M(t) = M_m(t) M_e(t) M(T_0, t) M_{i\alpha\alpha}(t, \lambda^{**}_{i\alpha}); \quad (12)$$

the sought-for parameters $\lambda^*_{i\alpha}$ are computed using the $M_{i\alpha\alpha}(t)$ matrix;

the sought-for parameters λ^* are computed using the $M(t)$ matrix.

In a general case the process described above can be represented in the form

$$\hat{r} = \hat{F}_i(\hat{\lambda}). \quad (13)$$

Then in a linear approximation

$$\hat{R}_i = G_{i\alpha}^T K_{i\alpha\alpha} G_{i\alpha}, \quad (14)$$

where $G_{i\alpha}$ is a gradient matrix containing the partial derivatives of the vector function $F^*_{i\alpha}$ for the components λ^* and the parameters of physical libration of the moon τ, σ, ρ . This matrix is computed using the central finite-difference approximations of each derivative entering into it; $K^{**}_{i\alpha\alpha}$ is the covariation matrix of errors of the parameters $\lambda^{**}_{i\alpha}$ and the parameters τ, σ, ρ , which is stipulated in the form

$$\hat{K}_{i\alpha\alpha} = \begin{bmatrix} \hat{K}_{i\alpha\alpha} & 0 \\ 0 & K_{\tau\sigma\rho} \end{bmatrix}.$$

The submatrix $K_{i\alpha\alpha}$ is determined on the basis of studies of the accuracy of the libration models used at the present time [6].

In computer simulation of the process of coordinate-time referencing of the results of studies from an LPS orbit the makeup and program of navigational measurements were selected on the basis of the real conditions for their application and were varied from experiment to experiment in the following way.

Experiment R + G. The orbit is determined only from surface radiotechnical (R) measurements once at 12^h. Orientation data are received by telemetry from gyroscopic systems at any moment in time during operation of the onboard scientific instruments.

Experiment R + S. The orbit is determined the same as in the preceding case. Orientation by the stars (S) is carried out at any moment in time.

Experiment R + T + S. The orbit is determined from surface radiotechnical measurements once at 12^h and from photogrammetric (T) measurements of onboard videomages of the lunar surface on each survey transit, that is, once at 6^h. The orientation is determined from the stars for any moment in time.

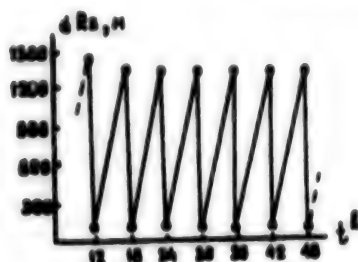


Fig. 4. Graph of "prediction-evaluation" process for numerical experiment R + T + S when predicting LPS orbit in interval 2 days.

The software which we developed for computer-aided simulation of the navigational referencing process allows variation of virtually any parameters on which this process is functionally dependent. However, in this case the referencing accuracy which can be attained when operating existing equipment is of interest. This also determined the makeup of the parameters adopted as the initial parameters when making the experiments:

topographic videocamera: focal length $f = 400$ mm, length of frame edge, $l = 180$ mm; star camera: $f_s = 70$ mm, $l = 10$ mm;

accuracy in measurements of the coordinates x, y in the videoimage field $\sigma_{xy} = 0.2 \times 10^{-1}$ mm;

the surface trajectory measurements were stipulated in the form of LPS phase vectors q^{**} , in a selenocentric dynamic system as the results of processing of sessions of direct measurements of range and radial velocity. The accuracy q^{**} , was stipulated on the basis of data from the Zond-8 spacecraft [2]: $\sigma_{Rz} = 500$ mm, $\sigma_{vz} = 0.1$ m/s;

the gyroscopic system formed the orbital orientation, the accuracy in maintaining which was determined in conformity to the data in Fig. 3: $\sigma_{\lambda} = 1,800''$;

orbital photogrammetric measurements. The trajectory was stipulated in the form of a series of coordinates of the LPS centers of mass at the times of survey in a dynamic selenocentric system. They were obtained as a result of construction of a photogrammetric network along the survey path, as described in [2]. Their accuracy was determined as $\sigma_{R, \text{phot}} = 150$ m.

The simulation process involves repeated repetition of the following steps in the time interval of active existence of the LPS (26^h).

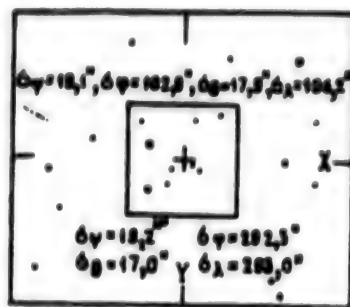


Fig. 5. Errors in angular orientation of star sensor for narrow- and wide-angle cameras.

The Cauchy problem is solved using the initial data

$$\hat{q}_s^+(t), \hat{K}_s^+(t)$$

for the differential equations (8) and (9) for the purpose of predicting q^{**} , K^{**} , at the moment t_{1+1} of the next measurement. As a result the predicted evaluations

$$\hat{q}_s^-(t_{1+1}), \hat{K}_s^-(t_{1+1})$$

are computed.

Depending on the type of trajectory measurements (surface radiotechnical or orbital photogrammetric) at the time t_{1+1} they are processed by a Kalman filter iteration algorithm (10). As a result the refined evaluations

$$\hat{q}_s^+(t_{1+1}), \hat{K}_s^+(t_{1+1})$$

are computed. These data occupy the corresponding places in the vector P^{**} (2) and the covariation matrix K^{**} , (3). Figure 4 shows a graph of the "prediction-evaluation" process in a steady state for the case R + T + S for determining the LPS orbit in an interval of 2 days. In a prediction interval 6 hours the error in LPS position attains 1,300 m, but after determining the orbit at the beginning of the survey half-transit it is about 80 m. Figure 4 shows that within the limits of a working half-transit (1 hour) the prediction error is about 217 m.

Simultaneously at the moment in time t_{i+1} , an evaluation is made of the orientation parameters λ^* . This evaluation is generated by a random process of a stipulated intensity if use is made of data from gyroscopic systems or is computed using data from x, y measurements of star images.

In any case the evaluation algorithm (11)-(14) is used for this purpose. As a result, the evaluations

$$\hat{I}^+(t_{i+1}), \hat{R}_1^+(t_{i+1})$$

are computed at the time t_{i+1} . These are entered into the vector P^{**} and the matrix K^{***} . Figure 5 shows the field of view of the star videoinstrument typical for this case and the errors in determining LPS orientation obtained from measurements of the coordinates of star images.

Such images for each moment of observation are formed using data from the star computer catalogue and the parameters of the computer videoinstrument. The size of the field of view changes, depending on the length of the frame edge. Figure 5 shows narrow- and wide-angle fields. In both cases the greatest error is for the angle ϕ of turning of the image about the optical axis. It is virtually an order of magnitude greater than for the

other angles and is decisive when assessing the accuracy in LPS orientation. It also is interesting to note that the errors in the angles ψ and θ are in actuality not dependent on the size of the frame within the limits of the stipulated variations.

Uniformly positioned points are selected in the zone of overlap of topographic camera images registered at the times t_i, t_{i+1} . The coordinate vectors R_T^* of the observed points and the covariation matrices K_{RT} of their errors are computed for each of these points using the algorithm (1) and employing evaluations of the position

$$\hat{R}_T^+(t_i), \hat{R}_M(t_i), \hat{R}_T^+(t_{i+1}), \hat{R}_M^+(t_{i+1})$$

and the orientation

$$\hat{I}_T(t_i), \hat{R}_{1T}(t_i), \hat{I}_T^+(t_{i+1}), \hat{R}_{1T}^+(t_{i+1}),$$

positioned in the vector $P^{**}_s(t_i, t_{i+1})$ and the matrix K^{***}_s . The norms of the traces of these matrices σ_{RT} characterize the accuracy in referencing of the results of operation of the onboard instruments at the times t_i, t_{i+1} to the system rigorously coupled to the moon.

Table 2

Time, hours	Error in determining position, orientation and referencing in experiment								
	R + G;			R + S;			R + T + S		
	σ_{RS}, m	$\sigma_{IS}, ^\circ$	σ_{RT}, m	σ_{RS}, m	$\sigma_{IS}, ^\circ$	σ_{RT}, m	σ_{RS}, m	$\sigma_{IS}, ^\circ$	σ_{RT}, m
6							85	99	266
12	150	1804	1240	150	211	424	79	47	242
-									
-									
-									
30							82	54	254
36	167	1802	2195	167	274	612	85	116	328
-									
-									
-									

Time, hours	Error in determining position, orientation and referencing in experiment								
	R + G;			R + S;			R + T + S		
	σ_{RS} m	σ_{AS}	σ_{RT} m	σ_{RS} m	σ_{AS}	σ_{RT} m	σ_{RS} m	σ_{AS}	σ_{RT} m
54							77	101	255
60	150	1804	733	150	368	460	85	185	282
66							78	121	297
72	156	1802	1786	156	294	533	82	106	302
Mean			1398			492			273

In Table 2 we give the results of an evaluation of the accuracy in referencing obtained using numerical experiments on a computer. The greatest referencing accuracy $\sigma_{RT} = 273$ m can be attained if for determining the LPS orbit joint use is made of data from surface trajectory measurements and onboard surface videoimages, but for determining the actual LPS orientation — data from onboard videoinstruments containing images of sectors of the star sky (experiment R + T + S). In this case the referencing error is almost five times less than in determinations by the standard method (R + G).

There is still another possibility for increasing the accuracy of navigational referencing when using instruments with the adopted parameters. As was noted above, the worst accuracy in determining orientation is for the angle ϕ of turning of the star camera relative to the optical axis. If there are two star cameras mounted aboard the LPS at an angle about 90° the accuracy in determining the actual orientation increases substantially, which also results in an increase in referencing accuracy. Appropriate computations were made for confirming this point. They gave the following results: $\sigma_{RS} = 81$ m, $\sigma_{AS} = 13^\circ$, $\sigma_{RT} = 63$ m, that is, the accuracy increases by a factor of approximately 4 in comparison with the R + T + S method and by a factor of almost 20 relative to the standard R + G method.

The cited results show that for navigational referencing of experiments from a LPS orbit with the required accuracy it is necessary that it carry aboard instruments making it possible to refine the orbit from videoimages of the lunar surface and to determine the actual orientation from videoimages of sectors of the star sky. Depending on the purposes of the studies, in the operation of a LPS it is necessary to select the elements of the initial orbit and the required accuracy in navigational referencing. Precisely these data are the point of departure in a search for the optimum operating programs, makeup and parameters of onboard instrumentation which will ensure navigational referencing with the stipulated accuracy. In this case algorithms and modeling program

systems similar to those described in this study may be useful.

Bibliography

1. Aleksashin, Ye. P., A priori assessment of the accuracy in determining the orientation of a spacecraft from the stars, Tr. TsNIIGAiK (Transactions of the Central Scientific Research Institute of Geodesy, Aerial Mapping and Cartography), No 228, pp 39-64, 1981.
2. Aleksashin, Ye. P., Timofeyev, Yu. S. and Shirenin, A. M., Selenotsentricheskaya sistema koordinat "Zond-8." Metody postroyeniya i katalog koordinat opornykh tochek. Sb. nauch. tr. (Zond-8 Selenocentric Coordinate System. Construction Methods and Catalogue of Coordinates of Reference Points. Collection of Scientific Papers), Moscow, Izd. TsNIIGAiK, 1989, 216 pages.
3. Astromicheskii yezhegodnik SSSR na 1990 g (USSR Astronomical Yearbook), Leningrad, Nauka, pp 663-668, 1988.
4. Proskurin, V. F. and Batrakov, Yu. V., First-order perturbations in motion of artificial satellites caused by the Earth's oblateness, in: Iskusstvennyye sputniki Zemli (Artificial Earth Satellites), Moscow, No 3, pp 32-38, 1959.
5. Seydzh, E. and Mels, Dzh., Teoriya otsenivaniya i yeye primeneniye v svyazi i upravleniye (Evaluation Theory and Its Application in Communications and Control), Moscow, Svyaz, 1976, 495 pages.
6. Shirenin, A. M., Comparison of models of physical libration of moon relative to problem of determining position of a spacecraft relative to the moon, in: Kinematika i fizika nebesnykh tel (Kinematics and Physics of Celestial Bodies), Vol 2, No 5, pp 68-73, 1986.
7. Aleksashin, E. P., Timofeev, Yu. S. and Shirenin, A. M., Zond-8 selenocentric coordinate system: design concepts and some results, in: 12-Soviet-American Microsymposium: Abstracts, Moscow, pp 10-11, 1990.

8. Aleksashin, E. P., Timofeev, Yu. S. and Shirenin, A. M., Analysis of navigational support accuracy of experiments by lunar polar satellite (LPS), in: 10-Russian-American Microsymposium: Abstracts, Moscow, pp 9-10, 1990.
9. Doyle, F. J., Ellassal, A. A. and Lucas, J. R., Selenocentric Geodetic Reference Systems, NOAA Tech. Rep., No 70, 977, 53 pages.
10. Eckhardt, D. H., Theory of the libration of the moon, Moon and Planets, Vol 25, No 1, pp 3-49, 1981.
11. Pieters, C. M., Recent Results from Clementine mission to the moon, in: 20-Russian-American Microsymposium: Abstracts, Moscow, p 2, 1990.

Modeling a Plasma-Tuned Satellite Antenna

964D0072A Nizhny Novgorod IZVESTIYA VYSSHIKH UCHEBNIKH ZAVEDENIY. RADIOFIZIKA in Russian Jun 95 Vol 37 No 6, pp 707-714

[Article by L.Ye. Kurina, G.A. Markov, and A.L. Umnov, Nizhny Novgorod State University; manuscript received 31 Dec 93; first paragraph is IZVESTIYA VYSSHIKH UCHEBNIKH ZAVEDENIY. RADIOFIZIKA abstract]

[FBIS Translated Text] Experimental and theoretical studies were conducted to examine the effect that a radio-frequency [RF] discharge excited in rarefied gas by the field of a radiating antenna has on the antenna's input and radiating characteristics. The conditions of the experiment were such that the inhomogeneity plasma was self-localized near the end of a dipole antenna and the parameters of plasma formation could be altered by varying the pressure of the gas, frequency of the signal, and power fed to the antenna. Excitation of an RF discharge results in modification of the antenna's near field and, consequently, in alteration of its electrodynamic characteristics.

It is a known fact that using a large-signal operating mode on satellites and descent vehicles may result in excitation of an RF discharge in the rarefied gas surrounding the antenna. Spontaneous development of a discharge (a plasma inhomogeneity) generally results in deterioration of the radiator's characteristics, detuning of the feeder section, and (consequently) partial or

even complete loss of radio communications. As recent studies have shown, however, a controlled RF discharge may be self-localized in the vicinity of the end of the dipole. The antenna's near field changes during the process of formation of the plasma inhomogeneity, which leads to redistribution of the antenna current and modification of the radiator's input impedance. This article is devoted to studying the possibility of using an end plasma load to control the characteristics of a thin antenna ($a \ll l_0 = \lambda$, where a and l_0 are the radius and length of the dipole and λ is the vacuum wavelength). The results of an experimental study and numerical modeling of such an antenna are presented in the article.

Figure 1 illustrates the laboratory model on which the experimental study was conducted. An asymmetric dipole located over a metallic shield was studied, and the end of the dipole was placed in an evacuable tank. The antenna was excited by an RF generator that created and maintained a plasma inhomogeneity around the end of the dipole. All of the antenna's parameters were measured by recording the distribution of current along the antenna. The mean square value of the antenna current was recorded by using an azimuthal magnetic field sensor. The sensor was based on an oscillatory circuit that had a microminiature incandescent-filament lamp connected to it. The light signal from the sensor, which was a function of the value of the antenna current, was fed along a lightguide to the photoreceiver unit and recorded by a voltmeter or oscillograph. The effect of the end plasma load was studied with a constant voltage at the RF generator's input. Figures 1 and 2 present the results of the experiment.

In the case of a short antenna ($l_0 \leq \lambda/4$ [Figure 1]), after the end plasma load had been formed, the antenna current increased as a result of resonance tuning. The maximum antenna current was shifted to the antenna's free end, which in turn increased its radiation resistance. Both the resonance tuning of the dipole and the increase in radiation resonance led to an increase in the power emitted by the antenna. In the case of a long antenna ($l_0 \geq \lambda$ [Figure 2]), both standing and traveling wave conditions occurred. In both cases, an increase in the power radiated by the antenna could be observed.

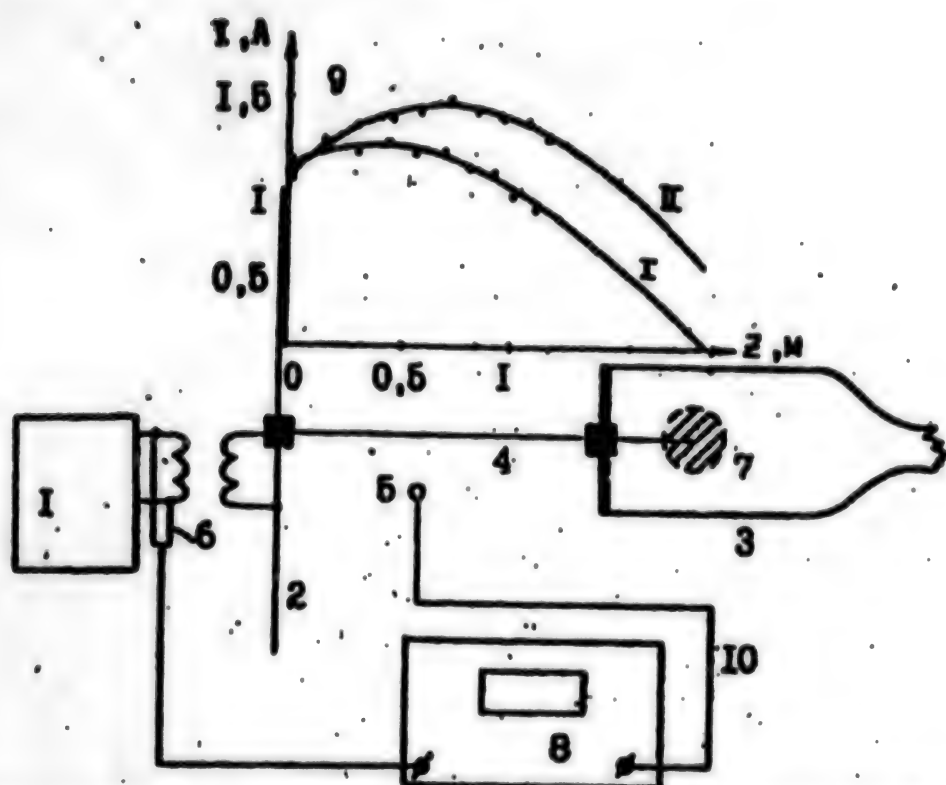


Figure 1. Diagram of the experiment: 1, radio-frequency generator; 2, metal screen; 3, glass discharge bulb; 4, antenna; 5, current sensor; 6, capacitance divider; 7, plasma inhomogeneity; 8, oscillograph; 9, distribution of current along the antenna (I, without a plasma load; II, with a plasma load; $f = 50$ MHz; $p = 3$ torr; —, theory; ---, experiment); 10, lightguide.

All of the principal distinctions of the operation of an antenna with a plasma load may be explained within the framework of the method of equivalent circuits. In accordance with the said method, an antenna with a plasma inhomogeneity is replaced by an equivalent long line that is loaded at its end with a complex impedance. The parameters of the substitution are as follows: l_0 is the wavelength equal to the length of the dipole's arm; $Z_w = 60[\ln(\lambda/2a) - 0.58]$ is the wave impedance of the line; $h = \beta - ia$ is the complex wave number; $\beta = 2\pi/\lambda$; $a = R_l/Z_w$; and R_l is the line's per-unit-length resistance as selected by proceeding from the requirement of equality of the radiation losses and losses in the line. The distribution of current in a line with an equivalent length and complex load Z_L at its end is given by the expression

$$|I| = |I_0| \left| 1 - \frac{Z_L/Z_w - 1}{Z_L/Z_w + 1} \exp[2ih(l_0 - z)] \right|,$$

where z is the longitudinal coordinate and I_0 is a constant. Figures 1 and 2 present the results obtained within the framework of this method. The values of Z_L were selected by proceeding from the requirement of the best consistency with the data obtained in experiments. Traveling wave conditions occur in the case where the impedance of the plasma load equals the antenna's wave impedance (Figure 2, curve 2). Standing wave conditions occur when the said impedances are unequal (Figure 3, curve 3). In both cases, the input impedance and radiation resistance of the antenna are modified.

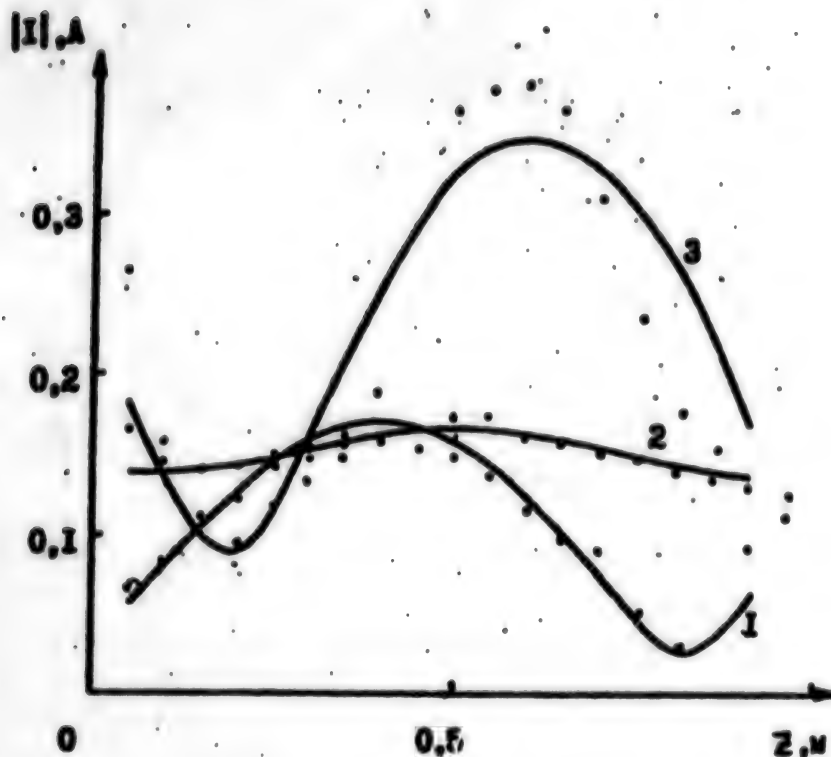


Figure 2. Distribution of current along the antenna ($l_0 = 1.5$ m; $f = 180$ MHz) outside the bulb. 1, without a plasma load; 2 and 3, with a plasma load; 2, $p = 0.5$ torr; 3, $p = 0.1$ torr; ..., experiment; —, theory.

A stricter analysis of the operation of a dipole antenna with a plasma load was performed within the framework of the integral equation method.³ An asymmetric thin dipole that has an end plasma load and is located over an infinite metallic plate and excited by the aperture of a coaxial cable (Figure 3) was examined.

The electrical field in the coaxial cable's aperture has the form

$$E_z = \frac{U}{r' \ln b/a},$$

where U is the voltage applied to the antenna, a and b are the radii of the coaxial cable's cylinders, and r' is the distance from its axis. Thanks to its symmetry, the model under consideration may be replaced by the model of a symmetric dipole located in a free space and excited by a ring of magnetic current with a density of

$$K_\phi = -\frac{2U}{r' \ln b/a}.$$

The requirement that the total electrical field on the antenna's axis equal zero may be used to obtain an integral equation relative to the antenna current. The total electrical field on the antenna's axis is created by the following sources: the annular magnetic current, the antenna current, and the current of the plasma space. The effect of a plasma load on the total electrical field may be viewed as the field of radiating polarization currents $j = i\omega(\epsilon\epsilon_0 - \epsilon_0)E$, where D is the total electrical field, $\epsilon =$

$$\epsilon = 1 - \frac{\omega_p^2}{\omega(\omega - i\nu)},$$

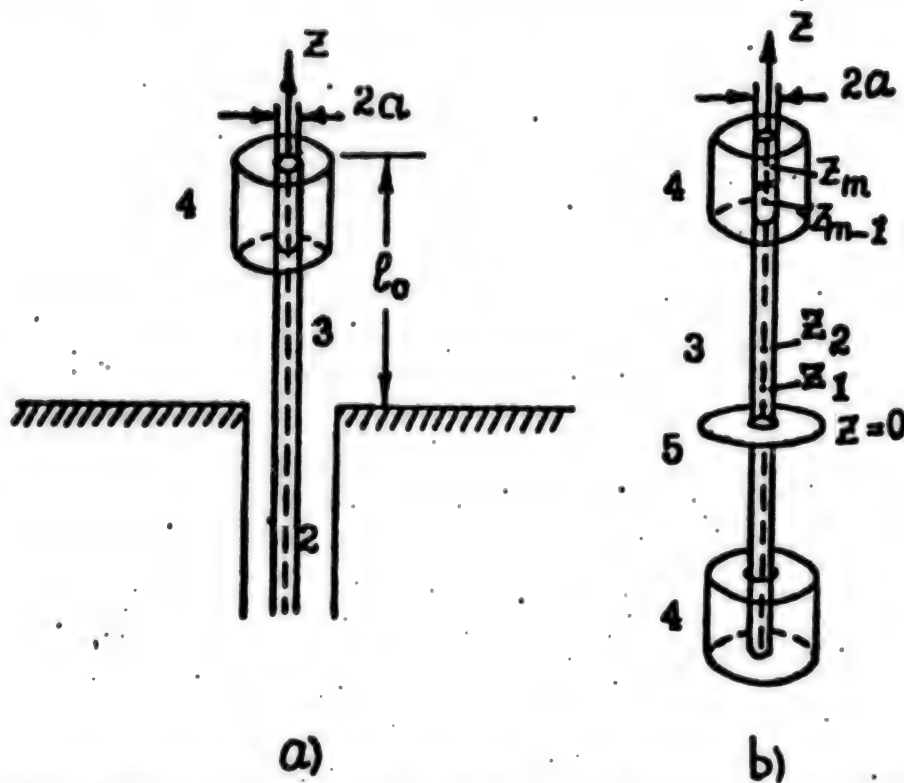


Figure 3. Model of the antennas: a, monopole excited by a coaxial antenna; b, dipole excited by an annular magnetic current. 1, metal plane; 2, coaxial line; 3, antenna arm; 4, plasma space; 5, annular magnetic current.

ω_p is the plasma frequency, ω is the frequency of the signal, and ν is the frequency of collisions of electrons with neutrals. In the case where the plasma layer is rather thin, the electrical field has only a radial component that may be expressed through the distribution of current along the antenna conductor:

$$E_r = \frac{1 - \epsilon}{\epsilon} \frac{dI}{dz} \frac{\rho_0}{2\pi\rho},$$

where I is the antenna current and ρ, z are cylindrical coordinates. The condition for the electrical field on the antenna axis makes it possible to write the following expression:

$$E_{ax}(z) + E_{px}(z) + E_{mx}(z) = 0, \quad (1)$$

where $E_{ax}(z)$, $E_{px}(z)$, and $E_{mx}(z)$ are the z components of the electrical fields excited by the antenna current, plasma current, and annular magnetic field, respectively. It is known that the electrical field may be represented as

$$\mathbf{E} = \frac{1}{i\omega\epsilon_0\mu_0} (\nabla \text{div} \mathbf{A} + k^2 \mathbf{A}) - \frac{1}{\epsilon_0} \text{grad} \mathbf{F},$$

where k is the wave number,

$$\mathbf{A} = \frac{\mu_0}{4\pi} \int_V \mathbf{j} \frac{e^{-ikr}}{r} dV, \quad \mathbf{F} = \frac{\epsilon_0}{4\pi} \int_V k \frac{e^{-ikr}}{r} dV,$$

are vector potentials, \mathbf{j} is the current source, and r is the distance between the point of the source and the

observation point. By using the latter two expressions, we can obtain the following:

$$E_m(z) = \frac{1}{4\pi i \omega \epsilon_0} \int_{-b}^b I(x') [(2r_1^2(1 + ikr_1) - a^2(3 + 3ikr_1 - k^2 r_1^2)) \frac{e^{-ikr_1}}{r_1^3} dx']$$

$$E_{np}(z) = \frac{1}{4\pi i \omega \epsilon_0} \int_{a_p}^{b_p} \int_{a_1}^{b_1} (z - x') \{k^2 r_2^2 - 3ikr_2 - 3\} \left\{ \frac{\omega_p^2 / \omega(\omega - i\nu)}{1 - \omega_p^2 / \omega(\omega - i\nu)} \cdot \frac{dI}{dx'} \right\} \frac{e^{-ikr_2}}{r_2^3} dx' dz'$$

$$E_m(z) = \frac{U}{\ln b/a} \left[\frac{e^{-ik\sqrt{a^2 + (z-x')^2}}}{\sqrt{a^2 + (z-x')^2}} - \frac{e^{-ik\sqrt{b^2 + (z-x')^2}}}{\sqrt{b^2 + (z-x')^2}} \right],$$

$$r_1 = \sqrt{a^2 + (z-x')^2},$$

$$r_2 = \sqrt{b^2 + (z-x')^2},$$

where a , and b , are the inner and outer radii of the plasma space and z_1 and z_2 are the longitudinal coordinates of the plasma's boundaries. Condition 1 thus yields an integral equation relative to the known current I . The method of moments, which has been described elsewhere,⁴ is used to obtain a numerical solution of the integral equation.

In accordance with that method, the antenna current is represented in the form

$$I = \sum_{n=1}^N I_n \cos \left\{ \frac{\pi(n-1)}{2l_0} x' \right\}. \quad (2)$$

To find I_n , we replace the strict condition (1) with the following less strict condition:

$$\sum_n E_m(z_m) + E_{np}(z_m) + E_m(z_m) = 0,$$

where E_m^* and E_{np}^* are components of the total electrical field linked to the n -th harmonic (2) and z_m represents the coordinates of a discrete set of points spaced evenly along the antenna axis. By taking this condition into consideration, we can obtain a system of linear algebraic equations equivalent to the integral equation system:

$$\begin{cases} x_{11}I_1 + \dots + x_{1n}I_n = V_1 \\ x_{21}I_1 + \dots + x_{2n}I_n = V_2 \\ \dots \\ x_{m1}I_1 + \dots + x_{mn}I_n = V_m, \end{cases}$$

where

$$x_{mn} = \frac{E_m^*(z_m) + E_{np}^*(z_m)}{I_n}, \quad V_m = -E_m(z_m).$$

This system was solved relative to I_n . The rapid convergence of the solution and small amount of required computer time were achieved by replacing series (2) when calculating E_{np} with the series

$$I' = \sum_{k=1}^M I_k(x')^2.$$

The values I_k were expressed through I_n by proceeding from the requirement of mean-square consistency of I and I' at those segments of the antenna covered with plasma. Thanks to the condition $l_p \ll l_0$ (l_p being the length of the plasma) M may be much lower than N , which speeds up the computation significantly.

Figure 4 presents selected results of the numerical modeling. The formation of a plasma load close to the end of the dipole results in an evening out of the distribution of current in the dipole and its resonance tuning.

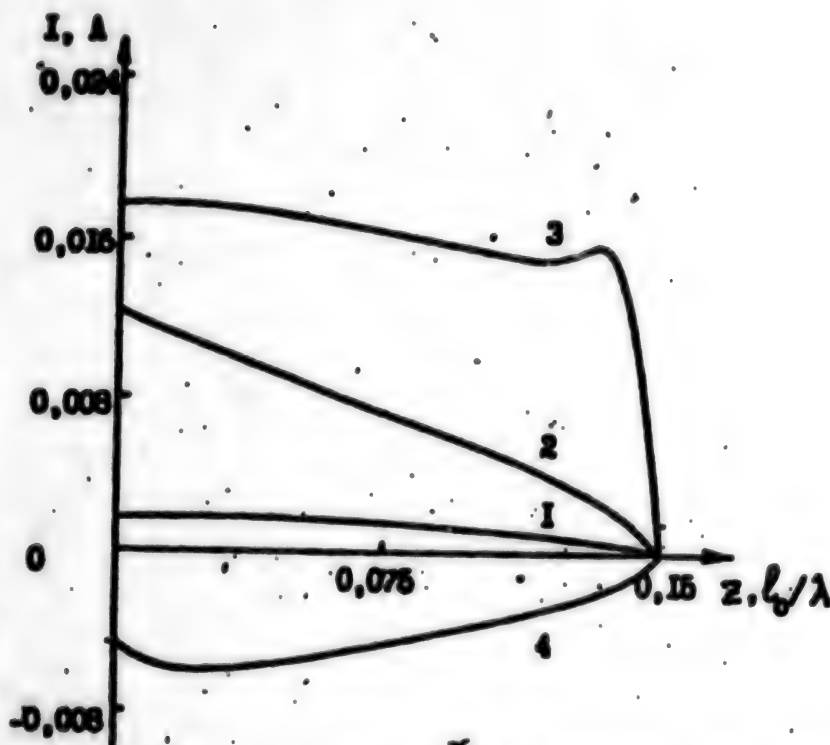


Figure 4. Current distribution along the antenna ($l/\lambda = 0.15$, $a/\lambda = 0.007$) obtained by numerical calculations; 1 and 2 are the real and imaginary parts of the antenna current without a plasma load, and 3 and 4 are the real and imaginary parts of the antenna current with a plasma load ($\omega/\omega = 1.5$, $\nu/\omega = 0.1$, with the length and radius of the plasma load equal to 0.02λ and 0.014λ , respectively, and with $U = 1$ V).

These factors in turn result in an increase in the power radiated by the antenna. A similar result was observed in the experiment (Figure 1). This confirms the adequacy of the description of the real physical situation.

The results of the experiments and theoretical examination make it possible to conclude that a plasma load that is located near an antenna's end and formed by the antenna's field expands the radiator's capability. This fact should be taken into consideration and may be used when formulating recommendations regarding the conduct of active ionospheric and space experiments.

This study was conducted with funding from the Russian Basic Research Fund, Grant No. 93-02-824.

References

1. S. Altshuler, USSR Patent 633.263, 1986.
2. A.V. Kim, G.A. Markov, A.L. Umnov, PISMA V ZhTF, Vol 15, No 5, 1989, p 34.
3. G.A. Markov, A.L. Umnov, PISMA V ZhTF, Vol 19, No 3, 1993, p 46.

4. G.A. Markov, A.L. Umnov, M.V. Likhodeyev, Fifteenth General Assembly of the URSI, Kyoto, Japan, Abstracts, 1993, p 423.

5. R. Mittra, ed., Computer Techniques for Electromagnetics, Pergamon Press, Oxford, 1973.

Comparative Analysis of Multiply Reusable Space Transport Systems

964D0097A Moscow PROBLEMY
MASHINOSTROYENIYA I NADEZHNOСТИ MASHIN
in Russian

No 4, Jul-Aug 95 (manuscript received 24 Mar 95) pp 3-12

[Article by G. Ye. Lozino-Lozinskiy and E. N. Dudar; the first paragraph is an abstract; UDC 621.01]

[FBIS Translated Text] The results of research carried out at the NPO [Scientific Production Association] Molniya are presented. Different concepts of multiply reusable space transport systems are examined and the requirements on such systems are formulated. In particular, three types of winged orbital aircraft

with liquid-propellant rocket engines are discussed: an aerial-launched orbital aircraft with a jettisonable external fuel tank (MAKS concept), an aerial-launched orbital aircraft with internal tanks (HOTOL-Interim concept) and a single-stage orbital aircraft with a vertical takeoff and horizontal landing (SSTO concept). The dependence of payload mass on orbital altitude and inclination is determined for the three studied orbital aircraft variants.

The NPO Molniya has studied possible ways to develop future multiply reusable space transport systems [1, 2]. Considerable efforts are being undertaken in the United States for studying the possibility of replacing the Space Shuttle at the beginning of the next century [3-6]. Despite some differences in the approach to this problem, it can be concluded that the development of single- and two-stage launch systems with promising ramjet engines with subsonic combustion and with supersonic combustion is a task for the remote future. Different variants of multiply reusable space transport systems using only jet engines are regarded as the most preferable variants of new launch systems since they make it possible to reduce the specific cost of launch of payloads into circumterrestrial orbit. It is possible to define two principal directions in research on multiply reusable space transport systems with rocket engines for a vertical launch from the earth and a horizontal launch from a subsonic mother aircraft.

Two-stage fully reusable systems of the Shuttle-II type require solutions of the complex problem of guaranteed engine-free return of the first stage to the launch site. It is possible that for this reason over the course of the last several years the United States has concentrated its research primarily on the concept of a single-stage carrier (SSTO) [3]. There is the widely known project for the Delta Clipper — a conical carrier for vertical takeoff and vertical rocket landing — developed by McDonnell Douglas, constituting one of the possible variants of construction of a single-stage carrier (Fig. 1,a). A winged single-stage carrier for vertical takeoff and horizontal landing is another direction in research on promising single-stage carriers [3] (Fig. 1,b).

The multipurpose aerospace system (MAKS), based on a heavy subsonic An-225 aircraft (horizontal takeoff and horizontal landing), will ensure a new quality due to the mobility of the launch. The MAKS system provides for three variants of the second stage positioned on top of the An-225 fuselage [7]. Variant 1 includes a manned or unmanned orbital aircraft outfitted with rocket engines and a jettisonable external fuel tank (Fig. 1,c). Variant 2 includes a launch unit, used a single time, atop which is placed a payload (space vehicle with a space tug). This is a cargo variant of the system, known as the MAKS-

T. Variant 3 is a multiply reusable orbital aircraft with liquid-propellant sustainer rocket engines and internal fuel tanks. Variants 1 and 2 may become the first stage in developing a highly efficient aerospace launch system because both these variants are based on actually existing technologies. As a result, in the first stage of construction of the aerospace system the technical risk is reduced and the time and cost of designing and producing system components are reduced. Variant 3 requires the perfecting of new technologies related to the problem of integration of multiply reusable heat shielding, structure and cryogenic insulation. This variant is regarded as the second stage in a multipurpose aerospace system. The technical risk in the second stage must be reduced by use of the experience accumulated in the first stage. This variant also is known under the name An-224/HOTOL-Interim (Fig. 1,d). Some aspects of this concept were examined in the course of an international investigation which was carried out by the organizations British Aerospace (Great Britain), NPO Molniya, Central Aerohydrodynamics Institute, Central Institute of Aviation Engine Building (Russia) and ANTK Antonov (Ukraine).

The principal results given in this article relate to investigations of a winged single-stage carrier with a vertical takeoff and a horizontal landing (SSTO concept), variants 1 and 2 (MAKS concept) and variant 3 (HOTOL-Interim concept). The launch characteristics of all variants of multiply reusable space transport systems are improved in the case of use of the three-component liquid-propellant rocket engine RD-701, developed at the NPO Energomash (Russia). It provides for the consumption of three fuel components in the first mode (kerosene, liquid hydrogen and liquid oxygen) and two components in the second mode (liquid hydrogen and liquid oxygen).

We will examine the requirements on multiply reusable space systems. One of the early systems was developed in 1965 by the Mikoyan Design Bureau. It was the two-stage Spiral aerospace system based on a supersonic mother aircraft. A great number of concepts for multiply reusable space systems are now being studied in different countries: NASP, Delta Clipper (United States), HOTOL (Great Britain), Zenger (Germany), MAKS (CIS), Ariane-5/Hermes (France), H2/Hope (Japan) and others. Such a diversity makes it necessary to formulate some fundamental requirements on multiply reusable launch systems. These requirements can be divided into three parts.

Mandatory requirements: a substantial decrease in the cost of launch and return of payloads; ecologic cleanliness; reliability; safety; high operational characteristics; maximum use of experience with aerospace technology.

Special requirements: routine servicing of orbital stations and other orbital objects; launch into equatorial orbits for countries located in the middle latitudes; possibility of use of the orbital stage as a satellite for the solution of various problems in orbit; realization of manned and unmanned variants; high landing accuracy.

General requirements: good prospects for improvement and development; use of individual system components for other branches of the economy; assurance of capability for handling not less than 70-80 percent of all future payloads.

existing subsonic mother aircraft it is necessary to use liquid hydrogen LH_2 and liquid oxygen LO_2 . A shortcoming related to the great volume of the hydrogen tank can be partially offset by the three-component sustainer engine. The RD-701 engine ensures a 40-percent decrease in the working mass of hydrogen fuel and has a low weight-to-thrust ratio about 0.009. In the first mode the RD-701 has a specific thrust in a vacuum of 415 s (with a 6-percent LH_2 content in the total per-second fuel consumption and 461 s in the second mode (with a 14-percent LH_2 content) with a thrust reduced to the level 40 percent. Despite some decrease in the mean specific thrust along the trajectory, the RD-701 ensures a substantial gain in MAKS system payload mass due to a reduction in the mass of the external fuel tank and orbital aircraft. The gain in payload mass in the manned MAKS variant (with a takeoff mass of the second stage 275 tons) is estimated at 1.8 tons in comparison with the two-component engine of the Space Shuttle sustainer type (SSME) with a specific thrust in a vacuum of 455 s.

The HOTOL-Interim variant is more sensitive to the use of three-component liquid-propellant engines: the gain in payload mass is about 3 tons in comparison with engines using LH_2/LO_2 components having a specific thrust in a vacuum of 463 s. It must be noted that the "kerosene, liquid oxygen" components do not ensure launch of any appreciable payload quantity in the HOTOL-Interim variant and in MAKS system variant 1. Thus, the RD-701 is the optimum choice for aerospace systems with restricted takeoff mass. Similar conclusions concerning the advantages of the RD-701 for the An-225/HOTOL-Interim system were drawn in [8].

Although the restriction on the takeoff mass in the concept of a single-stage carrier is not as rigorous as in an aerospace system, the use of three-component liquid-propellant engines gives a substantial effect. The RD-701 engine has a high thrust level during takeoff (first mode), which is very important for reducing the gravitational losses of characteristic velocity during a vertical launch. The second mode with a low thrust level makes it possible to dispense with strong throttling at the end of the trajectory. Thus, a high thrust during takeoff and a high specific thrust in the final part of the launch, being characteristic features of the sustainer engines of the first and second stages of an ordinary booster, are ensured in the very same three-component sustainer engine of a single-stage carrier.

For a vertically launched winged single-stage carrier with a fixed takeoff mass of 550 tons data were obtained characterizing the advantages of the three-component liquid-propellant RD-701 rocket engine in comparison

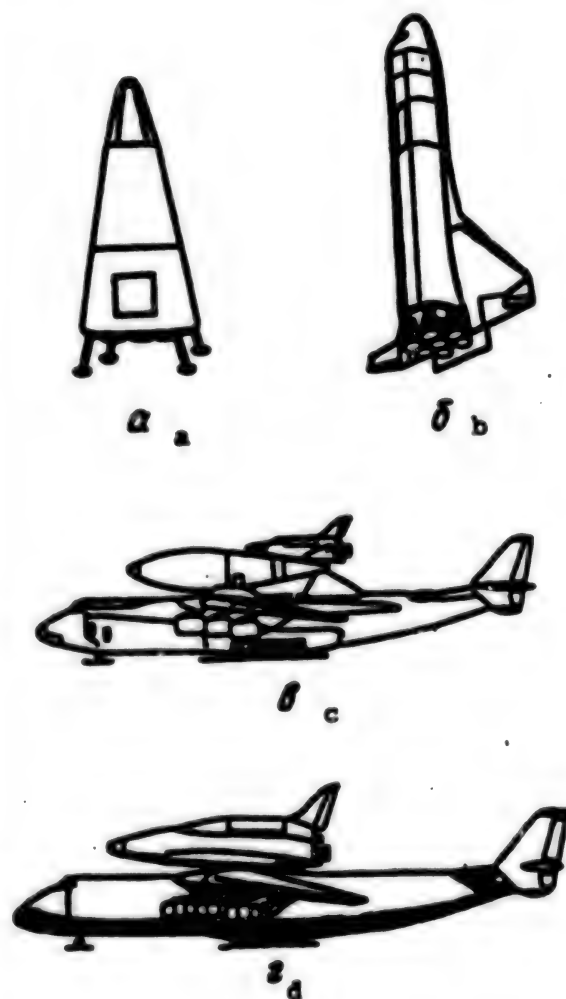


Fig. 1.

Three-component liquid-propellant jet engines: Research has shown that for the launch of payloads of considerable mass in the case of an aerial launch from

with the Space Shuttle sustainer engine (SSME); the mass launchable into an elliptical orbit is 70,720 and 73,460 kg; the SSTO dry mass is accordingly 50,880 and 61,980 kg and the payload mass in circular orbit is 10,400 and 1,940 kg. Calculations were made for the case of use of an extensible nozzle at altitudes greater than 9 km in each sustainer engine variant. Reference orbit: altitude 200 km, inclination 51°.

A considerable gain in payload mass (about 8.5 tons) is related to a decrease in SSTO dry mass by 18 percent. If a study is made of the problem with a fixed payload mass the effect in a decrease in SSTO dry mass will be more significant (according to [3], up to 22 percent).

The results give basis for assuming that the success of future multiply reusable space transport systems is related to the use of three-component engines and other key technologies. This conclusion can be applied to the single-stage vertically launched SSTO and to aerospace systems of the MAKS and An-225/HOTOL-Interim type.

Use of aerodynamic load-carrying properties for improving launch characteristics. The subsonic mother aircraft creates optimum initial conditions for launch of the second stage of the aerospace system as a result of performance of a prelaunch maneuver in the longitudinal plane. After separation the orbital aircraft performs flight with optimum longitudinal control, taking into account the influence of aerodynamic lift [9]. This part of the trajectory and launch can be called the aerodynamic turn. In contrast to aerospace systems, an ordinary booster does not use aerodynamic lift and executes a so-called gravitational turn. Nevertheless, if the single-

stage SSTO carrier is a multiply reusable winged vehicle, it can execute a gentle launch after a short vertical segment. In this case gravitational losses are reduced and the consumption of fuel necessary for launch of a single-stage carrier into circumterrestrial orbit is reduced.

Table 1 gives data on the influence of aerodynamic load-carrying properties on the launch characteristics of three variants of multiply reusable space transport systems (MSTS). Two possible launch methods are examined for a vertically launched single-stage carrier. The characteristics are given for a reference orbit with an inclination 50° and an altitude 200 km. The following annotations are used in Table 1: h_0 , V_0 , θ_0 , G_0 , altitude, velocity, trajectory angle and mass of the second stage of the aerospace system at the point of separation or SSTO at the point of launch from the Earth; ΔV_{gr} , ΔV_{aer} , ΔV_{com} , ΔV_{pr} , losses of characteristic velocity caused by gravitation, aerodynamic braking, presence of an angle between the thrust vector and the velocity vector and atmospheric pressure; V_{id} is the ideal characteristic velocity; G_{end} is the mass of the orbital aircraft at the point of sustainer engine shutdown; G_p is payload mass in a circular reference orbit.

It must be noted that the takeoff mass of the second stage of the MAKS and HOTOL-Interim variants was assumed equal to 275 tons. The orbital aircraft rocket engines are fired before separation and in the prelaunch maneuver segment of the An-225; the second MAKS stage consumes 5 tons of rocket fuel, but in the HOTOL variant — about 2 tons. Thus, at the separation point the G_0 values are 270 and 273 tons respectively.

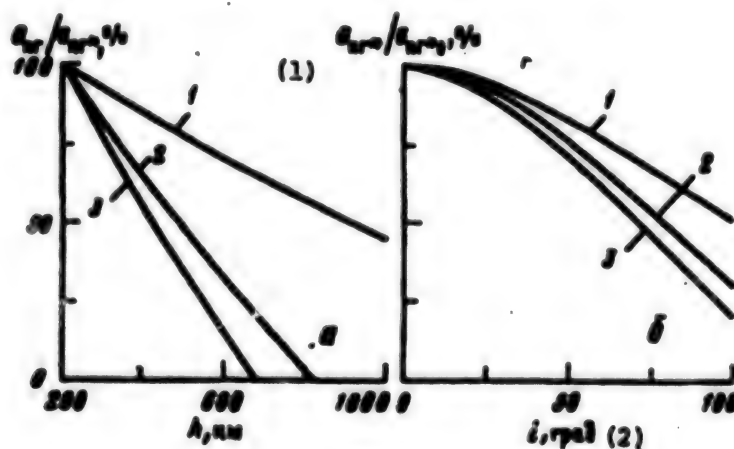


Fig. 2.

Key: 1. G_0 2. i , degrees

The results presented in Table 1 show the good contribution of the mother aircraft to launch energetics. However, the An-225 mother aircraft plays more than the role of a first stage. It is a moving launch platform making possible approach to the equatorial plane and considerable reduction of the fuel necessary for rocket-dynamic rotation of the orbital plane, for example, in

the case of launch of satellites into a geostationary orbit by means of the transport variant MAKS-T. High operating qualities are a second fundamental advantage of the aerospace system. The mobility of the launch from the mother aircraft makes it possible to minimize the total time expended on flight and docking with an orbital object.

Table 1

MSTS	MAKS	HOTOL	SSTO	
Initial conditions:				
h_0 , m	8,180	7,600	0	
V_0 , m/s	196	206	0	
θ_0 , degrees	36	24	90	
G_0 , tons	270	273	550	
Launch method	aerodynamic turn			gravitational turn
Velocity losses, m/s				
ΔV_{gr}	-700	-646	-979	-1224
ΔV_{un}	-312	-271	-267	-93
ΔV_{con}	-114	-87	-304	-286
ΔV_{pr}	-42	-45	-69	-62
V_{id} , m/s	8505	8419	8996	9070
G_{fu} , tons	37.9	38.7	68.7	67.7
G_{pl} , tons	8.4/9.5	5.4	8.5	7.5
Crew	2.0	unmanned		

The aerodynamic characteristics of the orbital aircraft exert a substantial influence on the launch trajectory and on the working fuel supply. The total mass put into an elliptical orbit is dependent on the aerodynamic quality [9]. As a result, the HOTOL-Interim variant has a higher launchable mass G_{un} , but the MAKS, due to the effect of the jettisonable fuel tank, ensures a higher maximum payload G_{pl} .

A vertically launched winged single-stage carrier has a possibility for improvement in launch characteristics by use of an aerodynamic turn. The gain in payload mass in this case is about 1 ton or 13 percent in the case of a stipulated takeoff mass of 550 tons.

Range of attainable orbital inclinations and altitudes. The relative payload mass in a circumterrestrial reference orbit is characterized by a ratio G_{pl}/G_{un} , where

G_{pl} , and G_{un} , respectively are the payload mass and the total mass of the orbital aircraft in a circular reference orbit with an altitude $h^* = 200$ km and an inclination $i = 51^\circ$ (the asterisk denotes parameters applying to the indicated reference orbit with an altitude 200 km, but with other altitudes the payload masses G_{pl} are denoted without an asterisk). The payload mass in higher orbits with altitudes $h > h^*$ is dependent on the dimensionless parameter G_{pl}/G_{un} , where G_{un} is the dry mass of the orbital aircraft, including the structure, fuel remnants in the orbital maneuvering engines and jet control system and crew. The values of the dimensional parameters G_{pl}/G_{un} and G_{fu}/G_{un} are 0.320 and 0.648 respectively for a manned orbital aircraft of the MAKS system with a crew of two persons, but for the unmanned HOTOL — 0.143 and 0.825 and for the SSTO — 0.112 and 0.856.

Table 2

MSTS	MAKS	HOTOL	SSTO
G_{μ} , kg	26,370	38,033	67,081
$G_{\mu 0}$, kg	8,440	5,440	7,540
$\mu \times 10^4$, km ⁻¹	7.975	17.846	22.786
$-v$, kg/km	6.730	9.706	17.119

Approximately $G_{\mu}/G_{\mu 0} = 1 - \epsilon - G_{\mu}/G_{\mu 0}$, where $\epsilon = \Delta V_{\text{orb}}/g_0 J_{\text{orb}}$; ΔV_{orb} is the characteristic velocity reserve expended on maneuvering in a circular reference orbit and on the braking impulse for descent from an altitude $h^* = 200$ km; $g_0 = 9.80665$ m/s²; $J_{\text{orb}} = 319$ s is the specific thrust of the orbital maneuvering engines; $\epsilon = 0.032$ is a dimensionless parameter which is identical for all orbital aircraft variants.

For the case of orbits with a great altitude $h > h^*$ it is possible to obtain a linear approximation for a payload mass $G_{\mu}/G_{\mu 0} = 1 - \epsilon - G_{\mu}/G_{\mu 0} - \beta \Delta h$, where $\Delta h = h - h^*$, $\beta = c/g_0 J_{\text{orb}}$, $c = \text{const}$. For all variants of orbital aircraft it can be assumed that $\beta = 0.0002552$ km⁻¹.

The change in the relative payload mass with altitude is $G_{\mu}/G_{\mu 0} = 1 - \mu \Delta h$, where $\mu = \beta/(G_{\mu}/G_{\mu 0})$. The gradient of change in dimensional values of payload mass relative to orbital altitude h is dependent on the parameters β and $G_{\mu 0}$: $v = \delta G_{\mu}/\delta h = -\beta G_{\mu 0}$.

Table 2 gives the values of the μ and v parameters characterizing the influence of orbital altitude on payload mass. These parameters were obtained using precise mathematical simulation.

Figure 2,a shows the precise dependencies of relative payload mass on orbital altitude obtained as a result of trajectory and weight calculations (1 — MAKS, 2 — HOTOL, 3 — SSTO).

Due to the jettisonable external fuel tank the MAKS orbital aircraft may attain circular orbital altitudes up to 1,500 km. The small maximum altitude in the SSTO variant is attributable to the greater fraction of structural mass in the total mass of an orbital aircraft launched into a low circumterrestrial orbit. Thus, the presence of

an external fuel tank, which is jettisoned into remote regions of the ocean, is a good solution for a first-stage aerospace system. The tank does not constitute any ecological danger and the range of working orbits is considerably expanded.

With a change in orbital inclination i from 0 to 100° the G_{μ} values are reduced for the variants: MAKS — from 10,066 to 5,339 kg, HOTOL — from 7,242 to 2,239 kg and SSTO — from 10,480 to 2,227 kg.

The dependencies of the relative payload mass $G_{\mu}/G_{\mu 0}$ on orbital inclination i are shown in Fig. 2,b (G_{μ} is the payload mass for a stipulated inclination i , whereas $G_{\mu 0}$ is the payload mass for an equatorial orbit with the same altitude 200 km).

An increase in inclination results in greater losses of payload mass in the SSTO variant due to a greater total mass of the orbital aircraft, launched into a low circumterrestrial orbit, and the small fraction of payload mass in the total launchable mass.

The transport variant of the MAKS-T aerospace system ensures delivery of a payload with a mass of 18 tons into a low circumterrestrial orbit with an inclination 51° and up to 20 tons into a low equatorial orbit. In the case of use of a space tug with cryogenic fuel components the MAKS-T will make it possible to put 5 tons of payload into a geostationary orbit.

Economic efficacy is a highly important criterion in a comparative analysis of different concepts of multiply reusable space transport systems. Expenditures on designing, production, testing and certification are the principal cost components.

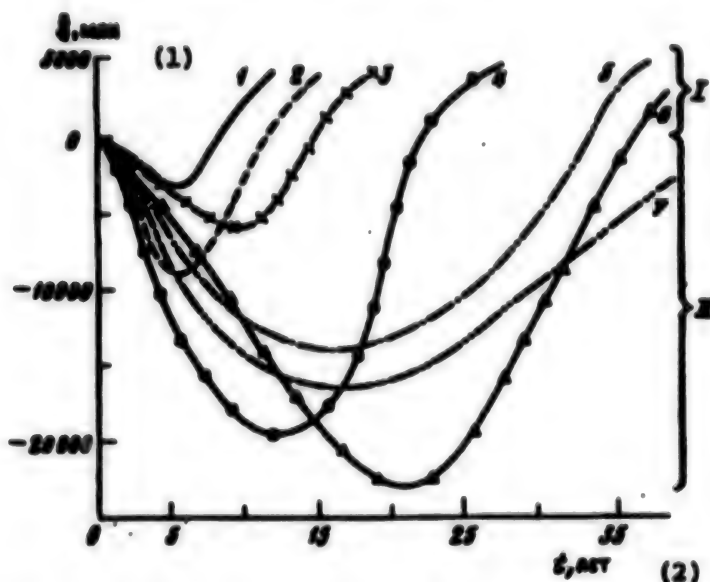


Fig. 3. 1) MAKS (Russia), 2) Delta Clipper (USA), 3) HOTOL-Interim (Great Britain), 4) Zenger (Germany), 5) SSTO (R) (United States), 6) NASP (United States), 7) TSTO (United States); I) decrease in specific cost of payload launch by a factor of 4, II) same by a factor of 2, t — number of years from onset of development work.

Key: 1) million, 2) t, years

The principal characteristics of projects for multiply reusable space launch systems developed in different countries are represented in Table 3. Figure 3 shows the dynamics of change in total expenditures and profit when constructing and using different multiply reusable space transport systems.

It can be concluded on the basis of data in [10] and research materials from the AO NIIEPU that the cost of development of multiply reusable space transport systems exceeds the construction cost by a factor of approximately 50-100. It must be noted that at the present time it is difficult to estimate the cost of construction of such a launch system as the NASP. The approximate estimates are about 50 billion dollars. Accordingly, 1 kg of NASP dry mass will cost approximately 500,000 dollars.

A two-stage horizontally launched system is most desirable in the case of additional use of an An-225 mother aircraft for other branches of the economy. There are good prospects for improving the launch characteristics and economic indices of the aerospace system due to future use of a superheavy mother aircraft

with a lift up to 400 tons. A design of such an aircraft, designated Hercules, has been developed. It has a triplane aerodynamic design in two fuselages [11].

A more detailed analysis of the cost must take a number of additional factors into account. The results make it possible to conclude that the MAKS pays for itself most rapidly. A project of the type An-225/HOTOL- Interim is the next best in this respect.

The development of single- and two-stage launch systems with promising ramjet engines with subsonic and supersonic combustion is a task for the more remote future. Different variants of multiply reusable space transport systems based solely on rocket engines are probable candidates for introduction as new space transport systems with a low specific cost of payload launch into circumterrestrial orbit.

The use of a three-component two-mode engine of the RD-701 type ensures a considerable gain in payload mass for different transport system variants. The most considerable decrease in dry mass when using the RD-701 is attained in the variant of a single-stage carrier.

Table 3

Project Parameters	MAKS (CIS)	MAKS-T (CIS)	An-225/ HOTOL (CIS-Gt. Britain)	Zenger (Germany)	NASP (USA)	Ariane-5 (France)	Delta Clipper (USA)
Launch weight, tons	630	630	630	366	180-230	620	460
Orbit (i, °/H, km)	51/200	51/200	51/200	28/200	28/400	28/460	90/400
Payload mass, tons	8.4-9.5	18	5.4	7.5	9-12	3	4.5
Crew, persons	2 or unmanned	-	-	4	2	3	2
% of total load quantity	71-75	92	50	32	70-73	25	60
Possibility of return to Earth	+	-	+	+	+	+	+
Cost of launch per payload kg, dollars	1,000	1,000	2,000	4,500	?	36,000	1,100
Parallax, km	2,000	2,000	2,000	2,000	?	0	0
Lateral range during descent, km	2,000	-	2,000	2,000	2,000	2,000	2,000

Multiply reusable two-stage vertical launch systems can fully ensure a great weight efficiency, but the construction of such systems is complicated by the problem of ensuring a guaranteed engine-free return of the first stage to the launch site. This variant requires additional research. A vertically launched single-stage carrier is simplest in operation. The launch characteristics of such a carrier can be improved by use of an aerodynamic turn.

The MAKS project is preferable for implementation in the immediate future with minimum expenditures of time and money. The An-225 mother aircraft is a moving launch platform which will make it possible to approach the equatorial plane and considerably reduce fuel expenditures on a rocket-dynamic rotation of the orbital plane, for example, in the case of launch of satellites into a geostationary orbit by means of the MAKS-T. A moving launch from an aircraft makes it possible to minimize the total time necessary for launch and docking with an orbital object. Due to the jettisonable external fuel tank the MAKS system has a minimum gradient of payload mass decrease relative to orbital altitude. This will make it possible for a manned orbital aircraft to attain a circular orbit altitude up to 1,500 km.

A fully multiply reusable variant of the An-225/HOTOL-Interim aerospace system requires use of new technologies.

An improvement in the launch characteristics and economic efficacy of the aerospace system is possible by future use of the superheavy Hercules mother aircraft with a lift up to 400 tons.

A multiply reusable aerospace system may become a real step along the path of next-generation multiply reusable launch systems.

Bibliography

1. Lozino-Lozinsky, G. E., Buran Development and Progress, 40th IAF Congress, Malaga, Spain, 1989.
2. Lozinsky, G. E., Skorodelov, V. A. and Plokhikh, V. P., International Reusable Aerospace System MAKS// AIAA/DGLR 5th Intern. Aerospace Planes and Hypersonic Technol. Conf., Munich, Germany, 30 Nov-3 Dec 1993.
3. Freeman, D. C., Stanley, D. O., Camarda, C. J., et al., Single Stage to Orbit — A Step Closer, 45th IAF Congress, Jerusalem, Israel, 1994.
4. Freeman, D. C., Wilhite, A. W. and Talay, T. A., Advanced Manned Launch System Study Status, IAF Paper 91-193, Oct. 1991.
5. Stanley, D. O., Talay, T. A., Lepsch, R. A., et al., Conceptual design of a fully reusable manned launch system, J. Spacecraft and Rockets, Vol 29, No 4, pp 529-537, 1992.

6. Stone, H. W. and Piland, W. M., An Advanced Manned Launch System Comparison, IAF Paper 92-221, Oct. 1989.
7. Lozino-Lozinsky, G. E., Dudar, E. N. and Plokhikh, V. P., Russian Sub-Orbital Commercial Passenger Transport System, SAE Paper. SAE Preprint Number 920aaa, 1992.
8. Parkinson, R. C. and Webb, E., AN-225/HOTOL//AIAA/DGLR, 5th Intern. Aerospace Planes and Hypersonic Technol. Conf., Munich, Germany, 30 Nov- 3 Dec 1993.
9. Filatev, A. S., The optimal space vehicle ascent using aerodynamic forces, Cosmic Res., Vol 29, No 2, 1991 (Consultants Bureau, N. Y.).
10. Access to Space Study, Summary Report, NASA, 1994.
11. Lozino-Lozinskiy, G. E., Triplane — a promising direction in development of aircraft design, Problemy mashinostroyeniye i nadezhnosti mashin (Problems in Machine Building and Reliability of Machines), No 3, pp 3-8, 1994.

Determining Structure of Meteor Streams From Radar Observations

964D0101A Moscow ASTRONOMICHSKIY VESTNIK

in Russian Vol 29 No 4, Jul-Aug 95 (manuscript received 17 Jun 94) pp 367-372

[Article by S. V. Kolomiyets and I. A. Milyutchenko, Kharkov State Technical University of Radio Engineering and Electronics, Kharkov, Ukraine; the first paragraph is an abstract; UDC 523.68]

[FBIS Translated Text] A method for determining the s parameter in the distribution of meteor bodies by mass and stream density is examined on the basis of the results of radar measurements of the number of meteors during the period of activity of meteor streams. The described method is used in analyzing data from radar observations of the meteor streams η -Aquadrids and Orionids at Kharkov in 1986. A value of the parameter $s = 1.65$ was determined for the dates of the maximum activity of both streams. The dependencies of the density of the stream of meteor bodies and the parameter s on solar longitude and the time of day when the stream is observed also were obtained. The mean density of the stream of meteor bodies with $M \geq 10^{-3}$ g for η -Aquadrids is $2.9 \times 10^{-11} \text{ m}^{-3} \text{ s}^{-1}$; for Orionids it is $2.5 \times 10^{-11} \text{ m}^{-3} \text{ s}^{-1}$.

In a study of the structure of meteor streams the problem always arises of separating a stream from the sporadic background. When making observations at Kharkov the registry is in the range of the faintest meteors 12^{m} .

14^{m} (the mean daily number of meteors is several tens of thousands) and the sporadic meteor background becomes very strong. Accordingly, in addition to a formal determination of the days of the stream and background, on the basis of data in the literature the background number of meteors N_{back} is determined by using data obtained on different days directly adjacent to days of stream activity and on more remote days (when such data are available).

When measurements are made of the number of radio meteors stream activity is manifested in the fact that there is a change in the shape of the diurnal curve of the number of meteors in comparison with the results of observations of sporadic meteors only. The time of visibility of the stream radiant is computed on the basis of the location of the observation point and the antenna directional diagram. The greatest difference of the $N(t)$ curve (N is the hourly number of registered meteors) for the dates of stream activity from the corresponding curves for the other cited dates should be observed precisely at these hours. The differences in the diurnal dependencies of the number of meteors for other time intervals characterize the range of random fluctuations of the sporadic background.

The mean number of sporadic meteors during the period of stream activity is determined separately for each hour using the formula $N_{\text{back}} = N_{\text{back } 1} + N_{\text{back } 2}/2$, where $N_{\text{back } 1}$ and $N_{\text{back } 2}$ are the hourly numbers of meteors on the days preceding the period of stream activity and on the days which follow respectively.

Specifically the dates of observations which can be adopted as background dates are established on the basis of an analysis of the diurnal curves of the number of meteors and the dispersion of the results obtained later.

The number of meteors of the observed stream is determined by subtracting the background number N_{back} for each hour from the hourly number N_{st} of meteors registered during the time of stream activity [sb is for the combination stream + background]. Negative N_{st} values have no physical sense and simply indicate random fluctuations in the number of meteors relative to the mean level, adopted as the background. The mean daily hourly number of faint meteors ($12^{\text{m}} - 14^{\text{m}}$) on days when a meteor stream occurs may almost not be discriminated against the sporadic background, in contrast to observations in the range $5^{\text{m}} - 7^{\text{m}}$.

The number of meteors was measured at Kharkov at 12 threshold levels differing from one another with respect to the amplitude of the registered signals by a factor of 1.6. The measurement data at the first, most sensitive registry level are usually not included in the processing because the influence of different kinds of interference on the measurement results is observed at this level.

The results of number measurements make it possible to determine the parameter k_1 of the distribution of radio meteors by amplitude and the parameter s of the distribution of meteor bodies by mass [2].

A theoretical formula for the distribution of the amplitudes of signals reflected from unsaturated trails was derived by T. Kaiser [8]. It was shown that in the case when the reflection occurs from the point of the ionization maximum and the maximum amplitude is proportional to the linear electron concentration, the distribution of signal amplitudes conforms to the Pareto law with a parameter related to s by the relation $s = c + 1$. This same law also is derived in a case when the reflecting points are uniformly distributed along the trail, but the shape of the ionization curve is not dependent on the mass and remains constant.

For assessing c it is customary to convert to an integral distribution of amplitudes. Then the curve constructed on a logarithmic scale approaches a straight line with a negative gradient.

$$k_1 = s - 1.$$

In this case the recorder is a statistical analyzer performing the quantization of amplitudes of the reflected signals and accumulating the numbers of events which exceed some threshold level. A k_1 assessment can be made by the least squares method or by a method which is based on the fact that with a changeover from the variable x to the new variable $y = \ln x$ the Pareto distribution is transformed into an exponential distribution. For such a distribution an assessment of the k_1 parameter is found using the maximum likelihood test:

$$k_1 = \left(\frac{1}{n} \sum_{i=1}^n \ln A \right)^{-1}.$$

This method is more convenient when automating measurements. When there is a detector with a logarithmic characteristic and a sufficiently broad dynamic range the problem of finding a k_1 assessment is essentially reduced in actuality to computation of the mean arithmetic value and is realized even without using a built-in computer operating in real time. For stream meteors the $K_{1,sw}$ parameter is determined for each hour using the formula [1]

$$K_{1,sw} = N_{sb} k_{1, sb} - N_{back} k_{1, back} / N_{sw}$$

where $k_{1, back}$ is an amplitude distribution parameter for sporadic meteors (background); $k_{1, sb}$ is this same parameter for the totality of stream and background meteors. This formula is a special case of the formula

$$N_0 k = \sum_{(i)} N_0 k_i.$$

The $k_{1, sb}$ and $k_{1, back}$ values are calculated using the formula

$$k_1 = \frac{\sum_{i=1}^n x_i y_i - \sum_{i=1}^n x_i \sum_{i=1}^n y_i}{\sum_{i=1}^n x_i^2 - \left(\sum_{i=1}^n x_i \right)^2 / n}, \quad (1)$$

where $y_i = \lg N_i$ is the logarithm of the integral number at the corresponding registry level.

In the further processing of meteor stream measurements use is made of the dependencies $s = f(k_1, V)$, obtained by the statistical simulation method on a computer [3]. The s parameter for stream meteors is determined using the dependence $s = f(k_1)_{V_0}$, computed for the velocity V of meteors of this stream (Fig. 1).

Simultaneously the s parameter and its diurnal variation are determined for the sporadic background and for the totality of the background and the meteor stream. Usually there is a great scatter of values of the s parameter for stream meteors at different hours, on different days and in different observation years, in contrast to the $s(t)$ curve for the sporadic background. This is associated not so much with the structure of the streams as with measurement errors due to difficulties in discriminating the stream against a strong and fluctuating background. At the activity maximum of the streams the stream parameter s is usually less than for sporadic meteors. By averaging the s parameter for those hours when there is a maximum number of stream meteors the mean s value is determined for different observation days and a graph of the dependence of s on solar longitude λ is determined. This dependence can serve as a cross-sectional characteristic of stream structure.

In order to determine the relative change in the spatial density of meteor bodies in the swarm cross section there is need only to measure the total number of meteors during those same hours of the day when the

stream is visible (or the mean hourly number). Then the results of measurements on different days give a transverse profile of the stream under the condition that the instrument parameters remain stable; such profiles are constructed for different amplitude levels $N_i = f(\lambda)$.

For determining the absolute density of the stream of meteor bodies $Q(M^*)$ with the mass $M > M^*$ we determine the effecting collecting surface of the antenna S_{eff} in the plane perpendicular to the direction to the stream radiant (in the echo plane) and the minimum mass M^* of the registered meteor bodies. S_{eff} is a function of time of day t because the horizontal coordinates of the stream radiant change continuously. The stream density in this case is determined using the formula

$$Q(M^*) = N(t)/S_{eff}(t). \quad (2)$$

if the number of meteors is known. S_{eff} and M^* are determined when calculating the geometric and physical detectability factors. On the basis of the dispersion of $Q(M^*)$ values, computed for adjacent hours of the very same day, it is possible to judge the measurement errors and the correctness of allowance for the geometry factor of meteor detectability because during the course of several hours of observations the spatial density of particles in the meteor swarm can be considered constant.

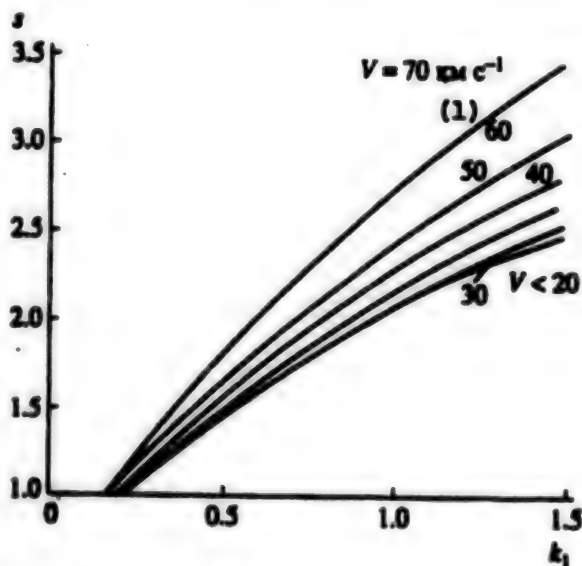


Fig. 1. Dependence of s parameter of distribution of meteor bodies by mass on parameter k_1 of distribution of amplitudes of reflected signals.

Key: 1. s^{-1}

The algorithm for processing the results of observations of the number of meteors is illustrated in Fig. 2.

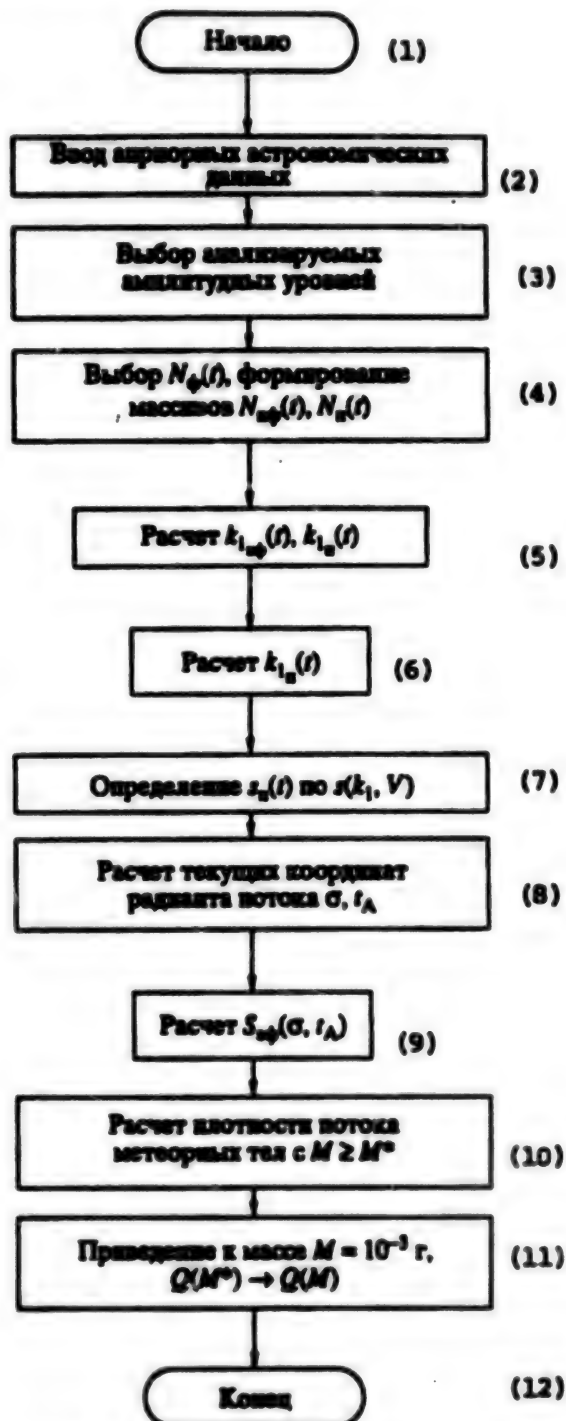


Fig. 2. Algorithm for processing results of observations of number of meteors during a period of stream activity.

Key: 1. Beginning; 2. Input of a priori astronomical data; 3. Choice of analyzed amplitude levels; 4. Choice of $N_{\text{back}}(t)$, formation of $N_{\text{st}}(t)$, $N_{\text{sp}}(t)$ files; 5. Computation of $k_{1,\text{st}}(t)$, $k_{1,\text{sp}}(t)$; 6. Computation of $k_{1,\text{st}}(t)$; 7. Determination of $s_{\text{st}}(t)$ from $s(k_1, V)$; 8. Calculation of momentary coordinates of stream radiant σ , t_A ; 9. Calculation of $S_{\text{st}}(\sigma, t_A)$; 10. Calculation of density of stream of meteor bodies with $M \rightarrow M^*$; 11. reduction to mass $M = 10^{-3}$ g, $Q(M^*) \rightarrow Q(M)$; 12. End

The cited method was used in processing the results of radar observations of the number of meteors in 1986 during the period of occurrence of the streams η -Aquadrids and Orionids [5]. A computation method at two levels (second and fourth) was used for assessing $k_{1,\text{st}}$ and $k_{1,\text{back}}$. In this case (1) is written as

$$k_{1,\text{st}} = 2.5 \times \frac{N_{\text{st}}^{(2)} (\lg N_{\text{st}}^{(4)} - \lg N_{\text{st}}^{(2)}) - N_{\text{st}}^{(4)} (\lg N_{\text{st}}^{(2)} - \lg N_{\text{st}}^{(4)})}{N_{\text{st}}^{(2)}}$$

where the superscripts (2) and (4) denote the number of the level. [The subscripts are for "stream," "stream-

background" and "background," as used in the preceding formulas.]

The following dates were adopted for the background: 27 and 30 April, 14, 15 May — for η -Aquadrids; 13, 18, 25, 26 October — for Orionids. For the principal maxima — 6 May and 24 October respectively. The values of the coefficient $k_{1,\text{st}}$ were computed for stream days for each hour during which the radiant was located in the visibility region of the meteorological radar. The $k_{1,\text{st}}$ value for a given day was determined by averaging of the weighted hourly values $k_{1,\text{st}}$. The $s(k_1, V)$ dependence with a known velocity of meteors in the studied streams $V = 64$ – 66 km s^{-1} was used to construct a file of values of the s parameter. Figure 3 shows the dependence of the s parameter on time and solar longitude λ for meteors of the streams and sporadic background.

The curves confirm the comment made above that there is a great scatter of s parameter values. For calculating the stream density of meteor bodies it is customary to use the minimum s value near the stream activity maximum. Using the graph in Fig. 3b for both streams we obtain $s = 1.65$.

Table 1. Density of stream of meteor particles belonging to η -Aquadrids

		λ_{\odot}	42	43	44	45	46	48	49	51	52	\bar{Q}
		U.T.										
$M \geq M^*$	$Q \times 10^{-3}, \text{m}^{-2} \text{s}^{-1}$	$6^{\text{h}}30^{\text{m}}$	1.2	0.78	1.3	2.5	1.2	—	0.75	1.4	1.5	1.3
$M \geq M_1$			0.02	0.013	0.02	0.04	0.02	—	0.012	0.023	0.025	0.02
$M \geq M^*$		$7^{\text{h}}30^{\text{m}}$	0.64	0.47	0.31	1.5	0.72	0.36	0.22	0.56	0.72	0.61
$M \geq M_1$			0.01	0.008	0.005	0.025	0.012	0.006	0.004	0.002	0.012	0.01
$M \geq M^*$		$8^{\text{h}}30^{\text{m}}$	4.5	3.8	—	14	8.5	—	—	—	4.2	7
$M \geq M_1$			0.07	0.06	—	0.23	0.14	—	—	—	0.07	0.12
$M \geq M^*$	$\sum_{i=1}^n N_i Q_i / n$			1.6	1.3	1.1	5.0	3.2	0.36	0.6	1.1	1.6
$M \geq M_1$				0.028	0.021	0.018	0.083	0.052	0.006	0.001	0.018	0.028

The equatorial coordinates of the stream radiant — the hour angle t_A and declination δ — are computed using well-known astronomical formulas for the radiant visibility region. The effective collecting surface of the meteorological radar $S_{eff}(t_A, \delta)$ determines the geometry factor for detectability of this radiant. The geometry factor curve for the Kharkov radar complex [7], computed by the graph analysis method, was employed when using formula (2) for calculating $Q(M^*)$. By knowing the minimum admissible registrable mass M^* and the s parameter it is possible to determine the density of the stream of meteor bodies with $M \leq M_1$ (for example, $M_1 = 10^{-3}$ g) using the formula

$$\frac{Q_s(M^*)}{Q_s(M_1)} = \left(\frac{M_1}{M^*} \right)^{s-1}.$$

The minimum linear electron density of meteor trails α_{min} was calculated using the well-known L-C method cited in [4]. In this case allowance is made for the dependence of meteor altitude H on velocity. (According to [6], with $V = 65$ km/s $H = 97$ km.) Then for the second amplitude level ($6.4 \mu V$) and a transmitter power 390 kW $\alpha_{min} = 9 \times 10^9$ cm $^{-1}$, which on the scale of radio meteor masses [4] corresponds to the maximum admissible registrable mass $M^* \cong 1.8 \times 10^{-6}$ g.

The results of calculations of the stream density of meteor bodies assigned to the η -Aquarids and Orionids for M^* and $M_1 = 10^{-3}$ g are given in Tables 1, 2. In the tables for several λ values there are no data due to strong interference. Curves of the dependence $Q(\lambda)$ for the studied streams are shown in Fig. 3b.

Bibliography

1. Belkovich, O. I., *Statisticheskaya teoriya radiolokatsii meteorov* (Statistical Theory of Radar Observation of Meteors), Kazan, Izd-vo KGU, 1971, 103 pages.
2. Voloshchuk, Yu. I. and Kashcheyev, B. L., Reflection of radio waves from meteor trails. II. Interpretation of distribution of amplitudes of meteors, *Radiotekhnika* (Radio Engineering), Kharkov Institute of Radio Engineering and Electronics, No 31, pp 51-57, 1974.
3. Voloshchuk, Yu. I. and Kashcheyev, B. L., *Raspredeleniye meteornykh tel vblizi orbity Zemli* (Distribution of Meteor Bodies Near the Earth's Orbit), Moscow, Nauka, 1981, 188 pages.
4. Voloshchuk, Yu. I., Kashcheyev, B. L. and Kruchenko, V. G., *Meteory i meteornoye veshchestvo* (Meteors and Meteoric Matter), Kiev, Nauk. dumka, 1989, 296 pages.
5. Milyutchenko, I. A., Radar observations of meteor streams η -Aquarids and Orionids at Kharkov in 1986, in: *Meteornyye issledovaniya: Rezultaty issledovaniy po mezhdunarodnym geofizicheskim proyektam* (Meteor Research: Results of Research Under International Geophysical Projects), Moscow, No 14, pp 69-72, 1988.
6. Oleynikov, V. N. and Smirnova, L. V., Assessment of detectability of radio meteors from observed dependence of mean altitude on velocity of meteors, in: *Meteornyye issledovaniya: Rezultaty issledovaniy po mezhdunarodnym geofizicheskim proyektam*, Moscow, No 12, pp 87-93, 1986.
7. Tkachuk, A. A., Detectability of weak radio meteors, *Problemy kosmicheskoy fiziki* (Problems in Space Physics), Kharkov State University, No 9, pp 92-98, 1974.
8. Kaiser, T. R., Radio echo studies of meteor ionization, *Advances Phys.*, Vol 2, pp 495-544, 1953.

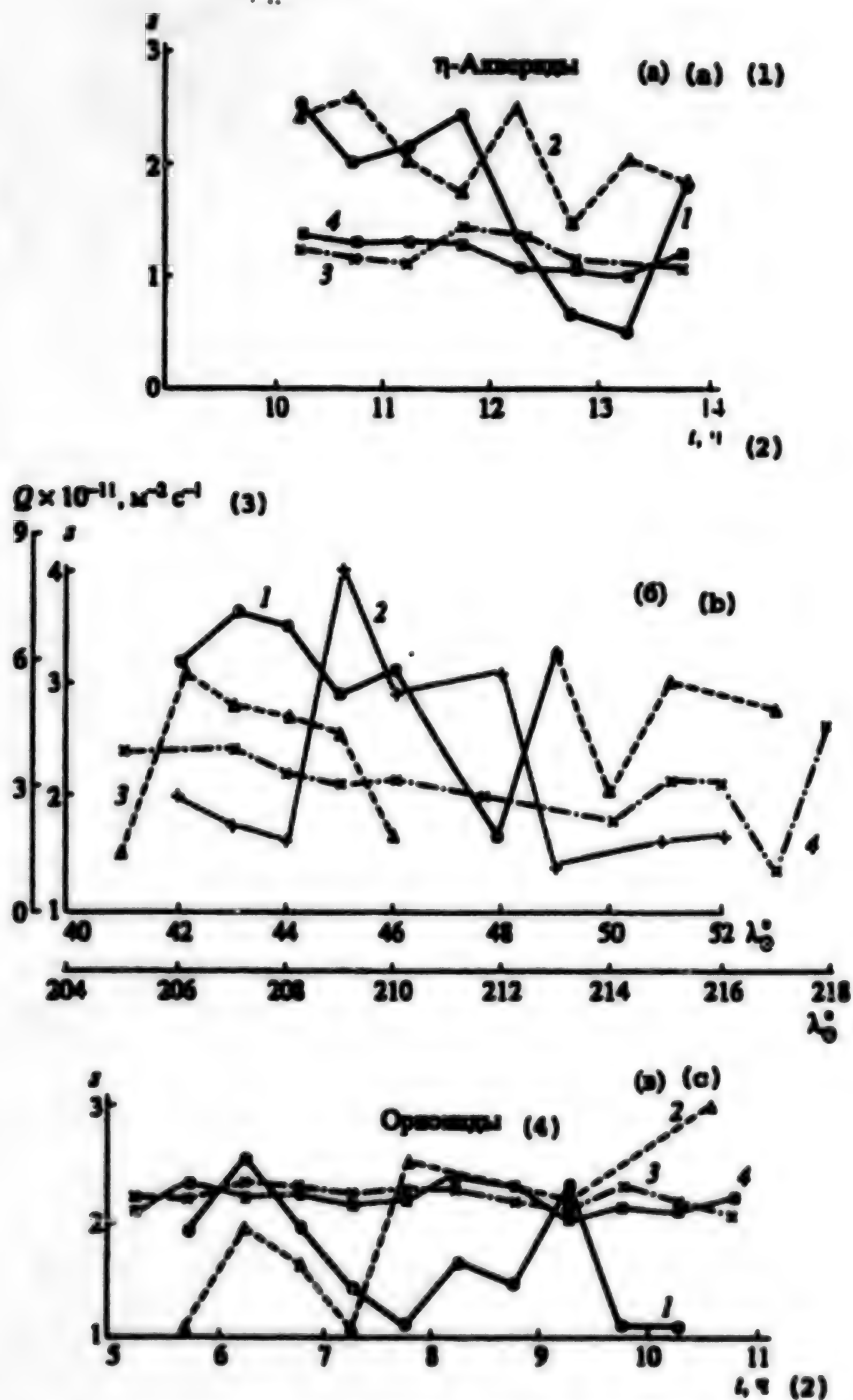


Fig. 3. Dependence of s parameter and stream density Q on solar longitude and time: s — $s_{\lambda=45^\circ}$ (1); $s_{\lambda=46^\circ}$ (2), $s_{\lambda=45^\circ}$ (3); mean $s_{\lambda=45^\circ}$ (4); b — $s_{\lambda=45^\circ}$ (1), Q , η -Aquarids (2); $s_{\lambda=45^\circ}$ Orionids (3), Q , Orionids (4); c — $s_{\lambda=205^\circ}$ (1); $s_{\lambda=210^\circ}$ (2); $s_{\lambda=210^\circ}$ (3); mean $s_{\lambda=210^\circ}$ (4).

Key: 1) η -Aquarids; 2) t , hours; 3) s^{-1} ; 4) Orionids

Table 2. Density of stream of meteor particles belonging to Orionids

		λ_{\odot}°	205	206	207	208	209	210	214	215	216	217	218	\bar{Q}
		U.T.												
$M \geq M^*$	$Q \times 10^{-9}, M^{-2} c^{-1}$	3^h30^m	4.6	2.2	4.2	4.1	2.9	3.4	2.8	3.7	0.36	0.97	5.6	3.2
$M \geq M_1$			0.076	0.036	0.07	0.067	0.048	0.056	0.046	0.06	0.009	0.016	0.092	0.053
$M \geq M^*$		4^h30^m	0.42	0.14	0.19	0.39	0.19	1.4	0.44	0.53	0.72	0.33	1.9	0.61
$M \geq M_1$			0.007	0.002	0.003	0.006	0.003	0.023	0.007	0.009	0.012	0.005	0.031	0.01
$M \geq M^*$		5^h30^m	0.67	1.9	0.86	1.0	1.3	0.69	0.63	0.64	1.7	0.19	2.4	1.1
$M \geq M_1$			0.011	0.031	0.014	0.016	0.021	0.011	0.01	0.01	0.028	0.003	0.039	0.018
$M \geq M^*$		6^h30^m	1.1	0.92	1.8	0.75	2.1	2.2	1.1	0.31	2.6	0.61	1.2	1.3
$M \geq M_1$			0.018	0.015	0.029	0.012	0.035	0.036	0.018	0.005	0.043	0.01	0.02	0.021
$M \geq M^*$		$\sum_{i=1}^n N_i Q_i / n$	2.3	1.6	2.3	2.0	1.9	2.0	1.35	1.9	1.9	0.54	2.8	1.87
$M \geq M_1$			0.039	0.028	0.039	0.033	0.03	0.033	0.022	0.03	0.03	0.008	0.047	0.025

Optimum Synthesis of Multiray Optical Interferometer For Making Observations Through Inhomogeneous Atmosphere

964D0113A Kiev KINEMATIKA I FIZIKA NEBESNYKH TEL

in Russian Vol 11 No 5, Sep-Oct 95 (manuscript received 2 Nov 94) pp 85-91

[Article by L. Ye. Kopilovich, Radio Physics and Electronics Institute, Ukrainian National Academy of Sciences, Kharkov; the first paragraph is an abstract; UDC 520.274]

[FBIS Translated Text] Problems in synthesis of the entrance aperture of an optical multiray interferometer ensuring single and double coverage of a maximum range of spatial frequencies with a stipulated number of subapertures and a corresponding exit nonexcess aperture of minimum size are examined.

The nonoptimality of a traditional optical telescope when making observations through an inhomogeneous atmosphere has motivated researchers to seek new image-forming methods more resistant to the destructive influence of atmospheric phase distortions. For this purpose it is possible to use an optical multiray interferometer [4, 19] ensuring measurement of the light flux coherence function in a stipulated spatial region. The idea of constructing a multiray interferometer involves the following: measurements are made using a primary (entrance) aperture which is excess in the sense that the base distances between the subapertures are not all dif-

ferent, but then the spatial spectral components of the signal, measured by pairs of subapertures with identical base distances, are "separated" on the secondary (exit) aperture plane in such a way that the exit aperture is already nonexcess with the same number of subapertures in it as in the entrance aperture. This makes it possible to extend the "phase closure" method [18, 8], which earlier was employed when using nonexcess aperture masks and therefore could be suitable only for retrieving the images of bright sources, to the case of weak sources when the influence of noise is extremely appreciable. Different aspects of use of a multiray interferometer are discussed in [3].

However, until now no study has been made of the problems involved in optimizing an interferometer of such a type. This article is devoted to this subject. Here there are two optimization problems. First it is necessary to ensure the coverage of a maximum range of spatial frequencies (that is, registry of all frequencies in this region of the u, v plane) with a stipulated number of subapertures in the interferometer entrance aperture; second, it is necessary to construct a nonexcess mask of minimum size with the same number of subapertures on the exit aperture plane. These problems are solved in the article by the methods developed in [2, 14] and [1, 13] respectively.

Bases for rectangular grids. We will introduce the concept of a base for a rectangular grid [2, 14]. For this purpose on the aperture plane we will construct an integral grid and within it we designate a rectangular grid

measuring $(n_1 + 1) \times (n_2 + 1)$ (with side lengths n_1 and n_2 and on this grid we place K point elements (subapertures). The interval between two elements (points of intersection, subapertures) is called their vector (without allowance for its direction). If all possible intervals between grid points of intersection are encountered among these elements, then we say that these elements form a base for the grid.

The problem of optimizing the interferometer entrance aperture thus essentially involves construction of a base from a stipulated number of elements which would cover a grid of maximum size, that is, have a minimum excess (which ensures interferometer transfer of the maximum range of spatial frequencies). The excess of a base of K elements for a grid measuring $(n_1 + 1) \times (n_2 + 1)$ is determined by the ratio of the number of intervals between the base elements to the number of different intervals present in this grid, that is, by the quantity

$$\alpha^* = K(K-1)/[2(n_1n_2 + n_1 + n_2)] \approx K^2/(4n_1n_2)$$

where $K \gg 1$, $n_1 + n_2 \ll n_1n_2$. The following quantity [2, 14] will be used as a characteristic of base excess

$$\alpha = K/\sqrt{n_1n_2}. \quad (1)$$

and from the mathematical point of view is more convenient for research.

The simplest method for obtaining the base for a rectangular grid involves multiplication of the two bases for the segments which are the sides of this grid. Such one-dimensional bases (sets of K_1 whole numbers, among the differences between which are encountered all the numbers $1, 2, \dots, n_1$ [5]) having a minimum or small excess (characterized by the quantity

$$\alpha_1 = K_1/\sqrt{n_1})$$

found in [15] for all $K_1 \leq 11$ and in [16] — for $K_1 \leq 19$.

The one-dimensional bases with a large number of elements can be obtained in the form [5, 15]

$$\{jV_1 + d_j\}, \quad j = 1, \dots, K_1; \quad i = 1, \dots, A_1. \quad (2)$$

where γ_i is the one-dimensional base for a small segment (we will call it the initial base) and d_i is a cyclic difference set (CDS) with the parameters $V_1, k_1, \Lambda_1 = 1$. In a general case the CDS with the parameters V_1, k_1, Λ_1 is determined in the following way [9, 10]: this is such a set of k_1 whole numbers on a segment of the length V_1 that any whole number $0 < v < V_1$ has Λ_1 different representations in the form

$$v = d_i - d_j \bmod V_1. \quad (3)$$

A base of the type (2) covers a segment of the length

$$R_1 = (n_1 + 1)V_1 - r_1 - 1, \quad (4)$$

where $r_1 = d_{\max} - d_{\min}$. As γ_i in (2) it is most common to use the nonexcess base

$$\{0, 1, 4, 6\}, \quad n_1 = 6. \quad (5)$$

However, since CDS with $\Lambda_1 = 1$ exist only when $k_1 = q + 1$ (where q is the power of a simple number) [9], for constructing the base (2) with a stipulated number of elements as the initial bases it also is necessary to use other bases from [15] or [16].

Optimization of a base in the form (2) essentially involves choice of an initial base with a minimum excess (with a stipulated number of its elements), and also, as can be seen from (4), choice of the most compact CDS. The procedure for obtaining a CDS with stipulated parameters was set forth, for example, in [12]; CDS tables with $k_1 \leq 100$ are given in [10]. A CDS with a minimum r_1 can be determined using the procedure described in [2, 14] (for $k_1 \leq 48$ tables of such CDS with $\Lambda = 1$ were given in [6, pp 169-171]). With an optimum initial base and CDS, using formula (2) we obtain a base for a segment of maximum length (4).

Multiplication of two bases of the type (2) gives a base in the form

$$\{(\gamma_j V_1 + d_j, \delta_i V_2 + d'_i)\} \quad (6)$$

for a rectangular grid. In (6) taking $\gamma_j = \delta_j$, we obtain a base for a square grid with the side length (4). For example, we obtain an optimum two-dimensional base of 96 elements, in (2) taking the initial base (5) and a CDS with the parameters $V_1 = 553$, $k_1 = 24$, $\Lambda_1 = 1$ from [6]. We find from (4) that $R_1 = 3,445$ and the base (6) for a square grid in this case consists of 9,216 elements, and for it $\alpha = 2.675$.

It also was demonstrated in [2, 14] that by using the two-dimensional initial base γ_j, δ_j and a two-dimensional difference set (TDDS) (a_i, b_i with the parameters v_a, v_b, k, Λ_1 (being a generalization of the CDS) it is possible to construct a base for a grid with the side lengths

$$R_1 = (n_1 + 1)v_a - r_a - 1, R_2 = (n_2 + 1)v_b - r_b - 1, \quad (7)$$

where

$$r_a = a_{\min} - a_{\max}, r_b = b_{\min} - b_{\max}. \quad (8)$$

This base consists of $K = kK_0$ elements (where K_0 is the number of elements in the initial base) and has the form

$$\{(v_a \gamma_a + a_i, v_b \gamma_b + b_i)\}. \quad (9)$$

Bases of the form (9) have, generally speaking, a lesser excess than the base (6); however, when $\Lambda_1 = 1$ they cannot be constructed for strictly square grids and it is necessary to select the characteristics of the initial bases and TDDS parameters in such a way as to compensate approximately for the difference between R_1 and R_2 .

It must be noted that a small part of the elements of the bases (6) and (9) goes beyond the limits of the grids covered by them and therefore the size of the integral grid on the aperture plane must be somewhat greater than for the grid proper.

Generalization: multiple bases. The statement of the problem formulated in the preceding section can be generalized in the following way. We will assume that it is necessary to ensure total coverage of a stipulated range of spatial frequencies when one of the elements mal-

functions, which is especially significant with respect to the reliability of a space-based interferometer. In this case coverage can be ensured by means of a double base. In general such a set of point elements that any interval between the grid points of intersection is encountered at least Λ times among the intervals between the elements of this set can be called a Λ -multiple base for a rectangular grid. A double base is obtained when $\Lambda = 2$.

When constructing multiple bases with a stipulated number of elements the optimization problem also arises, and specifically, coverage of a maximum range of spatial frequencies. For a well-known system of radioastronomical arrays, the Mills cross [17] (see Fig. 1), constituting a double base, the quantity (1) is equal to

$$\alpha = 2(n_1 + n_2)/\sqrt{n_1 n_2} \geq 4, \quad (10)$$

attaining a minimum in the case of square grids and increasing with an increase in the n_1/n_2 ratio. By means of methods examined in the preceding section it is possible to obtain double bases with an excess less than for Mills crosses covering the corresponding regions of spatial frequencies. The next section is devoted to this problem.

Construction of double bases. Double bases can be obtained both by multiplying single and double linear bases and on the basis of two-dimensional difference sets (TDDS) and two-dimensional initial bases.

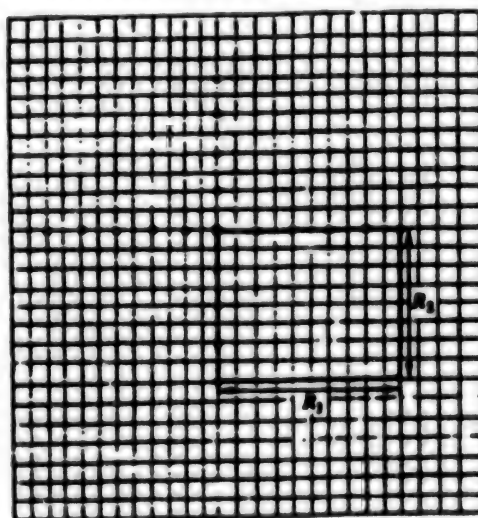


Fig. 1. Diagram of Mills cross with central element.

1. Double bases for small rectangular grids are obtained by multiplying single and double linear bases. Our research shows that among the double one-dimensional bases with $6 \leq K_2 \leq 11$ the quasioptimum characteristics have series in the form

$$\{0, 1, \dots, K_2 - 5, 2K_2 - 8, 2K_2 - 7, 3K_2 - 12, 3K_2 - 11\}. \quad (11)$$

doubly covering a segment of the length $n_2 = 3(K_2 - 4)$. When $K_2 = 12$ the best of the bases which we found doubly cover a segment of the length $n_2 = 25$ and has the form

$$\{0, 2, 3, 4, 6, 12, 13, 19, 20, 24, 25, 27\}, \quad (12)$$

but when $K_2 = 13$ a segment of the length $n_2 = 30$ is covered, but the base itself has the form

$$\{0, 2, 3, 4, 6, 13, 17, 20, 24, 25, 29, 30, 32\}. \quad (13)$$

If any of the bases (11)-(13) is multiplied by the single base (5), for the determined double two-dimensional base

$$\alpha = K_1 K_2 / \sqrt{n_1 n_2} \leq 4,$$

that is, less than for the Mills cross. However, by selecting pairs of segments covered by these bases and the single bases from [15] it is possible to obtain double bases for nearly square grids (Table 1). The last column gives the gain in the number of elements (M) in comparison with the corresponding Mills cross. It is obvious that the gain will be considerably greater for more extended grids.

Table 1. Characteristics of bases of type (6) for small grids

K	α	$(n_1 + 1) \times (n_2 + 1)$	M
32	3.771	13 x 7	4
35	3.889	10 x 10	1
48	3.843	13 x 14	2
54	3.868	16 x 14	2
70	3.889	19 x 19	2
88	3.920	22 x 25	2
96	3.918	26 x 25	2

2. Double bases for large grids also can be obtained by multiplying two one-dimensional bases — single and double — and the second of these can be constructed by two methods: on the basis of a double initial base and a CDS with $\Lambda_1 = 1$ or using a single initial base and a CDS with $\Lambda_1 = 2$. The first method ensures the possibility of constructing double bases of the type (6) for a broad set of grids because there are rather many CDS with $\Lambda_1 = 1$; at the same time only two types of CDS with $\Lambda_1 = 2$ are known: $V_1 = 11, k_1 = 5$ and when $V_1 = 37, k_1 = 9$ [10].

3. Two variants also are possible when constructing double bases on the basis of TDDS: using a double two-dimensional initial base and a TDDS with $\Lambda_1 = 1$ or a single two-dimensional initial base and a TDDS with $\Lambda_1 = 2$. In the first case as the initial base it is possible to take one of the bases found in #1, but TDDS with $\Lambda_1 = 1$ are obtained from the CDS with $\Lambda_1 = 1$ with the same k and with $V = v_1 v_2$ ($v_1, v_2 = 1$, using the formulas

$$a_i = d_i \bmod v_1, \quad b_i = d_i \bmod v_2. \quad (14)$$

By optimizing the TDDS by the method described in [2, 14] it is possible to construct double bases for a number of rectangular grids. The characteristics of several of

them, as well as the parameters of the corresponding TDDS and the initial bases, are given in Table 2.

Table 2. Characteristics of bases of type (9) and parameters of corresponding TDDS

K	α	$(R_1 + 1) \times (R_2 + 1)$	$(v_1, v_2; k)$	$(n_1 + 1) \times (n_2 + 1)$	M
320	3.856	83 x 85	(13, 7; 10)	7 x 13	12
432	3.846	120 x 107	(19, 7; 12)	7 x 16	18
2,176	3.759	567 x 593	(93, 49; 68)	7 x 13	140
2,252	3.795	591 x 588	(97, 39; 62)	7 x 16	122

With respect to a TDDS with $\Lambda_1 = 2$, only two types of such sets are known: with $k = 6$ and $v_1 = v_2 = 4$ with this same k and $v_1 = 8, v_2 = 2$ [20]. These TDDS cannot be obtained from the CDS. A TDDS with minimum r_1 and r_2 in the first case has the form:

$$\{(0, 0), (1, 0), (0, 1), (2, 1), (1, 2), (2, 2)\}. \quad (15)$$

If the initial base is taken in the form of the product of two bases (5), using formula (9) we obtain a double base for a square grid with a side length $R = 25$ and with $\alpha = 3.840$, represented in Fig. 2. In the second case the TDDS with minimum r_1, r_2 has the form:

$$\{(0, 0), (3, 0), (4, 0), (5, 0), (1, 1), (3, 1)\}. \quad (16)$$

and the initial base is taken in the form of the product of the base (5) and the base from [15] with $K_1 = 8$:

$$\{0, 9, 13, 19, 22, 24, 31, 39\}, \quad n = 24. \quad (17)$$

As a result we obtain a double base for a grid with side lengths $R_1 = 50, R_2 = 48$ and with $\alpha = 3.918$.

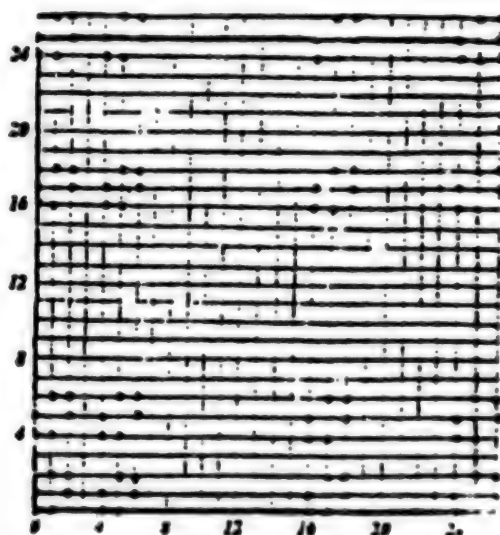


Fig. 2. Double base for square grid with side length $R = 25$ (enclosed by solid line), constructed on basis of two-dimensional difference set.

Optimization of exit aperture. The nonexcess configurations (NC) of an interferometer exit aperture with a stipulated number of subapertures K positioned in a $K \times K$ grid S_K can be computed by the method developed in [1, 13]. As a point of departure we use the set [11]

$$(i, j \bmod p), \quad i = 0, 1, \dots, p-1, \quad (18)$$

where p is a simple number. The elements of the set (18) form a NC in the S_p grid, the same as the elements of any set obtained from it with cyclic shifts along the grid axes or with multiplication of the coordinates of the elements of the set (18) by $(\bmod p)$ for pairs of numbers reciprocally simple with p . It was demonstrated in [1, 13] how by operations of this type the table obtained from (18) (if the value 1 is assigned to the set elements and a 0 is assigned to the remaining grid points of intersection) can be reduced to such a form that by successive deletion of pairs of lower rows and right-hand columns from it both the order of the table and the number of set elements in it is reduced by unity, that is, a NC of n elements on S_p is obtained with $n = p-1, p-2, \dots, p-c+1$, where

$$c = \max(l_{j+1} - l_{j-1}), \quad (19)$$

and l_j is a series of $i^2 \bmod p$ values written in an increasing order. In actual practice, proceeding on the basis of the closest simple number $p > K$ by such a method it is usually possible to obtain an NC of K elements in the S_K grid. In the example considered above the number of NC elements must be equal to $K = 9,216$ and therefore in formula (18) we assume that $p = 9,221$ (for example, see the table in [7]). In order to obtain the sought-for NC it is necessary to reduce the order of the matrix (18) by 5, which is known to be less than the quantity (19).

Summary. The methods for optimizing optical interferometer configuration developed in this article evidently also will find application when developing large multi-element radio telescopes operating in the millimeter and submillimeter ranges, in the construction of which it is necessary to reckon with the high cost of each structural component.

The author expresses appreciation to Yu. V. Korniyenko, who drew his attention to the problem of

synthesis of optical interferometers, as well as making a number of comments on the text.

The work was done with the financial support of the State Fund for Fundamental Research, Ukrainian State Committee for Science and Technology (Project No 2.3/474).

Bibliography

1. Kopilovich, L. Ye., Signals with minimum indeterminacy function for simultaneous determination of range and velocity of object, *Radiotekhnika i elektronika* (Radio Engineering and Electronics), 32, No 7, pp 1545-1546, 1987.
2. Kopilovich, L. Ye., Optimization of two-dimensional aperture synthesis systems, *Radiotekhnika i elektronika*, 33, No 9, pp 1918-1923, 1988.
3. Korniyenko, Yu. V., Interferometric approach to problem of vision through a turbulent atmosphere. I, *Kinematika i fizika nebes. tel* (Kinematics and Physics of Celestial Bodies), 10, No 2, pp 98-106, 1994.
4. Korniyenko, Yu. V. and Uvarov, V. N., Signal accumulation during observation of astronomical object through a turbulent atmosphere, *Dokl. AN USSR. Ser. A* (Reports of the Ukrainian Academy of Sciences. Series A), No 4, pp 60-63, 1987.
5. Redei, L. and Reni, A., Representation of numbers $1, 2, \dots, n$ in form of differences, *Mat. sb.* (Collection of Articles on Mathematics), 24(66), No 3, pp 385-389, 1949.
6. Sverdlik, M. B., *Optimalnyye diskretnyye signaly* (Optimum Discrete Signals), Moscow, Sov. radio, 1975, 200 pages.
7. Abramovich, M. and Stegan, I. (editors), *Spravochnik po spetsialnym funktsiyam* (Handbook on Special Functions), Moscow, Nauka, 1979, 832 pages.
8. Uvarov, V. N., Possibility of obtaining images with diffraction resolution when making observations through an inhomogeneous medium, *Dokl. AN USSR. Ser. A.*, No 10, pp 839-841, 1979.
9. Kholi, M., *Kombinatorika* (Combinatorial Analysis), Moscow, Mir, 1970, 424 pages.
10. Baumert, L. D., Cyclic difference sets, *Lect. Notes Math.*, 182, 1971, 166 pages.
11. Elliott, J. E. N. and Butson, A. T., Relative difference sets, *Ill. J. Math.*, 10, No 4, pp 517-531, 1966.
12. Kopilovich, L. E., Non-redundant aperture mask systems for interferometric image synthesis. A regular

method of construction, *Opt. acta*, 31, No 12, pp 1409-1415, 1984.

13. Kopilovich, L. E., Construction of nonredundant masks over square grids, *Opt. Commun.*, 68, No 1, pp 7-10, 1988.

14. Kopilovich, L. E., New approach to constructing two-dimensional aperture synthesis systems, *IEE Proc., Ser. F*, 139, No 5, pp 365-368, 1992.

15. Leech, J., On the representation of 1, 2, ..., n by differences, *J. London Math. Soc.*, 31, No 122, pp 160-169, 1956.

16. Miller, J. C. P., Difference bases, three problems in additive number theory, in: *Computers in Number Theory*, edited by A. D. Atkin and B. J. Birch, London, Acad. Press, pp 299-322, 1971.

17. Mills, B. Y., Cross-type radio telescopes, *Proc. IRE Australia*, 24, No 2, pp 132-140, 1963.

18. Rhodes, W. T. and Goodman, J. W., Interferometric technique for recording and restoring images degraded by unknown aberrations, *J. Optic. Soc. Amer.*, 63, No 6, pp 647-657, 1973.

19. Roddier, F., Redundant versus nonredundant beam recombination in an aperture synthesis with coherent optical arrays, *J. Optic. Soc. Amer.*, A4, No 8, pp 1396-1401, 1987.

20. Tutyn, R. J., Character sums and difference sets, *Pacif. J. Math.*, 15, No 1, pp 319-346, 1965.

Eko-Psi-95 Experiment in Mir Complex Described

964D0110A Moscow *SEGODNYA* in Russian
2 Nov 95 p 9

[Article by Viktor Gritsenko]

[FBIS Translated Text] A few days ago the State Center of Medical-Biological Problems (formerly the Institute of Medical-Biological Problems) began the Eko-Psi-95 experiment (ecology and psychology). Three volunteers will face total isolation for 90 days in an experimental complex on Earth which recreates the Mir manned orbital complex.

The main goal of this research is to study psychological compatibility, mechanics of conflict situations, and methods of getting out of them. As the scientific director of the experiment, Vadim Gushin, explained, "they will study the dynamics of psychological comfort and productivity."

The experiment was prompted by the fact that while working in space, despite the existing special psychological selection process, the crew cannot always manage to avoid problems. In 1976 the flight of the military orbital station Almaz-3 (officially called Salyut-5) was concluded prematurely because of the psychological incompatibility of military cosmonauts Boris Volyanov and Vitaliy Zholobov. Or a very recent example. Vladimir Dezhurov and Gennadiy Strekalov were part of this fall's eighteenth main expedition with American Norman Tagard on the Mir orbital complex. The cosmonauts were fined 15 percent of the total sum of the contract for "violation of seniority in the crew."

In order to avoid such complications, the State Center of Medical-Biological Problems decided to "repeat" them on Earth. Moreover, the crew's problems will be created intentionally. On the twenty-second day of the "flight" there are plans to "dock" with a ship whose crew will "visit." However, at this time the automatic controls will "fail" and the "docking" will have to be done manually. The cosmonauts will spend 60 hours doing this, during which they will not have the opportunity to even sleep. When the "docking" finally occurs, three more researchers will arrive and live an entire week there. The specialists promise to provide the "cosmonauts" with many other problems.

The State Center of Medical-Biological Problems has its own team of seven cosmonaut-researchers, of which only Valeriy Polyakov has been fortunate enough to fly in space, twice. Thus, the center is especially famous because those who have not flown in space participate in the ground-based experiments as a consolation here. In September 1994-January 1995 the HUBES experiment, lasting 135 days, was carried out under contract with the ESA. Three representatives of the center participated: cosmonaut-researchers Vladimir Karashtin and candidate of medical sciences Vasily Lukyanyuk, as well as candidate of medical sciences Igor Nichiporuk.

The experienced 48-year-old Colonel Aleksandr Andryushkov is participating in the current experiment. He is a correspondent of KRASNAYA ZVEZDA who underwent training at the Mission Control Center in 1990-1992 in preparation for space flight as part of the team from the Journalists Union of the USSR. However, he was not the first Soviet cosmonaut-journalist (he was preceded by a Japanese journalist). Also participating in the experiment are two students of the Moscow Aviation Institute, Aleksandr Ivyanskiy and Yaroslav Balakhontsev. At the end of the experiment each of them will receive \$1,500.

Mir Leak Described

964D0110B Moscow SEGODNYA in Russian
2 Nov 95 p 1

[Article by Mikhail Chernyshov]

[FBIS Translated Text] Tuesday evening Mir telemetry recorded a drop in temperature and a small leak of heat transfer fluid in the station's heating system. It seems the incident caused a mild panic among those in charge of space matters. The next day a hastily created commission consisting of representatives of Energiya, the Mission Control Center, and Military Space Forces were at work. The situation was complicated by the fact that the pipelines for the station's "central heating" are behind panels and instrument shields. The specific location of the heat transfer fluid leak was not determined over the course of the day. The specialists stated that nothing strange had occurred; only a small leak in the heat regulation system. The vapors of the leaking heat transfer fluid, like automobile antifreeze, poses no danger to the crew's respiration. All remember, however, the "ice age" which occurred on Salyut-7, when a similar "small" flaw turned the internal sections of the orbital complex into an ice cave. In addition, the batteries discharged and the lights went out. Only desperate measures taken by cosmonauts Vladimir Dzhanibekov and Viktor Savinyi, resulted in a "thawing" of the station, returning it to life.

The current situation, according to the assurances of the Mission Control Center, is much simpler. Mir is not threatened with the onset of an ice age. "The heat transfer fluid leak is small, and deviations of temperature from the norm are insignificant." Nonetheless, all current and proposed operations to repair the station have for some reason been kept secret and withheld from the press. The attempt to hide something that will come out anyway is completely in the spirit of the traditions of domestic cosmonautics. However, there is a small complication: in addition to our countrymen, Yuriy Gidzenko and Sergey Avdeyev, who could be persuaded to keep quiet, ESA astronaut Thomas Rafter is on board Mir. A Western researcher, by terms of his contract, is obliged to promptly report to his home agency all failures which occur on the station. There has been no talk of reexamination of the program of operations or emergency evacuation of the crew from on board Mir yet. The specialists promise to finally put the situation in order today.

Russian Space Industry Described

964D0122A Moscow KRASNAYA ZVEZDA
in Russian 11 Nov 95 p 5

[Interview with Sergey Zhiltsov, department head at the State Space Science and Production Center imeni M.V.

Khrunichev, by KRASNAYA ZVEZDA correspondent Mikhail Rebrov; place and date not given: "Iridium-Eurasia; New Company Promises Russian New Quality of Space Communication"; first two paragraphs are boldface KRASNAYA ZVEZDA introduction]

[FBIS Translated Text] Today it is difficult to imagine our business and everyday lives without radio receivers, televisions, telephones, and computers. Such technology feeds us information, connects us with the outside world, and makes leisure time interesting.

Even back in the dawn of their development, humankind had ways to send "meaningful signals" across great distances by using the beating of drums, torches, campfires, and smoke. Space has brought a new level of quality to the task. As they say, it seems like only "yesterday" we dreamed of a time when we would be able to call a person anywhere on earth by simply dialing a number. We supposed that communication with that person would automatically be established regardless of whether he was in the middle of the ocean, in the center of a big city, or crossing the desert. It was from such a historical digression that I began my conversation with Sergey Zhiltsov, department head at the State Space Scientific and Production Center imeni M.V. Khrunichev—an enterprise that is among other things working on designing space communications.

[Rebrov] Sergey Aleksandrovich, in our stormy era a man deprived of communication is deprived of practically everything. Information is a resource. An inexhaustible and important resource. Not that long ago ordinary relay satellites were fantastic, whereas today we talk about completely new concepts on a global scale.

[Zhiltsov] I would put it more precisely. We are not simply talking about them but are actually developing them. You are correct: Each day, common-use communication occupies a bigger place in society. Today virtually all people have the opportunity to use telephone communication. But life is being dictated by new conditions. And supporting business activity now requires more than constantly being on the telephone. Today the telephone services market offers a wide selection of equipment needed by modern businessmen. This includes data transmission, paging, facsimile communication, and confidential communication. A significant shift in clients' preferences in favor of mobile communications, namely, a preference for pocket devices, has been observed.

[Rebrov] As far as I know, progress in the field of telecommunications and communication, as well as developments in rocket and space technology, enabled the U.S. firm Motorola, Inc., to begin developing the

IRIDIUM satellite system of mobile communications back at the end of the eighties. The system, which is based on the use of low-orbiting spacecraft, would enable subscribers to use an ordinary portable telephone to establish communications regardless of their location.

[Zhiltsov] Such a project is in fact being implemented at the present time. It is intended first and foremost to provide communication services to governmental and business organizations and to services requiring immediate communication in emergencies. I would add that this is extremely important to populations living in hard-to-reach regions and in territories without ground systems of collective communication. I am not speaking about those members of population in middle and high income brackets, representatives of business circles, travelers, and so forth.

[Rebrov] Let's clarify something. Is this system an international system?

[Zhiltsov] Yes. In 1993, an international consortium called Iridium, Inc., was formed to implement the IRIDIUM project. The work is continuing. After the system has been put into operation, Iridium, Inc., will own its space segment. The consortium includes leading firms in the field of telecommunications, as well as developers and manufacturers of communications equipment and rocket and space technology in the United States, Canada, Russia, Italy, Japan, China, and other countries.

Extra capital and "brains" from such well-known firms as Lockheed Corporation, Siemens, Telespacio, Motorola, McDonnell Douglas, Stet, and Vebak [transliteration] have been brought in to work on the project. Russia is represented on the list by the leading rocket and space company State Space Scientific and Production Center imeni M.V. Khrunichev [GKNTPTs].

[Rebrov] What is the relative extent of your involvement? In other words, what do you have to invest and what will you receive?

[Zhiltsov] As an investor, the space center must, first and foremost, create a financial base of operations in Russia, purchase the required equipment and construct ground interface stations, and set up a network of system service providers. In addition, in January 1993, a contract was signed with the U.S. company Motorola for three launches of the rocket Proton to put 21 IRIDIUM communication satellites into orbit (seven satellites each

time). The first launch is slated for the end of 1996. Our center is developing and manufacturing carrier rocket containers to hold seven satellites, as well as a system to separate them from the Proton's final stage and put them into orbit. This is a commercial project.

[Rebrov] What guarantees are there that it will be implemented?

[Zhiltsov] A number of decisions of the State Commission on Electronic Communication and the "Memorandum Concerning Mutual Understanding and the Basic Principles of Cooperation in Implementation of the IRIDIUM System on Russian Federation Territory" between the Russian Federation Ministry of Communications and the Space Center imeni M.V. Khrunichev have permitted successful implementation of the project on Russian Federation territory.

[Rebrov] Is everything going "smoothly" as the space specialists say?

[Zhiltsov] In general, yes. The amount of work scheduled, short time frame, and plans to begin regular operation of the system in 1998 have all necessitated the creation of the new company Iridium-Eurasia, which should solve problems regarding the IRIDIUM system in Russian territory and provide the communication system's services within the territories of a number of governments as well as in those served by the base interface station that is being created. And that company has already been created. In the future, the State Center imeni Khrunichev will grant the company the right to operate the interface station and provide the communications services of the IRIDIUM system, as well as equip the interface station. I don't think that we will have a problem.

[Rebrov] Sergey Aleksandrovich, tell us a little about the partners.

[Zhiltsov] The GKNTPTs' partner is the closed joint-stock company Zond syvaz, which is the operator of a digital satellite network linking a number of Russia's cities.

[Rebrov] And what's next?

[Zhiltsov] There are plans to create a second system interface station, preferably in the Asian part of Russia. This will make it possible to increase the number of subscribers served, reduce rates, and increase the quality of services provided. The preferred use of the system is to provide electronic communications services in rural, sparsely populated, and difficult-to-reach regions,

including regions of the Far North, Siberia, Far East, the Chukotski Peninsula, the Kamchatka Peninsula, and Sakhalin, most of whose population centers are more than 100 km from telephone stations.

The IRIDIUM system must become a link in the world's infrastructure of mobile communications networks, including various ground and satellite mobile communications systems. We have had much of this prepared for many years now—both the satellite and the ground segment. We are using existing communications lines and do not need to create anything new. And we are already inviting all those operating telephone communications networks to join us.

At the beginning of our conversation, I called your attention to the fact that we have already advanced beyond the "conversation" stage and have gotten down to business. The Ministry of Communications, as the country's leading expert, is supporting our project. It therefore appears highly certain that Russia will have modern mobile communications, which will in turn open fundamentally new opportunities for the system's users.

[Rebrov] And now one final question, Sergey Aleksandrovich: How soon will the investments in the system be recouped?

[Zhiltsov] I'll tell you. The system's cost recovery period is estimated at a year and a half. After that, there will be a profit.

Russian Engines for American Rockets

964D0122B Moscow KOMMERSANT DAILY
in Russian 4 Oct 95 No 183, p 9

[Unattributed article: "Ministry of Defense Does Not Oppose Equipping American Rockets With Russian Engines"]

[FBIS Translated Text] Yevgeniy Gritsenko, general director of the Samara NTK Dvigateli NK [NK Engines], denied the numerous media reports in late September stating that the Russian Federation Ministry of Defense is blocking a joint Russian-American program to use NK-33 rocket engines. In his words, it was precisely in September that the Ministry of Defense approved the collaboration of the Samara NTK Dvigateli NK with the American company Aerojet. In July, two NK-33 engines were sent to the United States, where final preparations are being made for firing tests on Aerojet engine test beds in Sacramento (California). The NK-33, which was developed more than 25 years ago within the framework of the program to achieve manned flights to the Moon, is slated for use on new-generation American carrier rockets and to modernize existing rockets. If the Samara NTK Dvigateli NK program is implemented, significant amounts of capital could be obtained from the sale of NK-33 engines that have already been manufactured and from license fees. That capital could then be invested in the development and production of promising aircraft engines and commercial gas turbine units.

Degradation of the Interphase Si-SiO₂ Boundary Under Field and Radiation Effects

964D0047A St. Petersburg PISMA V ZHURNAL
TEKHNICHESKOY FIZIKI in Russian 26 May 95
Vol 21 No 10, (manuscript received 7 Nov 94; after
revision 16 Feb 95) pp 1-5

[Article by I. V. Klimov, Yu. M. Listopadov, A. I. Nazarov]

[FBIS Abstract] It is important to understand the reasons for the degradation of metal-dielectric-semiconductor transistors due to "hot carriers" (i.e., X-rays, avalanche hole and tunnel electron injection) to predict performance, optimize operating modes and improve production methods. This paper studies the structure of polycrystalline silicon-silicon dioxide-silicon with three types of oxides (vapor, pyrogenic, and dry) grown on an n-type silicon substrate. The radiation and avalanche-injected charge is formed in the same way in all oxide types. Study of the electric field strength showed that as the avalanche duration increases, the captured charge decreases, either due to leakage of the positive bulk charge from the trap into the electric field, or due to additional electron injection leading to recombination of electrons with the captured positive charge. A figure shows the dependence of surface state density on surface potential for various effects. Tunnel electron injection and avalanche hole injection with an electron component, as well as emission at a positive voltage at the gate causes a significant increase in surface states at the silicon-silicon dioxide interface. The greatest density is observed in samples with dry oxide. A study of the degradation of field metal-dielectric-semiconductor transistors after homogeneous avalanche injection of electrons showed an increase in the fluctuations of surface potential during injection. After a critical charge (10^9 pulses) the potential relief equalized. The most stable were transistors with a subgate dielectric manufactured using moist oxide. There is a clear relation between the density of surface states and the method of manufacturing the oxide layer when there is an electric

field in the dielectric and charges of both signs in the interphase carrier boundary. The effects of "hot carriers" are determined so that one can predict the degradation changes in metal oxide semiconductor structures. Figures 2; references 5: 2 Russian, 3 Western.

Growth of 3D Polytype 4H and 6H Silicon Carbide Crystals

964D0047B St. Petersburg PISMA V ZHURNAL
TEKHNICHESKOY FIZIKI in Russian 26 May 95
Vol 21 No 10, (manuscript received 20 Dec 94) pp
20-24

[Article by A. Yu. Maksimov, A. A. Maltsev, N. K. Yushin, I. S. Barash; A. F. Ioffe Physicotechnical Institute, St. Petersburg]

[FBIS Abstract] This paper describes an experiment to try to grow bulk silicon carbide crystals of polytypes 6H and 4H, as well as an attempt to obtain substrates (monocrystalline silicon carbide substrates) with a diameter of greater than an inch. The growth rate of polytype 6H monocrystals depends on temperature and argon pressure: too fast a growth rate and quality suffers; too slow and insufficient crystal height is obtained during the experiment. The optimal growth rate was 0.8 mm/hr at 2230°C and an argon pressure of 7 millibars. Boules of the 6H polytype 25 mm in diameter were obtained. The 4H polytype crystals were grown by placing a thick epitaxial layer of polytype 4H on a 6H substrate with an excess of carbon in the atmosphere and with the addition of a group IV element (Ge, Se, Pb). Later the substrate was removed. X-ray analysis demonstrated a sufficiently good crystal quality. The boules were used to manufacture substrates 25 mm in diameter (or a square shape 30x30 mm) 0.3-0.5 mm thick. The monocrystal plates of polytypes 4H and 6H had a polytype homogeneity of better than 80 percent, a dopant concentration between 10^{17} and 10^{18} cm⁻³, a pore concentration of 10^2 cm⁻³ and a dislocation density of 10^4 cm⁻². Figures 3; references 5: 1 Russian, 4 Western.

Diffusion Waveguides in Polycarbonate

964D0047C St. Petersburg PISMA V ZHURNAL
TEKHNICHESKOY FIZIKI in Russian 26 May 95
Vol 21 No 10, (manuscript received 14 Feb 95) pp
25-28

[Article by A. V. Tomov, Institute of Applied Optics,
Academy of Sciences of Belarus, Mogilev]

[FBIS Abstract] This paper examines waveguides manufactured at room temperature by submerging substrates of polycarbonate in a solution of methyl red indicator in a complex solvent based on orthoxylol. The diffusion time is from 0.5 to 16 minutes. The waveguides have a smooth, virtually linear function of the index of refraction from the surface to the substrate. There is a drastic change at the waveguide-substrate interface. In the best samples optical losses did not exceed 2.8 dB/cm ($\lambda = 0.633 \mu\text{m}$). A mathematical model is proposed which describes the index of refraction profile, which is of particular importance in the study of nonlinear phenomena in these waveguides. Figures 2; references 9: 4 Russian, 5 Western.

Effective Heating of Electrons and Ions by Low Hybrid Waves in an FT-2 Tokamak

964D0047D St. Petersburg PISMA V ZHURNAL
TEKHNICHESKOY FIZIKI in Russian 26 May 95
Vol 21 No 10, (manuscript received 16 Feb 95) pp 34-39

[Article by V. N. Budnikov, V. V. Dyachenko, L. A. Yesipov, Ye. R. Its, M. A. Irzak, S. I. Lashkul, K. A. Podushnikova, A. Yu. Stepanov; A. F. Ioffe Physico-technical Institute, Russian Academy of Sciences, St. Petersburg]

[FBIS Abstract] In low hybrid heating in an FT-2 tokamak wave absorption and ion heating is associated with the development of decay parametric instability of heating waves in the central plasma region. Generation of fast ions begins at the center at a minimum energy of eight times the ion temperature. As plasma density increases, the area of decay shifts to the periphery and local density increases slightly. The energy of the ions gradually increases due to the development of the longwave spectrum of the parametrically excited waves. Most ions are heated in this transition region. This is a detailed study of the heating of ions and electrons in the transition region of plasma densities. Installation and discharge parameters are given. The effect of low hybrid waves on plasma parameters and the dependence on density are shown in a figure. The highest efficiency

of heating is reached in a very narrow range of densities. Generation of fast ions begins at a density only somewhat lower than the low hybrid density. The central plasma region satisfies the conditions of low hybrid resonance and the heating can formally be considered classical. However, some facts point to a parametric mechanism, for example more slower ions than faster ions appear at lower densities, and the fact that the beginning of generation of fast ions occurs at the same time as a mechanism which leads to effective heating of electrons. It is stated that generation of fast ions and heating of electrons are associated with the development of parametric instability of the pump wave. A change in discharge parameters when a high-frequency pulse is used may cause a transition from a parametric to a classical mechanism of interaction. Figures 2; references 5 (Western).

Possibility of Establishing the Neutron Generation Mechanism in the Mechanical Effect on Deuterated Matter

964D0047E St. Petersburg PISMA V ZHURNAL
TEKHNICHESKOY FIZIKI in Russian 26 May 95
Vol 21 No 10, (manuscript received 15 Feb 95) pp 48-52

[Article by Ye. G. Fateyev, Institute of Applied Mechanics, Urals Division, Russian Academy of Sciences, Izhevsk]

[FBIS Abstract] In 1986 it was found that neutrons are emitted when there is a powerful mechanical effect on deuterated substances, but the neutron emission mechanism has remained a mystery. This paper discusses the possibility of establishing the mechanism of neutron emission which arises at the time of a rheological explosion or a rheological explosion-like process in impact loading and vibration disintegration of deuterated materials. It is more likely that the cause may be found using this type of process because a stage-by-stage analysis can be done. A classical mechanism of neutron generation is proposed which is associated with acceleration processes in the plasma discharges between the edges of microfractures. However, this type of discharge is only sporadic and one cannot unambiguously identify them with neutron emission bursts. Mechanical effects and low-frequency electric fields are used to determine the origin of neutron emissions. This paper discusses the method, but does not present results of the application of the model. Figure 1; references 18: 15 Russian, 3 Western.

High-Temperature Superconducting Compound
 $\text{YBa}_2\text{Cu}_3\text{Se}_x$, with $T_c = 371 \text{ K}$

964D0047F St. Petersburg PISMA V ZHURNAL
TEKHNICHESKOY FIZIKI in Russian 26 May 95
Vol 21 No 10, (manuscript received 7 Feb 95) pp 67-71

[Article by V. D. Shabetnik, S. Yu. Butuzov, V. I. Plak-
siy, Central Scientific Research Experimental Institute
of the Ministry of Defense of the Russian Federation,
Mytishchi]

[FBIS Abstract] A compound with the formula $\text{YBa}_2\text{Cu}_3\text{Se}_x$ (where x is disruption of the stoichiometry of Se, and varies from 0 to 0.5) was created to try to obtain a substance with a high temperature of transition to the superconducting state. X-ray analysis was used to study the compound. Specific features of its structure are discussed. The device used to prove the presence of superconducting properties in the compound is described. Superconductivity is signaled by a change in the sign of magnetic susceptibility and a drastic change in the resistance of the material. A figure shows the magnetic susceptibility and resistance for $\text{YBa}_2\text{Cu}_3\text{Se}_x$, and this is contrasted with the same information for $\text{YBa}_2\text{Cu}_3\text{O}_7$, a known superconductor. It is found that the transition temperature for the former is 371 K (93 K for the latter). The higher temperature is due to the presence of a selenide ion Se_2^{2-} in the crystalline lattice. The volume of material in the superconducting phase is 12 percent. Figures 4; references 2 (Russian).

Electric Conductivity of Heated Superdense Plasma

964D0047G St. Petersburg PISMA V ZHURNAL
TEKHNICHESKOY FIZIKI in Russian 26 May 95
Vol 21 No 10, (manuscript received 18 Jan 95) pp 89-92

[Article by V. V. Pogosov, I. T. Yakubov, Institute
of High Temperatures, Russian Academy of Sciences,
Moscow]

[FBIS Abstract] A superdense heated plasma arises when large energy fluxes affect matter, for example, irradiation of metal surfaces by strong subpicosecond laser pulses. The metal plasma does not expand, and retains its initial density. It cannot be described using common approximations. The plasma consists of ions of charge Ze and electrons with the parameters of ion-ion, electron-ion, and electron-electron interactions. The ion subsystem is described by a cellular model, each ion in a cell screened by Z electrons. The distribution of free electrons, which move unhindered from cell to cell, is found to be nearly uniform. The cell potential is defined and the effect of scattering on the ion core is considered. The time of flight through the cell is calculated classically. An equation is derived for the coefficient of electric conductivity. Comparison with experimental results shows that the cellular model developed here provides a good description, but can be refined. Figures 2; table 1; references 8: 2 Russian, 6 Western.

Estimation of the Thermodynamic Nonideality of the Detonation of an Emulsion Explosive

957A1198A Moscow *KHIMICHESKAYA FIZIKA* in Russian Nov 94 Vol 13 No 11, pp 79-87

[Article by V.V. Odintsov, V.I. Pepekin, and B.N. Kutuzov, Chemical Physics Institute imeni N.N. Semenov, Russian Academy of Sciences, Moscow; first paragraph is *KHIMICHESKAYA FIZIKA* abstract; manuscript received 5 Jul 94; UDC 534.222.2+536.7]

[FBIS Translated Text] *An attempt has been made to estimate the thermodynamic component of the nonideality of detonation in an ammonium nitrate-based mixture of emulsion explosive with glass microspheres as compared with the hydrodynamic component that is manifested in the effect of charge diameter on detonation rate. To obtain emulsion explosive and glass microsphere mixture detonation rates correlating with experimental data, the assumption was made that the reaction of products at the Chapman-Jouget point is incomplete. In other words, it was assumed that the products consist of three chemical subsystems and that each has its own chemical equilibrium established within it. The assumption of incomplete reaction of the emulsion explosive and glass microsphere mixture detonation products at the Chapman-Jouget point because of one of two factors (either the diffusion of the decomposition products of the emulsion matrix's components is insufficient or else the rate of the chemical reaction is insufficient on account of low temperatures) results in calculated and experimental relationships between the detonation rate and initial density that were consistent with one another. The order of the degree of thermodynamic nonideality numerically characterizing the degree of reaction of the products may be approximated by a linear dependence of the degree of reaction on the initial density with a slope coefficient on the order of 0.1-0.15 percent \times (kg/m³)⁻¹. According to the results of calculations performed by using a BKW-RDX model [BKW being an acronym for Becker-Kistiyakovskiy-Wilson equations of state], the diffusion factor should be the main reason for the increase in nonideality (decrease in the degree of reaction) as the concentration of hollow microspheres in the mixture with the emulsion matrix is increased. When a BKW-RR model is used, on the other hand, the effect of chemical kinetics cannot not be ignored.*

Emulsion explosives have come to be used extensively in the extraction industry thanks to their rather high detonation parameters, water resistance, and explosion-proof nature. The mixture's sensitivity is increased by adding hollow glass microspheres to the system, which reduces the density of the emulsion explosive and glass microsphere mixture.

Studying the process has made it possible to establish the characteristic features of an emulsion explosive's detonation as compared with other classes of explosives. It has, for example, been noted¹ that the density dependence of detonation rate indicates a behavior that is significantly different from that of powerful monomolecular explosives. The critical diameter of detonation increases exponentially as the emulsion explosive's density increases. It has also been noted² that the detonation rate of an emulsion explosive peaks at densities below its peak density. The deviation of experimental detonation rate values extrapolated for an infinite charge diameter from the values predicted on the basis of calculations performed by using the Becker-Kistiyakovskiy-Wilson [BKW] program or the Kemlet [transliteration] method will become greater as the initial density of the emulsion explosive and glass microsphere mixture is decreased.

Meyder³ [transliteration] noted similar detonation rate behavior for mixtures of solid ammonium nitrate with combustible components. The decomposition and reaction of the ammonium nitrate, part of which behaves as an inert component, has been hypothesized to be the cause. The experimental values of the detonation rate in Amatex-40 and Amatex-20 were successfully obtained in calculations performed under the assumption that 50 percent of the ammonium nitrate in the mixture reacts while 50 percent remains inert. The experimentally obtained values of the detonation rate in amatol are reproduced in calculations if 19 percent of the ammonium nitrate reacts while the rest remains inert.

In this study, an attempt has been made to estimate the thermodynamic component of the nonideality of detonation in an emulsion explosive and glass microsphere mixture as opposed to the hydrodynamic component that is manifested in the effect that charge diameter has on detonation rate.

The study is based on the results of a published experimental study¹ of the detonation of a emulsion explosive and glass microsphere mixture in which the starting mixture was obtained by adding unsorted hollow glass microspheres with a true density of 150 kg/m³ and average diameter of 70 μ m to an emulsion with the following composition (percent by weight): ammonium nitrate, 77; water, 16; oil, 6; and emulsifier, 1. The density of the matrix was specified as 1,353 kg/m³, and the particle size of the emulsion ranged from 1 to 5 μ m.

Table 1 presents the composition of the emulsion explosive and glass microsphere mixture and parameters of its components that were assumed in the thermodynamic calculations.

Table 1. Parameters of the Components

Component	Chemical Formula	Percent by Weight	Enthalpy, kJ/kg
Ammonium nitrate	$H_4N_2O_3$	77	-4,563
Water	H_2O	16	-15,860
Saturated hydrocarbon (liquid)	$(CH_2)_n$	6	-2,088
Oleic acid	$C_{18}H_{34}O_2$	1	-2,841
Glass	SiO_2	above 100 percent	-15,160

The calculations were performed by using Becker-Kistjakovskiy-Wilson equations of state with different sets of coefficients and the respective hypotheses regarding condensed carbon:

— BKW with an enthalpy of graphite formation of 15 kcal/mol⁴;

— BKW-RDX³ with the possibility of the formation of disperse diamond and graphite;

— BKW-TNT³ with the possibility of the formation of disperse diamond and graphite⁵;

— BKW-RDX³ with the possibility of the formation of disperse diamond and graphite⁵;

— BKW-R with an enthalpy of graphite formation of 12 kcal/mol⁴;

— BKW-RR with the possibility of the formation of disperse diamond and graphite.⁵

In all of the models, the graphite was assumed to be compressible and its behavior was described in terms of a Kovenko [transliteration] equation of state, whereas the glass and diamond were assumed to be incompressible.

Table 2 and Figure 1 present the results of equilibrium calculations of the detonation of an emulsion explosive and glass microsphere mixture within the framework of the aforesaid models. The points in Figure 1 represent experimentally obtained detonation rate data that have been extrapolated for an infinitely large charge diameter, which will for brevity's sake henceforth be termed the ideal detonation rate. The experimental value in Table 2, on the other hand, was obtained by a least squares approximation of the values of the ideal detonation rate¹:

$$D_i = 5.383\rho_0 - 152,$$

where the detonation rate is expressed in m/s and the density is expressed in kg/m³.

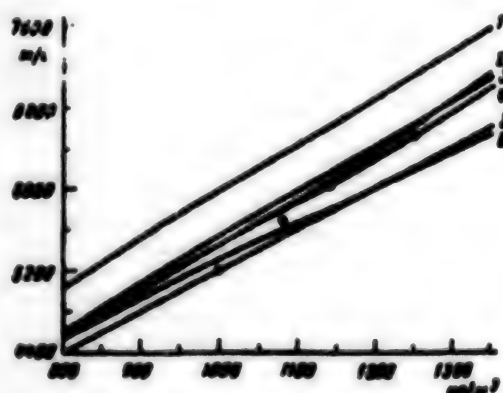


Figure 1. Dependence of the detonation rate of an emulsion explosive and glass microsphere mixture on initial density. Calculated lines: 1, BKW; 2, BKW-RDX; 3, BKW-R; 4, BKW-RDX; 5, BKW-RR; and 6, BKW-TNT. Points represent the extrapolation of experimental data for an infinitely large charge diameter. (Y-axis represents detonation rate in m/s.)

Table 2. Detonation Parameters of the Emulsion Matrix With a Density of 1,353 kg/m³

Model	Detonation Rate, m/s	Pressure, GPa	Temperature, K	Density, kg/m ³	Speed of Sound, m/s
BKW	7,584	18.41	974	1,772	5,791
BKW-RDX	7,134	16.04	976	1,764	5,473
BKW-TNT	6,547	14.53	1,254	1,805	4,907
BKW-RDX [*]	6,992	17.73	1,126	1,773	5,335
BKW-R	7,078	15.75	1,719	1,763	5,434
BKW-RR	6,613	13.95	1,781	1,770	5,054
Experiment ¹	7,131	-	-	-	-

A comparison of the lines in Figure 1 reveals that the density dependence of the detonation rate of an emulsion explosive and glass microsphere mixture differs for the different models. The slopes of the dependence are approximately identical for all of the models with the exception of the BKW-RR model, in which case the slope is noticeably smaller. The remaining models may be divided into three groups based on absolute value of the detonation rate: the BKW model yields the greatest value; the BKW-RDX, BKW-RDX^{*}, and BKW-R models yield mid-range values; and the BKW-TNT model yields the lowest value. The detonation rate values calculated on the basis of the BKW-RR model go from values characteristic for the middle group given low densities to the value calculated in accordance with the BKW-TNT model given near-peak densities. The slope of all of the calculated dependences is less than that of the experimental dependence in the case of the ideal detonation rate.

To obtain calculated rates of detonation of an emulsion explosive and glass microsphere mixture that correlate with data obtained in experiments, we assumed that the reaction of products at the Chapman-Jouget point was incomplete, which is just what Meyder assumed for mixtures of solid ammonium nitrate. Unlike Meyder, who considered part of the ammonium nitrate to be inert, we hypothesized that the products consist of three chemical subsystems and that each has its own established chemical equilibrium.

The first subsystem consists of products of the chemical decomposition of the aqueous solution of ammonium nitrate. The second subsystem consists of products of the chemical decomposition of the mixture of hydrocarbons. The third subsystem consists of products of the chemical interaction of all of the emulsion matrix's components. The ratio of components constituting each of the subsystems corresponds to the ratio of the same components in the starting emulsion matrix. In all remaining respects, the detonation products are considered to be a unified system, i.e., the state variables are one and the same for the entire system.

The said assumptions were all made on the basis of the diffusion theory of incomplete mixing of the products of the decomposition of the emulsion's components and the incompleteness of the chemical reaction, which is in turn the result of the products' rather low temperatures.

Figure 2 is a graph showing the calculated dependence of the detonation rate of an emulsion explosive and glass microsphere mixture on the degree of reaction of the products given an initial density of 1,000 kg/m³. The Y-axis represents detonation rate in m/s.

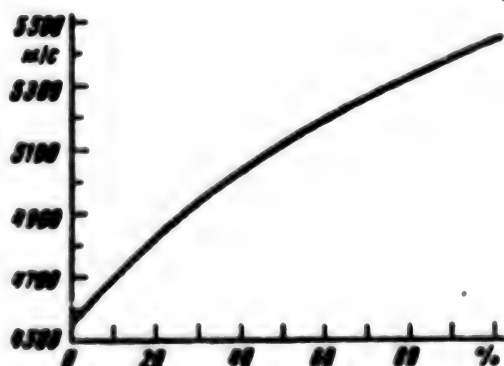


Figure 2. Calculated dependence of the detonation rate of an emulsion explosive and glass microsphere mixture on the degree of reaction of the products given an initial density of 1,000 kg/m³. (Y-axis represents detonation rate in m/s.)

It is proposed that the weight percent of the third subsystem, i.e., the weight percent of those products that have been completely mixed and that are in a state of chemical equilibrium, be considered the quantity characteriz-

ing the thermodynamic component of the nonideality of detonation. This quantity may henceforth be tentatively termed the degree of the products' reaction. The results of calculations of the detonation of an emulsion explosive and glass microsphere mixture presented in Figure 1 and Table 2 correspond to complete equilibrium in the products or a 100-percent degree of reaction.

It follows from the data presented in Table 2 that not only the detonation rate but also the other detonation parameters calculated within the framework of the various models differ markedly from one another. The very low detonation temperatures calculated in accordance with the BKW, BKW-RDX, BKW-TNT, and BKW-RDX* models are noteworthy. The detonation temperatures in the BKW-R and BKW-RR models correspond to the freezing temperatures of the detonation products of powerful explosives during the process of isentropic expansion.⁴

In the first model, the calculated and experimental values of the detonation rate of an emulsion explosive (without glass microspheres) virtually coincide, which makes it possible to assume that the detonation of the emulsion matrix is ideal and to calculate nonideality from the said value. In the calculations based on the BKW-RR model, it was not the absolute value of the detonation rate that was used as the criterion of thermodynamic nonideality of detonation but rather the decrease in detonation rate that occurred as the amount of glass microspheres in the mixture was increased and the mixture's density was thereby decreased.

Figures 2 through 4 present the results of calculations of thermodynamically nonideal detonation of an emulsion explosive and glass microsphere mixture by using the BKW-RDX model and assuming a density of 1,000 kg/m³. The very low temperature of the detonation products is noteworthy. Along with the other detonation parameters, Figure 4 presents the dependence of the amount of chemical heat released in the products at the Chapman-Jouget point on the degree of reaction. The amount of chemical heat was calculated as the difference between the values of the standard enthalpy of formation of the starting system and the detonation products at the Chapman-Jouget point given a temperature of 298.15 K

The sharp bend in the curve is the result of release of the heat of the phase transition of SiO₂ as the temperature of the products changes. The sharp bend does not affect the relationships of the other detonation parameters, however.

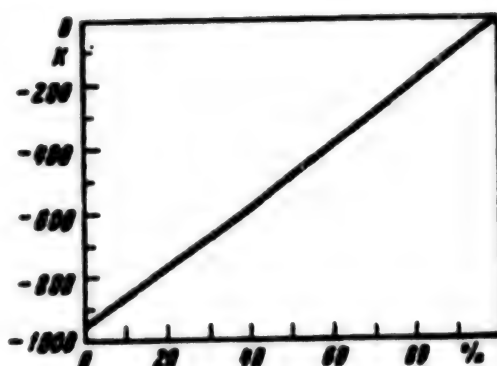


Figure 3. Calculated dependence of the change in detonation temperature of an emulsion explosive and glass microsphere mixture on the degree of product reaction given an initial density of 1,000 kg/m³.



Figure 4. Calculated dependence of chemical heat released in the products of the detonation of an emulsion explosive and glass microsphere mixture on the degree of product reaction given an initial density of 1,000 kg/m³. (Y-axis represents rate of heat release in kJ/kg.)

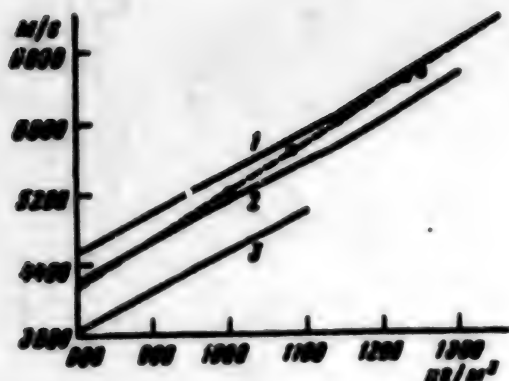


Figure 5. Dependence of the detonation rate of an emulsion explosive and glass microsphere mixture on initial density. Calculated lines represent different degrees of product reaction: 1 — 100 percent; 2 — 50 percent; 3 — 0 percent. Points and broken line represent the extrapolation of experimental data for an infinitely large charge diameter and their least squares approximation.¹ (Y-axis represents detonation rate in m/s, and x-axis represents initial density in kg/m^3 .)

When the degree of reaction of the products is changed from 100 percent to 0 percent, the detonation parameters are significantly altered. It may be anticipated that the experimentally obtained detonation rate value will correspond to some intermediate degree of reaction. Figure 5 presents the results obtained when the BKW-RDX model is used to calculate the dependence of the detonation rate of an emulsion explosive and glass microsphere mixture on the initial density for three different degrees of reaction of the products (100, 50, and 0 percent) as compared with data obtained in experiments. It is evident from Figure 5 that for each density value, it is possible to select a unique degree of reaction so that the calculated and experimental detonation rate values coincide.

Figures 6 and 7 present the values that are similarly obtained by using the BKW-RDX and BKW-RR models to calculate the degree of reaction as a function of the density of the emulsion explosive and glass microsphere mixture and weight percentage of glass microspheres in the mixture. Inasmuch as the detonation rate calculated for the emulsion matrix by using the BKW-RR model is much lower than the value obtained in experiments (see Table 2), the decrease in rate of detonation of the emulsion explosive and glass microsphere mixture that occurs as the content of glass microspheres in the mixture is increased and the density of the mixture is consequently reduced was therefore used as the criterion for selecting the degree of reaction instead of the absolute value of the detonation rate.

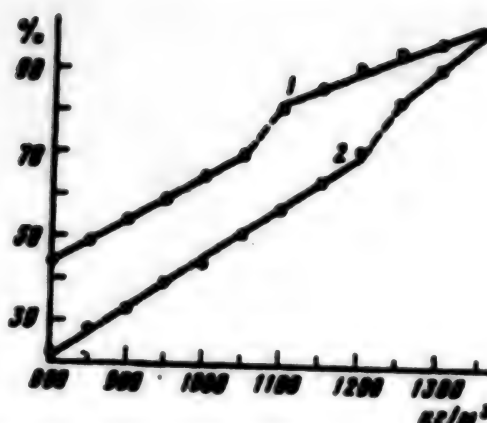


Figure 6. Dependence of the degree of reaction of products of the detonation of an emulsion explosive and glass microsphere mixture on initial density. Lines represent least squares approximations of the results of calculations (points) based on models: 1, BKW-RDX; 2, BKW-RR. (X-axis represents initial density in kg/m^3 .)

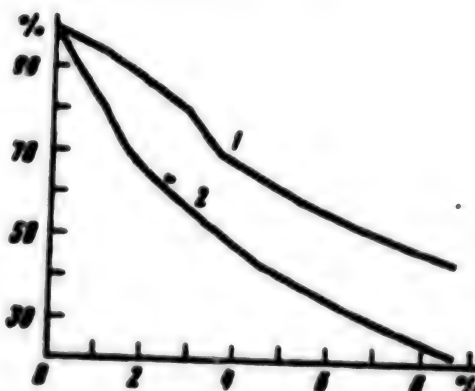


Figure 7. Dependence of the degree of reaction of products of the detonation of an emulsion explosive and glass microsphere mixture on weight percent of glass microspheres in the mixture. Lines represent calculations based on models: 1, BKW-RDX; 2, BKW-RR.

As is evident from the graphs presented in Figures 6 and 7, for an identical decrease in detonation rate, the BKW-RR model yields a degree of reaction that is an average of 15-20 percent lower than that yielded by the BKW-RDX model. The dependences of the degree of reaction on density of the mixture are more linear than are the dependences on weight percentage of glass microspheres in the mixture. Each of the dependences splits into two legs — a diamond leg and a graphite leg

depending on the structure of the free carbon formed in the products. The linear approximations (made by the least squares method) of the dependence of the degree of reaction of the products at the Chapman-Jouget point on initial density are expressed in terms of the following relationships:

For BKW-RDX:

diamond leg, $x = 0.7554\rho_0 - 0.8$;

graphite leg, $x = 0.1046\rho_0 - 39.9$;

For BKW-RR:

diamond leg, $x = 0.1651\rho_0 - 123.5$;

graphite leg, $x = 0.123\rho_0 - 75.9$;

where x is the degree of reaction expressed as a percentage and ρ_0 is the initial density of the emulsion explosive and glass microsphere mixture in kg/m^3 .

It may thus be concluded that the thermodynamic nonideality of the detonation of an emulsion explosive and glass microsphere mixture increases in a more or less linear manner as the density of the mixture decreases and is characterized by a rate of change in degree of product reaction at the Chapman-Jouget point on the order of 0.1 to 0.15 percent/(kg/m^3).

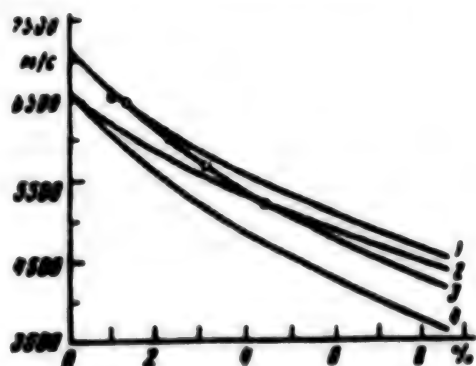


Figure 8. Dependence of the detonation rate of an emulsion explosive and glass microsphere mixture on weight percent of glass microspheres in the mixture. Calculated lines: BKW-RDX, 100-percent reaction; 2, BKW-RR, 100-percent reaction; 3, BKW-RDX, partial reaction; 4, BKW-RR, partial reaction. Points represent the extrapolation of experimental data for an infinitely large charge diameter. (Y-axis represents detonation rate in m/s .)¹

Figures 8 through 11 are graphs of the results of thermodynamically nonideal detonation of an emulsion explosive and glass microsphere mixture and the resultant values obtained for the degree of reaction. For the

sake of comparison, the same figures also contain the results of calculations performed for the case of completely ideal detonation. Except for temperature (Figure 10) and chemical heat (Figure 11), the detonation parameters as a function of density of the starting mixture behave similarly for all of the models considered.

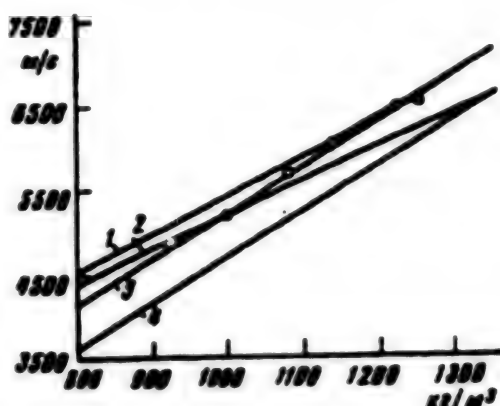


Figure 9. Dependence of the detonation rate of an emulsion explosive and glass microsphere mixture on initial density. Calculated lines: BKW-RDX, 100-percent reaction; 2, BKW-RR, 100-percent reaction; 3, BKW-RDX, partial reaction; 4, BKW-RR, partial reaction. Points represent the extrapolation of experimental data for an infinitely large charge diameter.¹ (Y-axis represents detonation rate in m/s .)

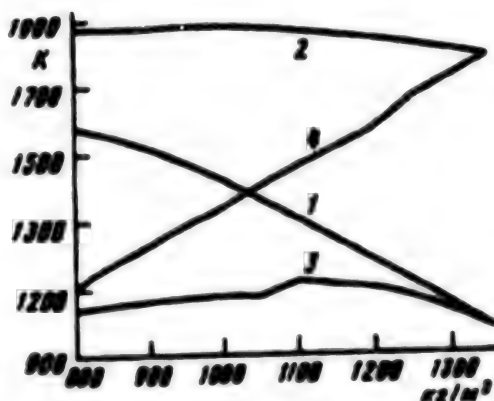


Figure 10. Dependence of the detonation temperature of an emulsion explosive and glass microsphere mixture on initial density. Calculated lines: BKW-RDX, 100-percent reaction; 2, BKW-RR, 100-percent reaction; 3, BKW-RDX, partial reaction; 4, BKW-RR, partial reaction. (X-axis represents initial density in kg/m^3 .)

In the calculations based on the BKW-RDX model the temperature of ideal detonation remains virtually unchanged and amounts to approximately 1,000 K, whereas using the BKW-RR model results in a decrease from a temperature of 1,800 K in the case of ideal detonation of the emulsion matrix to 1,100 K in the case of the maximum degree of nonideality. The amounts of chemical heat calculated for ideal detonation obtained by using the two models are virtually identical, whereas the values calculated for thermodynamically nonideal detonation differ significantly. This is because of the difference in the products' temperature behavior: Given the low temperature of the BKW-RDX model, silicon oxide undergoes two phase transitions, which in turn affects the dependence of chemical heat on initial density.

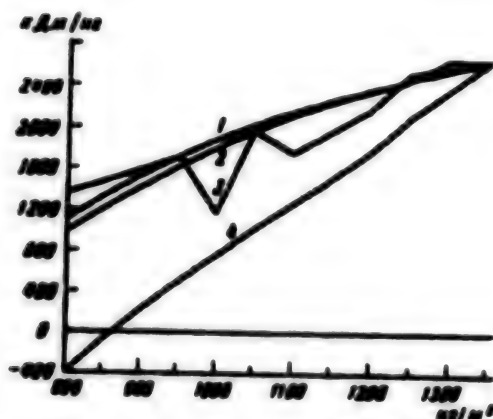


Figure 11. Dependence of the chemical heat released in the products of the detonation of an emulsion explosive and glass microsphere mixture on initial density. Calculated lines: 1, BKW-RDX, 100-percent reaction; 2, BKW-RR, 100-percent reaction; 3, BKW-RDX, partial reaction; 4, BKW-RR partial reaction. (X-axis represents initial density in kg m^{-3}).

The assumption that the reaction of products of the detonation of an emulsion explosive and glass microsphere mixture at the Chapman-Jouget is incomplete, possibly because of insufficient diffusion of the products of the decomposition of the emulsion matrix's components or

possibility because of the insufficient rate of occurrence of the chemical reactions on account of low temperatures, thus made it possible to achieve calculated dependences of the detonation rate on initial density that were comparable to the dependences obtained in experiments. The order of the degree of thermodynamic nonideality, which is a numerical characterization of the degree of reaction of the products, may be estimated by a linear dependence of the degree of reaction on the initial density with a slope coefficient on the order of 0.1 to 0.15 percent $\times (\text{kg/m}^3)^{-1}$.

According to calculations performed by using the BKW-RDX model, the diffusion factor should be the main cause for the increase in nonideality (decrease in degree of reaction) as the concentration of hollow microspheres in the mixture with the emulsion matrix is increased. The reason for this is that the temperature of the products of thermodynamically nonideal detonation remains virtually unchanged (see Figure 10). Using the BKW-RR model makes it possible to consider both the diffusion factor and the effect of chemical kinetics as result of the significant temperature drop of thermodynamically nonideal detonation.

References

1. J. Lee, F.W. Sandstrom, B.G. Craig, P.-A. Persson, Proc. Ninth Symp. (Int.) on Detonation. Res. Centr for Energ. Mater., New Mexico, 1989, p 263.
2. J. Lee, P.-A. Persson, PROPELLANTS, EXPLOSIVES, PYROTECHNICS, Vol 15, 1990, p 208.
3. Ch. Meyder, Numerical Modeling of Detonation, translated from English, Mir, Moscow, 1985.
4. M. Finger, E. Li, F. Khelm, et al., Detonatsiya i vzryvchatyye veshchestva (Detonation and Explosives), Mir, Moscow, 1981, p 70.
5. V.V. Odintsov, S.A. Gubin, V.I. Pepekin, L.N. Akimova, KHIMICHESKAYA FIZIKA, Vol 10, No 5, 1991, p 687.
6. S.A. Gubin, V.V. Odintsov, V.I. Pepekin, Termodinamicheskiye raschety detonatsii kondensirovannykh veshchestv (Thermodynamic Calculations of the Detonation of Condensed Materials), Preprint, Chernogolovka, IKhF AN SSSR, 1986, p 24.

Generation Mechanism of a Photodissociative Laser Based on the Electron Transition of the Fine Structure of a Chlorine Atom $^2P_{1/2} \rightarrow ^2P_{3/2}$

957A1206A Moscow *KHIMICHESKAYA FIZIKA* in Russian Dec 94 Vol 13 No 12, pp 3-13

[Article by A.I. Nadkhin (deceased) and Ye.B. Gordon, Chernogolovka Affiliate, Power Generation Problems Institute, Russian Academy of Sciences; first paragraph is *KHIMICHESKAYA FIZIKA* abstract; manuscript received 23 Dec 93; UDC 621.373.826.038.823]

[FBIS Translated Text] A study examined the lasing mechanism of a pulse laser at the transition between components of the fine structure of a chlorine atom, i.e., $^2P_{1/2} \rightarrow ^2P_{3/2}$ ($\lambda = 11.33 \mu\text{m}$) during photodissociation of iodine monochloride (ICl). The dependence of output power on the following was studied: energy and spectral composition of the pumping, pressure of the ICl and its chemical purity, and the number of pumping pulses before the mixture is replaced. The important role of processes of quenching of the Cl^* on the photolysis products, i.e., the I atoms and especially the Cl^* atoms that impede chemical purification of the lower laser level under conditions of high-power lamp pumping because of its preferential drain in reactions with the native ICl molecules, was noted. A quasi-continuous lasing model, including one with solar pumping, was shown to be possible in principle, and the conditions required for achieving it were discussed.

Introduction

In the past few years, the following two types of photodissociative gas lasers have aroused special interest:

1. Lasers with solar pumping (space or ground based) capable of converting solar energy directly into the energy of laser radiation. The success of such lasers is contingent upon having an active medium that is capable of operating with a high coefficient of converting solar energy in a closed cycle in a continuous or periodic pulse mode.
2. Lasers operating in the mid-infrared range and lasing in an atmospheric window ($\lambda = 11\text{-}13 \mu\text{m}$) for purposes of transmitting energy to satellites, probing deep space, and conducting space communications or else in a range ($\lambda = 2\text{-}5 \mu\text{m}$) where interference on the part of the earth's thermal radiation with laser communication is minimal provided that the lasers are located outside the atmosphere.

Three active media for gas lasers with solar pumping have been proposed and studied in the literature: the familiar iodine atom laser, which has a wavelength of $\lambda = 1.315 \mu\text{m}$ and uses photodissociation of various per-

fluoroalkyl iodides^{1,2}; the atomic bromine laser, which operates at a wavelength of $\lambda = 2.714 \mu\text{m}$ with photolysis of $\text{IBr}^{3,4}$; and the molecular CO_2 laser, which operates at $\lambda = 10.6 \mu\text{m}$ with photoinduction of Br_2/CO_2 by E-V transfer of energy from an excited bromine atom to carbon dioxide.^{5,6} None of these active media fully satisfies the aforementioned criteria. The search for new laser media for gas lasers with solar pumping is therefore both important and timely.

From that standpoint, this study examines the characteristics of a photodissociative ICl laser.

Iodine monochloride was first used as an active medium for a photodissociative laser with high-power lamp pumping in our laboratory.^{7,8} The wide and intensive band of continuous absorption of ICl between 360 and 600 nm ($\epsilon = 111 \text{ l/mol/cm}$ at 470 nm), which is the region of maximum solar radiation at the level of the earth, and the high quantum yield of chlorine atoms in the excited state $\text{Cl}(^2P_{1/2})$ during photodissociation of ICl ($\gamma_{\text{Cl}^*} \sim 0.55$ with wideband pumping⁹) make the said laser attractive for use with solar pumping.

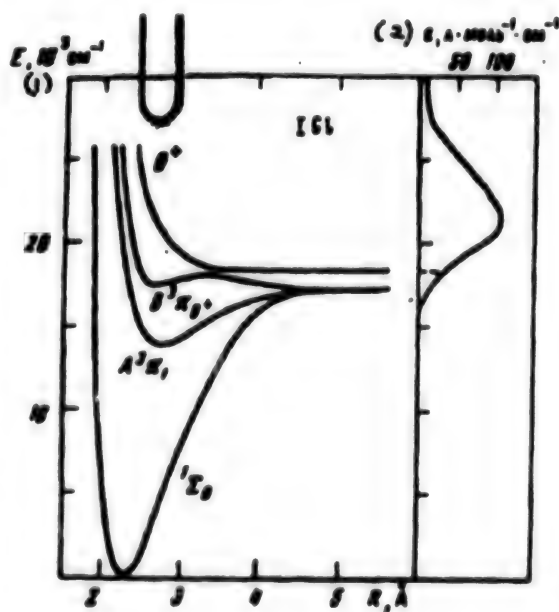
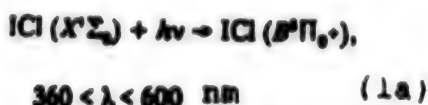


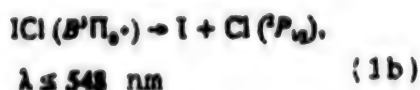
Figure 1. Potential energy curves and absorption spectrum of ICl. Key: 1, E , $10^3/\text{cm}$; 2, ϵ , l/mol/cm .

Figure 1 presents the potential energy curves and absorption spectrum of ICl. In the first absorption band, the probability of transition to the state $B^1\Pi_0^+$ is significantly higher than the probability of transition to

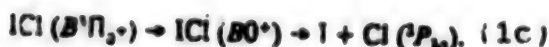
the state $A^3\Pi_1$ and $0^+. ICl is therefore initially excited into the state $B^3\Pi_{0+}$$



which may dissociate adiabatically

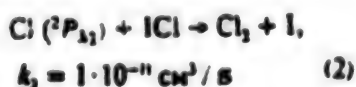


yielding a chlorine atom in an excited state, or nonadiabatically

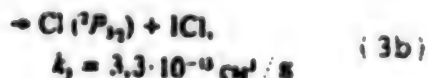
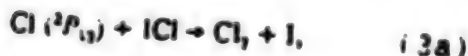


resulting in unexcited atoms. The domination of channel (1b) explains the inversion of the populations at the transition between levels of the fine structure $\text{Cl}(^2P_{1/2}-^2P_{3/2})$ ($\lambda = 11.33 \mu\text{m}$) in the very act of photodissociation.

The rapid secondary reaction of the unexcited chlorine (Cl) atoms with the native ICl molecules^{8,11,12}

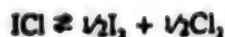


occurs at a rate that is more than 30 times faster than the total rate at which Cl^* is deactivated (here and henceforth $X^* = X(^2P_{1/2})$, $X = \text{Cl}, \text{Br}, \text{I}$)¹²



which additionally increases and maintains the inversion population at the laser transition thanks to selective depopulation of the lower laser level.^{*} The prerequisites for a laser with a continuous operating mode thus exist.

The radiative life time $\text{Cl}(^3P_{1/2})$ is very long (87.9 seconds¹³); however, the cross section of stimulated radiation is only half that in the analogous transition of the iodine atom used in the familiar laser with $\lambda = 1.315 \mu\text{m}$.¹⁶ At room temperature ($K = 3.2 \times 10^5$),¹⁷ the equilibrium constant



facilitates the regeneration of ICl molecules after photolysis and thus permits multiple lasing based on one mixture.

To clarify the mechanism of lasing, a study was conducted to determine the dependence of the laser's output power on the energy and spectral composition of light pumping, the pressure and chemical purity of the ICl, and the number of pumping pulses before the mixture was replaced. The effect of the addition of buffer gases to the working mixture was also examined. In addition, the method of laser atomic resonance spectroscopy was used to investigate the time profiles of inversion in the active medium.

1. Experimental Unit

Figure 2 is a diagram of the experimental unit. A quartz laser cell with a length of 120 cm and inner diameter of 2.8 cm and with NaCl Brewster windows had a 0.5-cm-thick outer "sleeve" that could be filled with gaseous or liquid materials when necessary to filter the pumping light. A quartz pulse lamp with xenon filling (pressure, Xe 1mF 15 torr; length, 120 cm) that was, together with the laser tube, located inside an aluminum foil reflector served as the light pumping source. The energy of the discharge loop ranged from 50 to 1,350 J, and the light pulse had a duration of approximately 6.5 μs at its half-height. An optical cavity with a base of approximately 2 m was formed by mirrors with a dielectric coating: an "opaque" mirror with a radius of curvature of 2 m and a flat mirror with a reflection factor of 95 or 90 percent at 11.33 μm . The energy of the laser radiation was measured with an IMO-2N calorimeter. The laser pulse's time characteristics were recorded by using a Ge: Au photoresistor (that had been cooled to 77 K) with a set of calibrated attenuators. An FEK-19 photoelement was used to control the lamp's light.

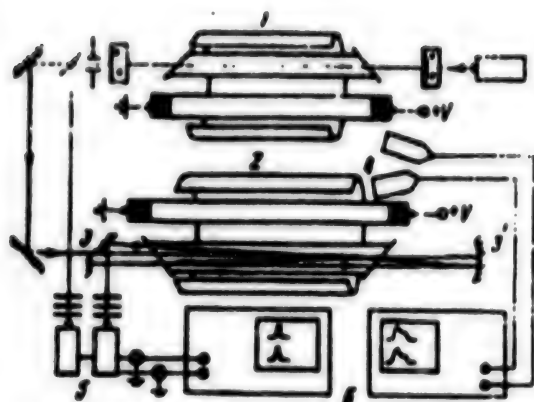


Figure 2. Diagram of the experimental unit: 1, sounding laser; 2, study laser (amplifier); 3 and 3', mirrors of the multipass circuit; 4, FEK-19 phototubes; 5, Ge:Au photoreceivers; and 6, oscillographs with memory.

All of the experiments were conducted under static conditions. The pressure measurements were taken with reference vacuum gauges and a type MAS-EZ pressure transducer with electrical output (upper limit, 30 torr) that was connected directly to a measuring cell. The iodine chloride was prepared as follows: Cl_2 with a grade of chemically pure was dried over P_2O_5 three times and subjected to vacuum distillation at 77 K. It was then mixed in a stoichiometric ratio (1:1) with I_2 . After the reaction had been completed, the composition of the gaseous phase over the ICl was analyzed and periodically checked based on its absorption spectra¹⁰ on a Specord UV-VIS spectrophotometer. The typical composition of the gas had a purity of approximately 99 percent.

2. Experiment Results

2.1. Characteristics of a Cl Laser

Even with pumping energies significantly above the threshold level and long pumping pulse durations (up to 15-20 μs), the lasing had the form of a pulse with $\tau_{1/2} \sim 5 \mu\text{s}$ and a delay relative to the beginning of light initiation of 1-2 μs . In view of the aforementioned effect of "eating away" of the lower laser level in the active medium of a chlorine laser (provided that the lower value of the constant k_1 is accurate), such short lasing pulses were somewhat unexpected because in a three-level laser with collision resettlement of the lower level, the duration of the lasing pulse is, as is well known, dictated by the duration of the pumping pulse. In a study⁴ that examined the characteristics of a Br laser operating with photodissociation of IBr and

having a kinetic diagram identical to that of a Cl laser, lengthening of the pumping pulse did not lead to a significant increase in the duration of lasing either. This indicates that in neither laser's kinetic diagram was consideration given to additional processes that either depopulate the upper laser level or slow down resettlement of the lower laser levels.

The pumping threshold amounted to 100 \pm 20 J, which is just 1.5 times higher than that of a bromine laser in the equivalent cavity.^{4,8} This corresponds to approximately 3,000 solar constants and, in principle, indicates the possibility of obtaining Cl lasing with solar pumping by using solar energy concentrators, which as is well known have a theoretical limit of approximately 20,000 solar constants.⁴ As the pressure of the ICl rises, the threshold lasing energy begins to increase when $[\text{ICl}] \geq 7$ torr (Figure 3). Consequently, operation under elevated pressures will only be possible given elevated degrees of solar energy concentration.

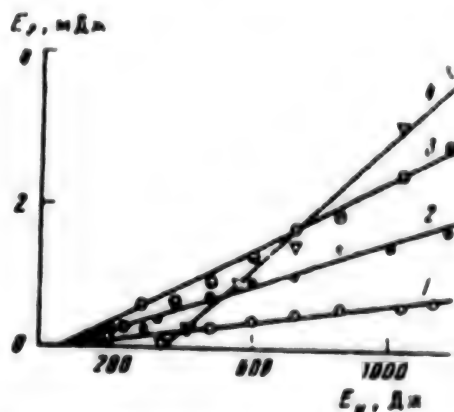
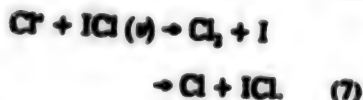
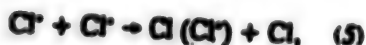


Figure 3. Dependence of the lasing energy of a Cl laser on pumping energies given different concentrations of ICl: 1.9 (1), 3.8 (2), 7.5 (3), and 25.3 (4) mm Hg. The x-axis represents pumping energy in joules, and the y-axis represents the lasing energy in millijoules.

The dependence of lasing energy on energy stored in the discharge loop (proportional to the light pumping energy) presented in Figure 3 is linear throughout the entire range of pumping energies ($E_{\text{pump}} = 0.1$ to 1.35 kJ) and ICl pressures (1 to 25 torr) studied. For a bromine laser, the increase in output power virtually ceased after $E_{\text{pump}} \cong 500$ kJ,^{4,8,10} which the authors of another study⁴ attributed to either heating of the active medium or quenching of the excited Br^* atoms on the iodine atoms. The absence of lasing energy saturation in an ICl laser may accordingly be explained as follows: a) the smaller

cross section of absorption of ICl compared with IBr and, consequently, the lesser amounts of heating; b) the stronger temperature dependences of the rate constants of the interaction of Cl^{*} and Cl atoms with ICl molecules as compared with the analogous dependences of the rate constants of the reaction of Br^{*} and Br atoms with IBr molecules; and c) the stronger quenching of Br^{*} atoms on the photolysis products of IBr (I, Br, and Br^{*} atoms and oscillation-excited molecules IBr(*v*)) as compared with the quenching of Cl^{*} atoms on the photolysis products of ICl (I, Cl, and Cl^{*} atoms and oscillation-excited molecules ICl(*v*)).



Unfortunately, the literature data regarding spin-orbital relaxation of Br^{*} and Cl^{*} atoms on atoms and radicals are extremely scant.^{2,19-21} The temperature dependences of the rate constants of the interaction of bromine atoms in ground and excited states with parent IBr molecules that were obtained by Boriyev et al.²² confirm that in an IBr laser, the effect of temperature is extremely important: k/k^* is approximately equal to 35 at 300 K versus only approximately 10 at 350 K. The temperature dependences of the rate constants of the reactions of Cl and Cl^{*} atoms with ICl are lacking in the literature.

The effect of inert gas additives on a Cl laser's output characteristics was studied to clarify the role of heating of the active medium. It turned out that the addition of He, Ar, and Xe does not result in an increase in the intensity and/or duration of the laser's lasing pulse. Moreover, a monotonic, albeit rather weak decrease in its output power was observed (the said decrease may well be explained by the collision broadening of the transition line Cl(²P_{1/2} - ³P_{2/2}) in the said atoms¹⁶). As is thus evident in Figure 4, for 9 torr, ICl, and $E_{\text{lase}} = 726$ J, adding 30 torr of He and Ar, as well as 40 torr of Xe, reduced E_{lase} by approximately half. Oxygen had a slightly stronger effect on lasing: When approximately 15 torr of O₂ was added, the laser's lasing energy [E_{lase}] dropped by half.

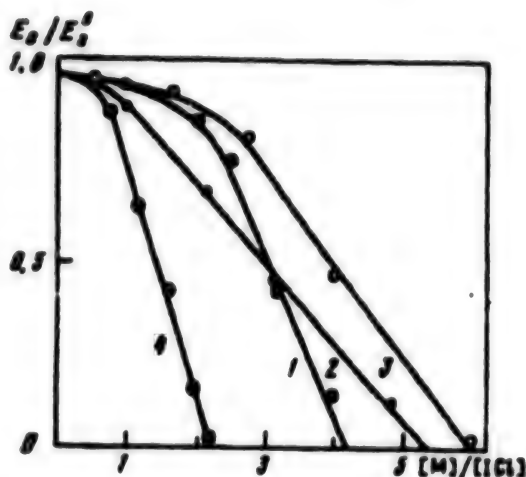


Figure 4. Dependence of the lasing energy of a Cl laser on concentration of the different additives to the active medium [M]: M = Ar (1), He (2), Xe (3), and O₂ (4); [ICl] = 3×10^{17} /cm³, $E_{\text{lase}} = 726$ J. The x-axis represents the concentration of a given additive, i.e., [M]/[ICl], and the y-axis represents the resultant lasing energy divided by the initial lasing energy, i.e., $E_{\text{lase}}/E_{\text{lase}}^0$.

Besides demonstrating that heating has no effect on the mechanism of lasing, the said results make it possible to estimate the upper bound of the rate constant of the quenching of Cl(²P_{1/2}) atoms on O₂ and noble gases. The estimates are consistent with data published in two studies^{12,23}; however, they contradict the results of other published studies.²⁴⁻²⁶ In one of those studies,²⁴ a rate constant of $2.1 \pm 0.5 \times 10^{-11}$ cm³/s was obtained by the method of vacuum ultraviolet adsorption spectroscopy for the process of quenching of Cl^{*} on O₂. That value was confirmed in a later study by the same team of researchers.²⁵ Clearly, with such a rate constant, adding even approximately 1 torr of O₂ with a lasing time scale of 10 μs should lead to a significant decrease in lasing energy. (Such behavior actually occurred when strong relaxants were used as additives: hydrogen and a number of multiatomic gases, i.e., CF₂Cl₂, CCl₄, CF₃Br, CF₃I, i-C₃F₇I, CH₃I, CD₃I, and SF₆, completely quenched the lasing energy even when added in very small concentrations (<1 torr), in total consistency with the values of the deactivation rate constants.⁶) Our estimate of the rate constant of the quenching of Cl^{*} on O₂ was $k \leq 3 \times 10^{-13}$ cm³/s.

A strong increase in rate constant in the series from He to Xe (from 3.8×10^{-13} cm³/s in the case of He to 1.8×10^{-11} cm³/s in the case of Xe) was discovered in one study²⁶ for the process of relaxation of an excited chlorine atom in collisions with atoms of inert gases. In another study,²⁷ the asymptotic method of plotting quasi-molecular terms was used to calculate the rate constants of spin-orbital relaxation, i.e., $F(^2P_{1/2})$ and $Cl(^2P_{1/2})$, during collisions with He, Ne, Ar, Kr, and Xe, and an inverse relationship was obtained: for the case of quenching of Cl^* , the rate constant decreases monotonically from 4.2×10^{-14} to 1.4×10^{-20} cm³/s in the series from He to Xe. As is evident from the curves presented in Figure 4, Ar and Xe are, at the very least, not more effective quenching partners for $Cl(^2P_{1/2})$ than He is. From our measurements and in view of experimental data on the quenching of excited chlorine atoms on Ar atoms^{12,21} and the results of a theoretical study,²⁷ it is obvious that the values presented elsewhere²⁶ for the rate constants of the relaxation of Cl^* on atoms of heavy noble gases are inflated by several orders of magnitude.

It is difficult to determine the reasons for so great a discrepancy between the data obtained in some published studies²⁴⁻²⁶ and our studies^{9,23} and other published data.^{12,20,28-30} This is especially true when consideration is given to the fact that the rate constants presented in the one group of studies²⁴⁻²⁶ for relaxation of Cl^* on O₂ and noble gases are highly inflated whereas the rate constants presented in the same studies²⁴⁻²⁶ for the cases of collision of $Cl(^2P_{1/2})$ atoms with molecules of H₂,^{21,23,28} CO₂,^{9,23} CH₄,²⁸ HCl,²⁹ Cl₂,¹² and H₂O³⁰ are low. Suffice it to present the opinion of the one team of researchers²⁹ that the time profile of the concentration, i.e., $[Cl^*(t)]$, with lamp photolysis of CCl₄ (the source of Cl^* atoms in the aforementioned group of studies²⁴⁻²⁶) is rather complicated and its decrease is not described in terms of a simple exponent as was proposed in the studies of Hussein's team.²⁴⁻²⁶

The relationships of lasing energy E_{lasing} on the concentration of ICl, i.e., $E_{\text{lasing}} = E([ICl])$, that are presented in Figure 5 are distinguished by the presence of saturation at an iodine chloride pressure above 10 torr. Because the layer of active substance under our conditions is optically transparent given ICl concentrations up to $[ICl] \geq 1.5 \times 10^{19}$ /cm³, the transition to saturation at such low pressures may be the result of either a decrease in the cross section of stimulated radiation in the laser transition as a result of collision broadening on the parent molecules (including when $[ICl]$ is 5 torr¹⁹) or the aforementioned processes (described in equations (3) through (7)) of spin-orbital relaxation $Cl(^2P_{1/2})$ of the

state on ICl and its photolysis products: iodine, chlorine atoms and oscillation-excited molecules $ICl(v)$.

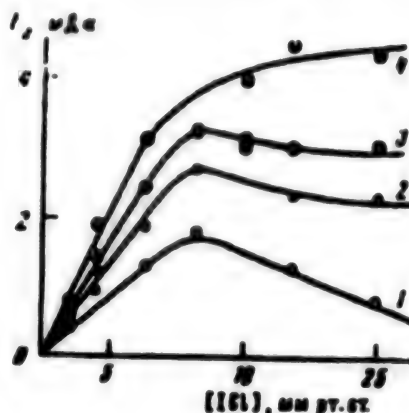


Figure 5. Dependence of the lasing energy of a Cl laser on the concentration of ICl at the following different pumping energies [E_{pump} : 600 (1), 864 (2), 1,037 (3), and 1,350 (4) J]. The x-axis represents the concentration of ICl in mm Hg, and the y-axis represents the lasing energy in millijoules.

The maximum energy of lasing obtained in a cavity with a 10% output mirror amounted to 4.5 ± 0.5 mJ with $E_{\text{pump}} \sim 1$ kJ and an iodine chloride pressure of approximately 18 torr. This is approximately one-third the lasing energy of a Br laser in an equivalent cavity in the optimum mode, which allowing for the difference in energy of the radiated quantum of $h\nu_{\text{Br}}/h\nu_{\text{Cl}} \cong 4$, indicates that both lasers have similar quantum efficiencies.

The absorption spectrum of ICl consists of two bands of identical intensity that are located in the visible (band 1) and ultraviolet (band 2) regions of the spectrum.¹⁰ Experiments involving filtration of a pulse lamp's radiation were performed to determine the contribution of the ultraviolet absorption band of ICl ($\lambda_{\text{max}} = 248$ nm, $\sigma_{\text{max}} = 4.4 \times 10^{-19}$ cm²)¹⁰ to the formation of $Cl(^2P_{1/2})$ excited atoms. For that purpose, gaseous Br₂ under a pressure of approximately 200 torr was let into the laser cell's "sleeve," which in turn weakened the luminous flux in the region $\lambda > 360$ nm by a factor of 7-10 virtually without touching the ultraviolet portion of the lamp's radiation. No laser radiation was observed when $E_{\text{pump}} = 1.3$ kJ and when the pressure of the iodine chloride amounted to about 9 torr. It is thus possible to draw the qualitative conclusion that during photolysis of ICl in the ultraviolet region of the spectrum with $\lambda < 360$ nm, the main atoms formed are chlorine

atoms in the ground state $^2P_{3/2}$ and $\gamma_{Cl} < 0.33$. It is thus the photodissociation of ICl in the visible band of absorption of light with $360 < \lambda < 548$ nm that is decisive to the formation of Cl * atoms. Consequently, with solar pumping of ICl, it is necessary either to cut off the ultraviolet portion of the radiation or, better yet, transform it into the visible region. Using a solution of the dye 490 RT (1.8-naphthylene-1',2'-benzimidazole) in benzene not only enabled us to eliminate photolysis of ICl in the ultraviolet region of the spectrum but also, thanks to the dye's luminescence, enabled us to increase the density of the luminous flux in the visible region of the spectrum and significantly improve the laser's operating stability.

Photodissociative Br lasers are known to be sensitive to molecular bromine impurities in IBr on account of the process of parasitic photodissociation of the Br $_2$ that mainly populates the lower laser level.^{4,18} An analogous effect may also be important for a Cl laser. Studies were therefore conducted to determine the effect that additions of Cl $_2$ to a Cl laser's active medium have on its lasing energy. It turned out that a chlorine laser is much more stable in the face of such impurities, and its lasing is completely cut off only when $[Cl_2]:[ICl] \cong 1$. Using the aforementioned dye 490 RT in the laser "sleeve" improves the stability of the laser's output characteristics when exposed to Cl $_2$ impurities by an additional factor of 1.5-2.

In cases of repeated photolysis (up to 50 flashes) without replacement of the active substance and with an interval of 1 minute between pulses, the intensity and shape of the laser signal and its delay time remained virtually unchanged from pulse to pulse. This confirms the effective regeneration of the starting ICl molecules in recombination processes and indicates that an ICl laser may operate in a sealed version.

2.2. Time Profile of an Inversion

Studies of the time behavior of inversion of the populations at the Cl($^2P_{1/2}$ - $^2P_{3/2}$) transition in the active medium of a Cl laser with different pumping levels are very important to assess the possibility of creating a quasi-continuous Cl laser with solar pumping. To take such measurements, the experimental unit was modified in accordance with a "generator-amplifier" circuit.¹⁶ An analogous photodissociative laser model was added to it (Figure 2) that served as a source of sounding laser radiation at the transition between levels of the fine structure of the chlorine atoms, and the study Cl laser was transformed into an amplifier (its resonator mirrors were removed and replaced with mirrors permitting multiple¹⁶ passage of the sounding radiation through the active medium). The sounding laser was triggered with a delay relative to the pulse of the amplifier lamp [τ_{Cl}], ranging from 0 to 1,000 μ s. The sounding laser's lasing

signal was a single pulse with a duration of 1.5 μ s. The gain [χ] of the laser's signals as it passed through the cell four times was found by using the relationship $\chi = \ln(I_1/I_2)$, where I_1 and I_2 are respectively the laser signal's measured intensities at the cell's entrance and exit and I_1^0 and I_2^0 are the analogous intensities for an empty cell.

The time dependence of the gain factor of a Cl laser, i.e., $\chi^{Cl}(t)$, was measured under the following conditions:

a) with an identical pumping energy, i.e., $E_{pump} = 1$ kJ (the degree of photodissociation of ICl was kept constant at $\alpha = 3$ percent) but with the ICl under different levels of pressure (0.5, 1.0, and 3.0 torr);

b) with an identical ICl pressure (3 torr) and different pumping levels, i.e., $E_{pump} = 1$ kJ ($\alpha = 3$ percent) and $E_{pump} = 270$ J ($\alpha = 0.9$ percent). Figure 6 presents the results. It turned out that the decrease in the curves plotted for $\chi^{Cl}(t)$ with one and the same pumping level but different ICl pressures is described by an identical overall constant [k_3^{eff}] of 5×10^{-12} cm 3 /s. At the same time, the drop in the curves given identical values of [ICl] but different values of α is described by significantly different values of k_3^{eff} , i.e., $(k_3^{eff})_1 = 5 \times 10^{-12}$ cm 3 /s ($E_{pump} = 1$ kJ, $\alpha = 3$ percent) and $(k_3^{eff})_2 = 8 \times 10^{-13}$ cm 3 /s ($E_{pump} = 270$ J, $\alpha = 0.9$ percent). The dependence of the value of k_3^{eff} on the degree of the active substance's collapse may be clearly traced, with the k_3^{eff} decreasing and approximating the published¹² value as α decreases. It is significant that channels (IV) through (VII) of the quenching of Cl($^2P_{1/2}$) on the photolysis products of ICl play an important role even with degrees of collapse as low as $\alpha \geq 1$ percent and must be taken into consideration in the kinetic diagram describing lamp photolysis of ICl with high-power pumping.

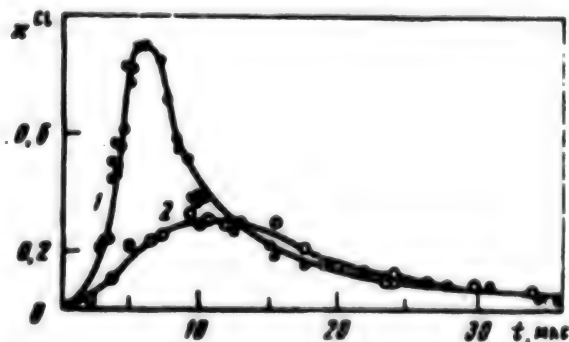


Figure 6. Dependence of intensification of a Cl laser's resonance signal during photolysis of ICl: $[ICl] = 1 \times 10^{17}$ /cm 3 ; $E_{pump} = 1,000$ (1) and 270 (2) J. The x-axis represents time in microseconds, and the y-axis indicates χ^{Cl} .

All of the photolysis products of ICl, i.e., atoms of Cl, Cl^{*}, and I, are easily observed in our method when the active medium is sounded with I and Cl lasers. Of course, the formation of oscillation-excited ICl(X, v) molecules is in principle possible when ICl is excited with white light. As is clear from the absorption spectrum of ICl that is presented in Figure 1, however, the relative concentration of such "hot" molecules barely exceeds 3-5 percent of the total number of dissociated molecules of ICl. It is therefore not likely that process (VII) plays an important role in the kinetic diagram of photolysis of ICl. (Therein lies one of the main differences between ICl and IBr. In the case of wideband photolysis of molecules of IBr, the quantum yield of the photodissociation may amount to approximately 0.25-0.5, which means that the concentrations of atoms and "hot" molecules, i.e., IBr(X, v) are comparable.²²)

We will note that the concentration of I atoms increases on account of process (II), reaching a stationary state at the level $2\alpha[\text{ICl}]$, whereas the concentration of chlorine atoms in the ground state [Cl] falls symbasically to zero ($k_2 = 1.5 \times 10^{-12}$ cm³/s). Using a Cl laser to sound a measuring cell containing ICl under a pressure of 3 torr mixed with CCl₄ under a pressure of 1 torr, which is an effective quencher of the state Cl(²P_{1/2}), demonstrated that there are virtually no Cl atoms left after about 5 μs following the beginning of the light pulse. At our request, the authors of one study²¹ measured the value of the constant k_6 by the method of electron paramagnetic resonance in a flow and obtained a value of $4.7 \pm 1.5 \times 10^{-12}$ cm³/s. It may therefore be hypothesized that the contribution of process (VI) to quenching of the Cl^{*} atoms is, in all likelihood, also small.

In addition, given the very different kinetics at short times, the rear "tails" of the amplification profiles $\chi^{\alpha}(t)$ at times $t \geq 12$ μs virtually coincide for degrees of collapse of ICl of 3 and 0.9 percent (see Figure 6) despite the fact that the concentration of iodine atoms under the said conditions differs by more than a factor of 3. This indicates that quenching of the Cl(²P_{1/2}) atoms on I atoms (process (IV)) is less important than is their relaxation in process (V). The profile of $\chi^{\alpha}(t)$ calculated by the Runge-Kutta method from a kinetic diagram that includes processes (I) through (VI) is consistent with the results of an experiment performed with values of $k_4 = 5 \pm 2 \times 10^{-12}$ and $k_5 = 10 \pm 5 \times 10^{-11}$ cm³/s, respectively. We will note that while the value obtained for k_4 by variation falls within the range of published values for the rate constants of the process of relaxation of X(²P_{1/2}) atoms on I atoms,^{19,20} the value obtained for k_5 appears to be anomalously high at first glance. However, the literature already mentions just such an anomaly for the quenching of I(²P_{1/2}) on Cl atoms.^{31,32}

Final clarification of the contribution of processes dictating the kinetics of inversion during photolysis of ICl requires experiments with independent sources of Cl^{*}, Cl, and I atoms. The results that have been obtained nevertheless demonstrate that during high-power lamp photolysis of ICl (when $\alpha > 1$ percent), additional channels of quenching of Cl(²P_{1/2}) on photolysis products appear and sharply increase the overall constant of its decomposition so that k_5^{eff}/k_5 comes to equal to approximately 1/2. Using reaction (II) to selectively purify the lower laser level and thereby create a quasi-continuous Cl laser, including a Cl laser with solar pumping, becomes problematic. Evidently, a continuous lasing mode can only be achieved in the case of "weak" pumping with degrees of dissociation (α) of markedly less than 1 percent, wherein quenching of the Cl^{*} atoms on the photolysis products is not yet significant.

The existing discrepancy between the values of the rate constant of the process of deactivation of Cl^{*} molecules by ICl molecules, i.e., k_5 , measured in published studies^{12,13} may be explained by proceeding from the results obtained. In one of the two studies,¹³ high-power lamp photolysis of ICl ($E_{\text{pump}} = 1.2$ kJ, $\alpha = 5$ percent) was used, and the measured value of $k_5 = 3 \times 10^{-11}$ cm³/s was evidently due to the effect of secondary processes of quenching on the photolysis products. In the other study,¹² laser photolysis of ICl ($\alpha \leq 0.5$ percent) was used, the likelihood of a contribution on the part of the secondary processes was low, and the value $k_5 = 3.3 \times 10^{-13}$ cm³/s obtained was obviously closer to reality. The reason why the value obtained for k_5 in a recent publication¹⁴ was inflated by nearly an order of magnitude is more difficult to determine inasmuch as the authors also used laser photolysis. It can only be speculated that either the degree of photodissociation of ICl in the said study¹⁴ was higher or else the accumulation procedures used (the said procedures were used¹⁴ to improve the signal:noise ratio) made it impossible to avoid the effect of secondary processes of quenching on the photolysis products.

3. Conclusion

The output characteristics of a pulse photodissociative Cl laser and the time behavior of the inversion in its active medium have thus been studied. The fundamental possibility of implementing a quasi-continuous lasing mode, including one with solar pumping, has been demonstrated. An analysis of the reasons for the rapid decomposition of the inversion indicated that processes of quenching of Cl^{*} atoms on the photolysis products, i.e., atoms of I and especially Cl^{*}, play an important role in the said laser's lasing mechanism. Chemical purification of the lower laser level by its preferential

drain in a reaction with the parent ICl molecules can therefore only be implemented with low levels of light pumping.

References

1. J.H. Lee, W.R. Weaver, APPL. PHYS. LETTERS, Vol 39, No 2, 1981, p 137.
2. J.H. Lee, B.M. Tabibi, D.H. Hummes, W.R. Weaver, OPT. COMMUNS, Vol 74, No 6, 1990, p 380.
3. L.I. Bubnova, Ye.B. Gordon, A.I. Nadkhin, et al., KVANTOVAYA ELEKTRONIKA, Vol 10, No 4, 1983, p 883.
4. L.E. Zapata, R.J. De Young, J. APPL. PHYS., Vol 54, No 4, 1983, p 1686.
5. W.L. Harries, J.W. Wilson, SPACE SOLAR POWER REVIEW, Vol 2, No 2, 1981, p 367.
6. B.F. Gordiets, V.Ya. Panchenko, UFN, Vol 149, No 3, 1986, p 551.
7. V.Ch. Bokun, Ye.B. Gordon, L.N. Krasnoperov, et al., KVANTOVAYA ELEKTRONIKA, Vol 13, No 7, 1986, p 1319.
8. A.I. Nadkhin, Dissertation for degree of candidate of physical and mathematical sciences, 31 October 1989, Chernogolovka, 1989, 209 pages.
9. K. Balasubramanian, CHEM. PHYS., Vol 95, No 2, 1985, p 225.
10. D.J. Seery, D. Britton, J. CHEM. PHYS., Vol 68, No 8, 1964, p 2263.
11. M.A.A. Clyne, H.M. Cruse, J. CHEM. SOC. FAR. TRANS. II, Vol 68, No 8, 1972, p 1377.
12. Chichinin, S.A. Chasovnikov, L.N. Krasnoperov, CHEM. PHYS. LETTERS, Vol 138, No 4, 1987, p 371.
13. R.J. Donovan, D. Husain, TRANS. FAR. SOC., Vol 64, No 9, 1968, p 2325.
14. J. Park, Y. Lee, G.W. Flynn, CHEM. PHYS. LETTERS, Vol 186, No 5, 1991, p 441.
15. A.C. Stanton, CHEM. PHYS. LETTERS, Vol 122, No 4, 1985, p 385.
16. S.A. Sotnichenko, V.Ch. Bokun, and A.I. Nadkhin, OPTIKA I SPEKTROKOPIYA, Vol 67, No 5, 1989, p 1013.
17. W.H. Evans, T.R. Munson, D.D. Wagmann, J. ES. NATL. BUR. STAND (U.S.), Vol 55, No 1, 1955, p 147.
18. Ye.B. Gordon, A.I. Nadkhin, S.A. Sotnichenko, KVANTOVAYA ELEKTRONIKA, Vol 12, No 8, 1985, p 1914.
19. M.B. Faist, R.B. Bernstein, CHEM. PHYS. LETTERS, Vol 64, No 7, 1976, p 2971.
20. J. De Juan, I.W.M. Smith, J. CHEM. SOC. FAR. TRANS. II, Vol 81, No 11, 1985, p 1695.
21. I.B. Bykhalo, Ye.B. Gordon, A.I. Perminov, V.V. Filatov, KHIMICHESKAYA FIZIKA, Vol 11, No 8, 1992, p 1097.
22. I.A. Boriev, E.B. Gordon, A.A. Efimenko, Proceedings of XIII Int. Conference on Photochemistry, Budapest, 1987, p 330.
23. S.A. Sotnichenko, V.Ch. Bokun, A.I. Nadkhin, CHEM. PHYS. LETTERS, Vol 153, No 6, 1988, p 560.
24. I.S. Fletcher, D. Husain, CHEM. PHYS. LETTERS, Vol 49, No 3, 1977, p 516.
25. R.H. Clark, D. Husain, J. CHEM. SOC. FAR. TRANS. II, Vol 80, No 1, 1984, p 97.
26. I.S. Fletcher, D. Husain, J. CHEM. SOC. FAR. TRANS. II, Vol 74, No 1, 1978, p 203.
27. A.I. Reznikov, S.Ya. Umanskiy, KHIMICHESKAYA FIZIKA, Vol 9, No 10, 1990, p 1299.
28. A.I. Chichinin, L.N. Krasnoperov, Proceedings of XIII Int. Conference on Photochemistry, Budapest, 1987, p 261.
29. E. Tiemann, H. Kanamori, E. Hirota, J. CHEM. PHYS., Vol 88, No 4, 1988, p 2457.
30. A.I. Chichinin, L.N. Krasnoperov, CHEM. PHYS. LETTERS, Vol 160, No 4, 1989, p 448.
31. M.D. Burrows, J. CHEM. PHYS., Vol 81, No 8, 1984, p 3546.
32. G.E. Hall, S. Arepalli, P.L. Houston, J. CHEM. PHYS., Vol 82, No 6, 1985, p 2590.

Footnote

*It should be noted that the spread between the values provided in the literature for the total rate constant of processes (3a) and (3b) is very large. Donovan and Husain¹³ give a value that is two orders of magnitude larger than that given elsewhere,¹² and a recent publication¹⁴ presented an intermediate value, i.e., $k_t = (4 \pm 1) \times 10^{-12} \text{ cm}^3/\text{s}$. One of the purposes of the present study was therefore to clarify the reasons for so great a discrepancy.

Using the Electrical Response of a Semiconductor Compound To Record the Chemical Transformation Behind the Front of a Shock Wave

957A1206B Moscow *KHIMICHESKAYA FIZIKA*
in Russian Dec 94 Vol 13 No 12, pp 175-176

[Article by S.S. Nabatov and A.V. Lebedev, Chemical Physics Institute, Russian Academy of Sciences, Chernogolovka; manuscript received 12 Jul 94; UDC 539.63+537.226]

[FBIS Translated Text] A method of recording exothermal reactions in shock wave conservation experiments based on the phenomenon of thermoelectromotive force in semiconductors has been proposed.¹ In essence, the method entails measuring the difference in potentials between the faces of a semiconductor element that is placed into a flat storage tube together with the study sample. It was noted that such a formulation can only be used to study processes in an unloaded state. The method was tested by way of the example of the reaction occurring during the synthesis of stannous monosulfide [SnS] from the elements. A thermoelement was made from SnS, which is a *p*-type semiconductor with a thermoelectromotive force coefficient of $+550 \mu\text{V}/^\circ$ under normal conditions. It turned out that with a loading pressure of 16 GPa, the reaction is initiated within several milliseconds after the shock wave enters the study specimen. There are, however, grounds for hypothesizing that at higher pressures, the synthesis may occur directly in a shock-compressed state. As has been shown elsewhere,² an SnS thermoelement generates electrical signals with a characteristic amplitude of 200-300 mV when a shock wave passes through it. This communication proposes that the said signals be used to observe the reaction occurring in the system $\text{Sn} + \text{S}$ during shock compression. The experiment consisted of sounding a shock-compressed mixture with a secondary shock wave. It was hypothesized that if a semiconductor compound forms behind the front of the first shock wave, it should give an electrical response to the second compression and that, possibly, uneven heating of the reaction product behind the shock wave front may result in a signal with a single compression. Preliminary experiments were conducted to study the response of the system $\text{Sn} + \text{S}$ to gradual loading with a pressure of approximately 10 GPa in the first shock wave and approximately 15 GPa in the second shock wave. It turned out that the two loading amplitudes were insufficient to effect a synthesis reaction in a shock-compressed state, which is consistent with findings reported elsewhere.¹ Additional experiments with higher pressures are planned to clarify whether it is possible to effect a synthesis reaction behind the front of a shock wave.

References

1. S.S. Nabatov, S.O. Shubitidze, V.V. Yakushev, *FIZIKA GORENIYA I VZRYVA*, Vol 26, No 6, 1990, p 114.
2. S.S. Nabatov, A.V. Lebedev, *KHIMICHESKAYA FIZIKA*, Vol 12, No 2, 1993, p 187.

Estimating the Parameters of a New Class of Detonation of Emulsion Explosives

957A1199A Moscow *KHIMICHESKAYA FIZIKA*
in Russian Dec 94 Vol 13 No 12, pp 131-144

[Article by V.V. Odintsov, V.I. Pepekin, and B.N. Kutuzov, Chemical Physics Institute imeni N.N. Semenova, Russian Academy of Sciences, Moscow; first paragraph is *KHIMICHESKAYA FIZIKA* abstract; manuscript received 9 Aug 94; UDC 534.222.2+536.7]

[FBIS Translated Text] This article is devoted to quantitative estimation of the parameters characterizing the detonation of mixtures of an emulsion explosive and gunpowder based on thermodynamic calculations of ideal and nonideal detonation. Two models of the equation of state of gaseous detonation products, i.e., the Becker-Kistjakovskiy-Wilson [BKW]-RDX and BKW-RR models, were used for the calculations. Three thermodynamic models of detonation were examined: 1) ideal detonation, i.e., complete chemical equilibrium of the detonation products at the Chapman-Jouget point; 2) slightly less than ideal detonation, i.e., the detonation products consist of two chemical subsystems (decomposition products of the emulsion matrix and gunpowder) such that a state of equilibrium exists within each subsystem and the two systems do not interact with one another; and 3) far-from-ideal detonation, i.e., the detonation products consist of three chemical subsystems (decomposition products of the aqueous ammonium nitrate solution, hydrocarbon mixture, and gunpowder) such that a state of equilibrium exists within each subsystem and the three systems do not interact with one another. It is demonstrated that estimates of detonation parameters based on thermodynamic calculations and general discussions of the mechanism of emulsion explosives' sensitivity make it possible to boost the said explosives' power characteristics by 10-20 percent or more by replacing the hollow glass microspheres or gas-forming additives with disperse explosives, especially gunpowder, the problem of whose recycling in view of conversion of the defense complex still remains far from solved.

It has been hypothesized elsewhere¹ that the power characteristics of emulsion explosives that are now in existence and used in practice may be increased significantly by adding gunpowder to them. This study

is devoted to quantitative estimation of the detonation parameters of mixtures of emulsion explosives and gunpowder.

Emulsion explosives possess good water resistance and are fairly explosion-proof, which is to say that they have a low sensitivity to initiation of detonation. While low sensitivity is a positive feature during manufacturing and transport, it becomes a drawback when the explosives are put to direct use inasmuch as the traditional method of boosting their sensitivity by adding hollow microspheres or a gas bubble-forming chemical reagent to the emulsion matrix results in a decrease in charge density and, accordingly, in a decrease in the efficiency of the detonation products of emulsion explosives.

Adding disperse gunpowder to the emulsion matrix instead of microspheres or gas-forming chemical additives

appears to be a promising way of overcoming the aforesaid drawback in using emulsion explosives. When that is done, a smaller reduction or possibly even an increase in detonation parameters as the amount of additive is increased may be anticipated instead of the rather sharp drop in detonation parameters that occurs when hollow glass microspheres are added to the emulsion matrix.²

Table 1 presents the composition of an emulsion matrix identical to the one considered elsewhere.² The composition of the gunpowder whose detonation parameters were studied in another study³ (gunpowder No. 3) and that was considered as an additive to commercial explosives in yet another study¹ are also presented in Table 1 along with the enthalpies of the various components.

Table 1.

Component	Chemical Formula	Weight Percent	Enthalpy, kJ/kg
Ammonium nitrate	$H_4N_2O_3$	77	-4,563
Water	H_2O	16	-15,860
Saturated hydrocarbon (liquid)	$(CH_2)_n$	6	-2,088
Oleic acid	$C_{18}H_{34}O_2$	1	-2,841
Gunpowder	$C_{24}H_{33.13}N_{13.19}O_{46.68}$	more than 100 percent	-2,272

The emulsion matrix's density was determined to equal 1,353 kg/m³.⁴ For the sake of generalization, two gunpowder density values, i.e., 1,600 and 1,353 kg/m³, have been considered. The latter value was selected to clarify the effect of adding gunpowder apart from the effect of the initial charge density.

Two different cases of determining charge density were thus considered: 1) an increase in charge density from 1,353 kg/m³ by adding gunpowder with a density of 1,600 kg/m³ and 2) a charge density of 1,353 kg/m³ that remains constant regardless of the amount of gunpowder in the mixture. Figure 1 is a graphic representation of the dependence of charge density on the amount of additive for each of the two aforesaid cases. The dependence of the density of the mixture of an emulsion matrix and hollow glass microspheres is presented for comparison's sake. In Figure 2 the relative increase in initial charge density when gunpowder is used as compared with when hollow glass microspheres are used to boost emulsion

explosives' sensitivity is presented as a function of the amount of additive.

The Automated System of Thermodynamic Calculations and Algorithms [ASTRAL] was used to perform the thermodynamic calculations of emulsion explosives' detonation based on a method described elsewhere.⁵ A Becker-Kistyakovskiy-Wilson [BKW] equation served as the equation of state of the detonation products' gaseous phase. The possibility of formation of disperse diamond and graphite was assumed for the condensed carbon.⁶ A Kovenko [transliteration] equation of state was used for the graphite, and the diamond was considered incompressible.

Two sets of coefficients were used for the BKW equation: BKW-RDX and BKW-RR. Selection of the two sets of coefficients for calculating emulsion explosives' detonation is discussed elsewhere.²

Table 2.

Explosive	Density, kg/m ³	Model	Detonation Rate, m/s	Pressure, GPa	Temperature, K
Gunpowder	1,353	BKW-RR	6,706	15.68	3,375
	1,353	BKW-RDX	6,568	15.44	2,834
Emulsion matrix	1,353	BKW-RR	6,613	13.55	1,781
	1,353	BKW-RDX	7,134	16.04	976

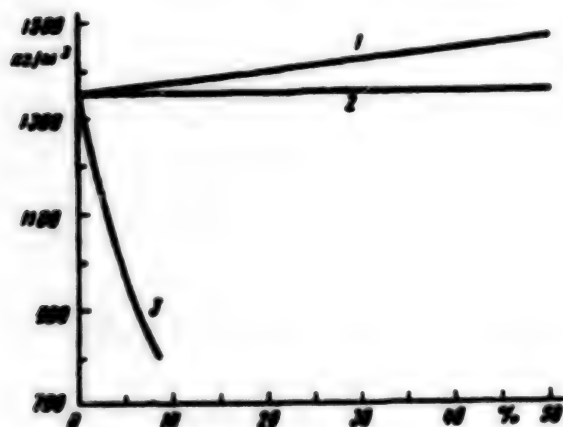


Figure 1. Dependence of mixture density on weight percent of additive to the emulsion matrix. Lines: 1, gunpowder, 1,600 kg/m³; 2, gunpowder, 1,353 kg/m³; 3, hollow glass microspheres, 150 kg/m³. Values on the y-axis represent quantities in kg/m³.

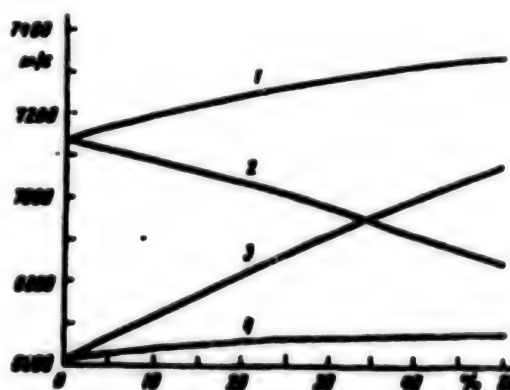


Figure 3. Dependence of the rate of ideal detonation on the weight percent of gunpowder in a mixture with an emulsion matrix. Lines: 1, BKW-RDX model and gunpowder density of 1,600 kg/m³; 2, BKW-RDX model and gunpowder density of 1,353 kg/m³; 3, BKW-RR model and gunpowder density of 1,600 kg/m³; 4, BKW-RR model and gunpowder density 1,353 kg/m³. Values on the y-axis represent quantities in m/s.

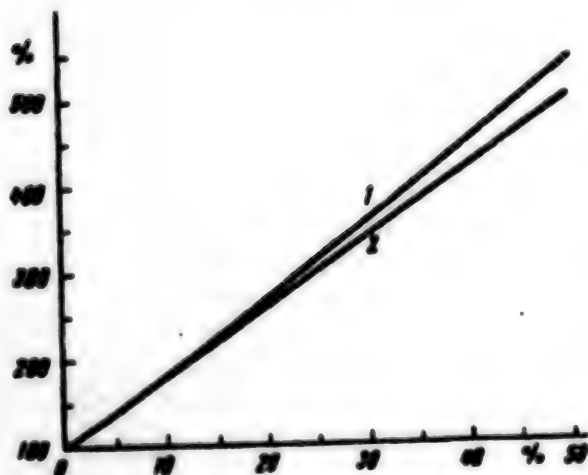


Figure 2. Dependence of the relative increase in mixture density when microspheres are replaced with gunpowder on the weight percent of additive. Lines: 1, gunpowder, 1,600 kg/m³; 2, gunpowder, 1,353 kg/m³.

Figure 3 is a graph representing the calculated equilibrium dependence of the detonation rate on the amount of gunpowder in a mixture with an emulsion matrix. The results of calculations based on the BKW-RDX and BKW-RR models differ not only from the standpoint of absolute values but also with respect to the nature of the dependences. In fact, when the initial charge density remains unchanged (1,353 kg/m³), the detonation rate calculated on the basis of the BKW-RDX equation moderates as the amount of gunpowder in the mixture is increased, whereas the BKW-RR equation yields a slight increase in detonation rate. This is a consequence of the fact that the calculated detonation rates of gunpowder are slightly different for the BKW-RDX and BKW-RR models, whereas the detonation rate of the emulsion matrix calculated according to the BKW-RDX model is significantly higher than that calculated by using the BKW-RR equation (Table 2). Moreover, the emulsion matrix detonation rate calculated on the basis of the BKW-RDX model is noticeably higher than that calculated for gunpowder with an identical initial charge density.

A somewhat different pattern is observed in the behavior of the dependence of the detonation pressure on the amount of explosive in the mixture that is graphed in Figure 4. When the initial density of the mixture remains unchanged ($1,353 \text{ kg/m}^3$), the detonation pressure remains nearly unchanged for the BKW-RDX model (changing from 16.04 GPa for the emulsion to 15.44 GPa for gunpowder), whereas it increases from 13.95 GPa (emulsion) to 15.68 GPa (gunpowder) for the BKW-RR model.

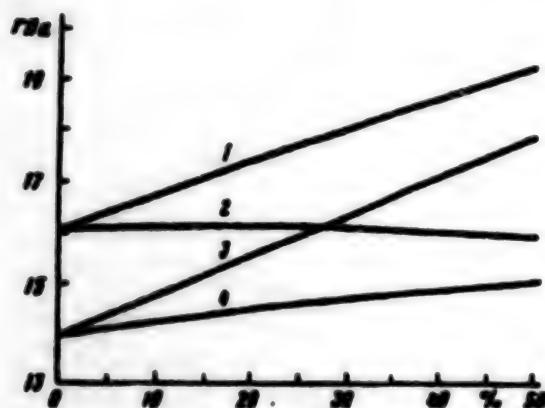


Figure 4. Dependence of the pressure of an ideal detonation on the weight percent of gunpowder in a mixture with an emulsion matrix. Lines: 1, BKW-RDX model and gunpowder density of $1,600 \text{ kg/m}^3$; 2, BKW-RDX model and gunpowder density of $1,353 \text{ kg/m}^3$; 3, BKW-RR model and gunpowder density of $1,600 \text{ kg/m}^3$; 4, BKW-RR model and gunpowder density $1,353 \text{ kg/m}^3$. Values on the y-axis represent quantities in GPa.

When the initial density of the mixture is increased on account of the gunpowder's higher density, the detonation rate and pressure both increase as the amount of gunpowder additive is increased.

Figure 5 presents graphs of the temperature of the detonation products of the study systems as a function of the amount of gunpowder in the mixture. The said temperature behaves similarly in both models and in both methods of determining initial density. This is because the temperature of gunpowder's detonation products is much higher than the temperature resulting from detonation of the emulsion matrix. As expected for the BKW equation, the detonation temperature of the mixture with the higher density was lower than the detonation temperature of the mixture with the lower density. The very low detonation temperature of the emulsion, as calculated in accordance with the BKW-RDX model (see Table 2), is noteworthy.

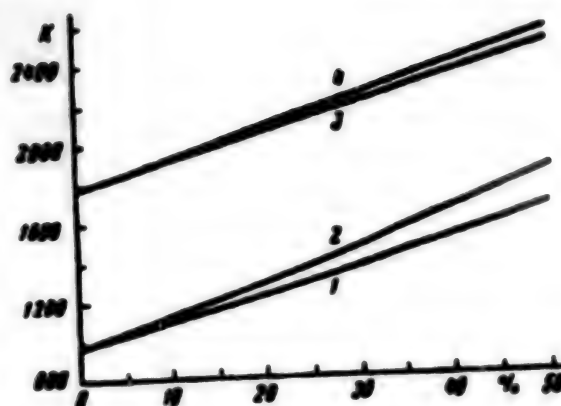


Figure 5. Dependence of the temperature of the products of an ideal detonation on the weight percent of gunpowder in a mixture with an emulsion matrix. 1, BKW-RDX model and gunpowder density of $1,600 \text{ kg/m}^3$; 2, BKW-RDX model and gunpowder density of $1,353 \text{ kg/m}^3$; 3, BKW-RR model and gunpowder density of $1,600 \text{ kg/m}^3$; 4, BKW-RR model and gunpowder density $1,353 \text{ kg/m}^3$. Values on the y-axis represent quantities in K.

The advantage of using gunpowder instead of hollow microspheres in a mixture with an emulsion matrix may be graphically illustrated by the ratio of the detonation rates of the said mixtures given an identical weight percent of additive in the mixture. Figure 6 is a graph representing the dependence of the ratio of the detonation rates of mixtures of emulsion with gunpowder and with microspheres for the two equation of state models and two methods of determining the charge density of a mixture with gunpowder. Previously calculated² values obtained by using the BKW-RDX and BKW-RR models and assuming partial reaction of the detonation products by matching the slopes of the calculated and experimentally obtained dependences of the detonation rate on initial charge density were used as values for the detonation rate of mixtures of an emulsion matrix and microspheres. As follows from the graph in Figure 6, when the amount of additive to the emulsion matrix is increased, the ratio of the detonation rates increases sharply. The calculated rate of the detonation of an emulsion explosive with gunpowder is thus approximately twice that of the detonation rate of a mixture with microspheres when the weight percent of additive is assumed to be approximately 10 percent.

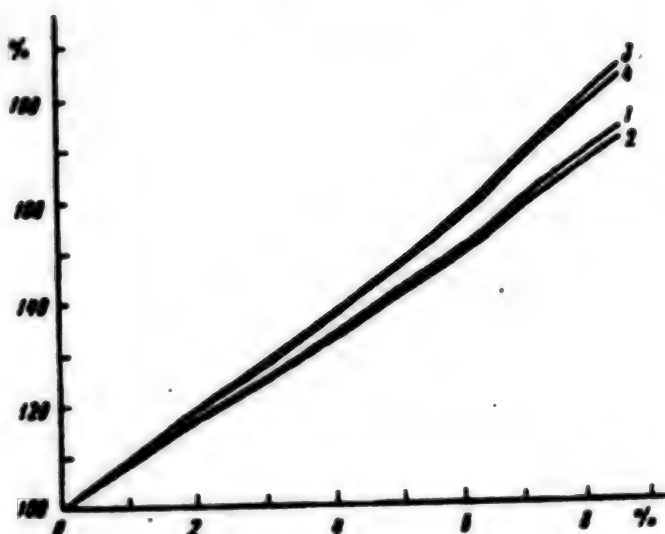


Figure 6. Dependence of the ratio of the rate of ideal detonation of a mixture with gunpowder to rate of ideal detonation of a mixture with microspheres on the weight percent of additive. Lines: 1, BKW-RDX model and gunpowder density of 1,600 kg/m³; 2, BKW-RDX model and gunpowder density of 1,353 kg/m³; 3, BKW-RR model and gunpowder density of 1,600 kg/m³; 4, BKW-RR model and gunpowder density of 1,353 kg/m³.

Those results were, however, obtained in the case where completely ideal detonation was assumed for the mixtures with gunpowder and thermodynamically nonideal detonation with incompletely reacted products at the Chapman-Jouget point was assumed for the mixtures with microspheres. For that reason, to examine the effect of the possibility of thermodynamic nonideality of the detonation of mixtures of an explosive emulsion with gunpowder, we will consider two additional cases. The first is the worst possible case, and it may serve as the lower bound of our estimate of the said mixtures' detonation parameters.

The first case of thermodynamic nonideality of detonation may be modeled by assuming that the detonation products of the emulsion matrix and gunpowder do not engage in a chemical reaction with one another. When such is the case, the entire system is assumed to consist of the following three chemical subsystems whose products are in a state of chemical equilibrium: 1) a solution of ammonium nitrate in water; 2) a mixture of hydrocarbons; and 3) gunpowder. There is no chemical interaction between subsystems, which is to say that the state variables at the Chapman-Jouget point are identical throughout the entire system.

The calculation results demonstrate that the absence of chemical interaction between the decomposition products of the emulsion matrix and gunpowder have virtu-

ally no effect on the parameters of the mixture's detonation. This is expressed in the indistinguishability of the lines depicting the dependence of the detonation parameters of mixtures of emulsion matrix and gunpowder in Figures 3 through 5 for completely ideal and thermodynamically nonideal (two subsystems) detonation. The dependence of the ratio of the detonation rate of a mixture of emulsion and gunpowder to the detonation rate of a mixture of emulsion and microspheres on the weight percent of additive in the case of thermodynamically nonideal detonation virtually coincides with the corresponding dependence for completely ideal detonation.

A different pattern is observed in the case of thermodynamic nonideality and the formation of three chemical subsystems in the detonation products. The said case corresponds to the case of thermodynamically nonideal detonation with a zero degree of product reaction that was examined elsewhere.² For brevity's sake, we will refer to the system in question (three subsystem) as thermodynamically nonideal detonation with a zero degree of reaction. Because the decomposition products of the oxidizing subsystem (solution of ammonium nitrate in water) do not react with the decomposition products of the burning subsystem (hydrocarbon mixture), a substantial portion of the chemical component will not be transformed into the thermal and elastic components of

the internal energy to the Chapman-Jouget point. As a result, the detonation parameters turn out to be significantly lower than in the cases considered previously.

Figure 7 is a graph representing the dependences of the rate of thermodynamically nonideal detonation of a mixture of emulsion matrix and gunpowder on the amount of additive as calculated by using the two equation of state models and two methods of specifying initial charge density in the case of a zero degree of product reaction. The dependences differ from the cases of ideal and slightly less than ideal detonation. The detonation rate values for a zero degree of reaction that are obtained with both models are significantly lower than that for a pure emulsion. As the amount of gunpowder in the mixture increases, the detonation rate increases and approaches the detonation rate of ideal and slightly less than ideal detonation.

The possibility of obtaining higher detonation parameter values when gunpowder is added to the emulsion matrix instead of hollow microspheres, even in the case of detonation with a zero degree of product reaction, is illustrated in Figure 8, which graphs the dependences of the ratio of the detonation rates of mixtures with gunpowder and a zero degree of product reaction to the detonation rates of mixtures with microspheres on the amount of additive in the emulsion mixture.

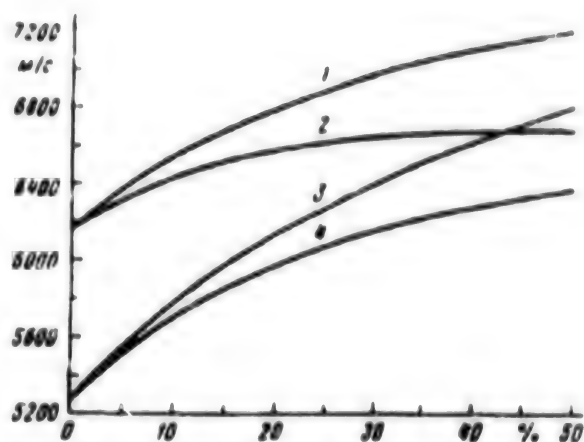


Figure 7. Dependence of the rate of far-from-ideal (with a zero degree of product reaction) detonation on the weight percent of gunpowder in a mixture with an emulsion matrix. Lines: 1, BKW-RDX model and gunpowder density of 1,600 kg/m³; 2, BKW-RDX model and gunpowder density of 1,353 kg/m³; 3, BKW-RR model and gunpowder density of 1,600 kg/m³; 4, BKW-RR model and gunpowder density 1,353 kg/m³. Values on the y-axis represent quantities in m/s.

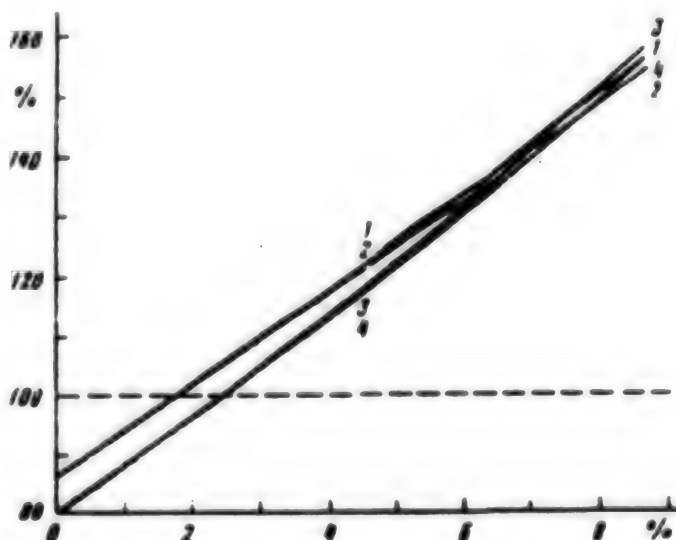


Figure 8. Dependence of the ratio of the rate of a far-from-ideal detonation (with a zero degree of product reaction) of a mixture with gunpowder to the rate of detonation of a mixture with microspheres on the weight percent of additive. Lines: 1, BKW-RDX model and gunpowder density of 1,600 kg/m³; 2, BKW-RDX model and gunpowder density of 1,353 kg/m³; 3, BKW-RR model and gunpowder density of 1,600 kg/m³; 4, BKW-RR model and gunpowder density 1,353 kg/m³.

The detonation rate of pure emulsion in the case of a zero degree of reaction is less than the rate of ideal detonation, which is what a comparison with experimental data⁴ indicates that detonation of pure emulsion is, and amounts to more than 80 percent of the rate of ideal detonation. When, however, the amount of additive in the mixture is increased to levels as low as 1.5-2.5 percent (by weight), the rate of far-from-ideal detonation of a mixture with gunpowder becomes comparable to the rate of somewhat nonideal detonation of a mixture with microspheres.

When the amount of additive is increased further, the ratio of the rates increases rapidly. At a concentration of additive equal to 9 percent (by weight), the detonation rate of a mixture with gunpowder and a zero degree of product reaction exceeds the rate of somewhat nonideal detonation of a mixture with microspheres by 50-60 percent.

It follows from experimental data⁴ that the critical diameter of detonation of a mixture of emulsion and microspheres, which characterizes the charge's sensitivity, reaches 25 mm and virtually stops decreasing at densities below 1,200 kg/m³, which corresponds to approximately a concentration of microspheres in the mixture equal to 1.6 weight percent. The experimentally obtained⁴ dependences of detonation rate on the initial density peak at approximately the same value. It may be assumed that the values of the rate of somewhat nonideal detonation of a mixture of emulsion and microspheres calculated on the basis of the BKW-RDX and BKW-RR models with the given charge density are optimum for actual use from the standpoint of the relationship of the detonation rate and critical diameter. The specified detonation rate values calculated in accordance with the two equation of state models may therefore be used as reference values for determining the effectiveness of adding gunpowder instead of microspheres. Specifically, detonation rates that have been calculated for mixtures of emulsion and gunpowder by using the respective models for the two methods of determining charge density may be referenced to the said values.

The graphs presented in Figures 9 and 10 represent the ratios of the detonation rates of mixtures of emulsion matrix with gunpowder to reference values of the detonation rate of a mixture of emulsion matrix and microspheres as a function of the amount of gunpowder in the mixture for the two different methods of determining mixture density.

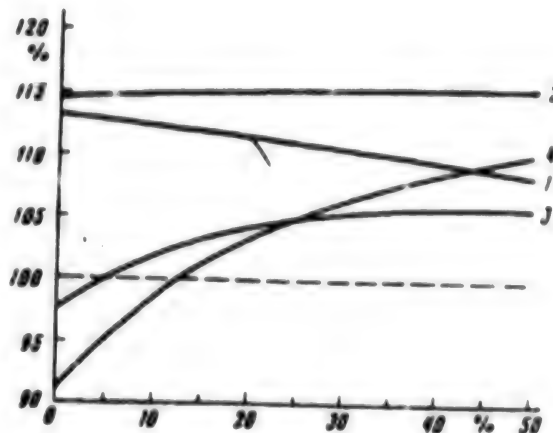


Figure 9. Dependence of the relative rate of detonation on a mixture's weight percent of gunpowder with a density of 1,353 kg/m³. Lines: 1, ideal detonation, BKW-RDX model; 2, ideal detonation, BKW-RR model; 3, far-from-ideal detonation, BKW-RDX model; 4, far-from-ideal detonation, BKW-RR model.

It is evident from Figure 9 that when the density of the mixture equals the density of the emulsion matrix, it may be expected that adding gunpowder will increase the detonation rate by 10-15 percent over the reference values. The anticipated detonation rate of a mixture of emulsion and gunpowder should lie in the region whose upper bound is the dependence for an ideal detonation rate and whose lower bound is the dependence for detonation with a zero degree of product reaction. We will note the different natures of the dependences for ideal detonation rate calculated in accordance with the different equation of state models. In the case of the BKW-RR model, the relative rate of ideal detonation increases slightly as the amount of gunpowder in the mixture is increased, whereas it decreases in the case of the BKW-RDX model. The values obtained for the relative rate of detonation with a zero degree of reaction increase with both models, but to different degrees. In any case, the rate of detonation with a zero degree of product reaction surpasses the reference detonation rate of a mixture of emulsion and microspheres given a concentration (by weight) of gunpowder in a mixture with an emulsion matrix of more than 12 percent.

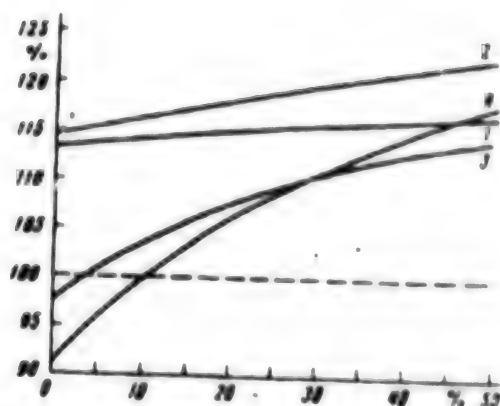


Figure 10. Dependence of the relative rate of detonation on a mixture's weight percent of gunpowder with a density of $1,600 \text{ kg/m}^3$. Lines: 1, ideal detonation, BKW-RDX model; 2, ideal detonation, BKW-RR model; 3, far-from-ideal detonation, BKW-RDX model; 4, far-from-ideal detonation, BKW-RR model.

In the case in which the density of the mixture increases as its content (by weight) of gunpowder with a density of $1,600 \text{ kg/m}^3$ is increased (Figure 10), the increase in the rate of ideal detonation when gunpowder is added reaches values 15-20 percent above the reference values for a mixture with microspheres. The nature of the dependences of the relative rates of ideal and maximally possible nonideal detonation is identical for both equation of state models: In all cases, the detonation rate increases as the concentration (by weight) of gunpowder in the mixture is increased. The only difference is in the dependences' slopes. The detonation rates, even with a zero degree of product reaction, are more than 10 percent higher than the reference values for the given concentration (by weight) of gunpowder in the mixture.

It has been hypothesized^{2,4} that detonation of an emulsion matrix is ideal from a thermodynamic standpoint, i.e., the detonation products are completely intermixed and react by the Chapman-Jouget point. Increasing the amount of hollow microspheres increases the mixture's sensitivity but results in an increase in the thermodynamic nonideality of detonation, as modeled² by an increase in the degree of chemical reaction of the decomposition products of the aqueous ammonium nitrate solution and hydrocarbon mixture.

Under the effect of the leading shock wave, the hollow glass microspheres collapse, thereby creating "hot spots" in whose vicinity chemical reactions in the emulsion matrix itself are initiated and accelerated in the initial stages. The creation of significant local temperature

spikes, i.e., hot spots, is, however, accompanied by a decrease in the total amount of energy per unit mass or volume of mixture because energy-releasing matter is displaced from part of the mixture's bulk and partially replaced by inert glass, which in turn results in a decrease in the degree of completion of the chemical reactions in the late stages of the reaction process after "dispersion" of the hot spots. As a result, the increase in temperature of the products in the chemical reaction zone as they move to the Chapman-Jouget point decreases significantly as a result of the lower average concentration of energy in the system, which in turn restrains the increase in the detonation product's temperature. The result is a closed circle, or in other words, a system with positive feedback. The decrease in the rate of energy release results in a decrease in temperature rise that in turn leads to a decrease in rates of energy release that in turn leads to a decrease in temperature rise, and so on.

Increasing an emulsion explosive's sensitivity by the addition of hollow glass microspheres thus leads to a decrease in the degree of reaction of the detonation products.

As has been noted,¹ achieving detonation conditions in gunpowder requires powerful initiation and a rather large charge diameter. Systematic experimental data regarding the sensitivity of gunpowder to shock wave initiation and its critical diameter are not to be found in the literature, however. Consequently, we can only make a few general remarks that must be verified by systematic experimental studies.

With regard to the possibility of the development of a detonation mode of propagation of the chemical decomposition of gunpowder under the effect of a shock wave passing from the emulsion matrix, we can only state that the rate and pressure of detonation of a pure emulsion are comparable with the detonation rate and pressure of gunpowder (see Table 2) and that it may therefore be anticipated that the strength of a shock wave is entirely adequate to initiate detonation in a gunpowder particle.

The critical diameter of detonation, even if it exceeds the dimensions of a gunpowder particle, is not directly applicable to the case under consideration inasmuch as the particle is surrounded by a dense medium subjected to shock wave compression.

The proposed mechanism of increasing the sensitivity of an emulsion explosive by adding gunpowder particles is based on the very same principle as in the case of hollow microspheres or gas bubbles. The temperature of the products of the gunpowder's detonation is significantly higher (by 1,500-2,000 K for different equation of state

models) than the temperature of the detonation products of pure emulsion. In that sense, the gunpowder particles will act as "hot spots." The products of the gunpowder's detonation act as "hot spots" not only in close-lying regions, as in the case of microspheres, but also in significantly more remote regions inasmuch as at least as much energy is stored in gunpowder molecules as is stored in the explosive emulsion itself.

Even with a very cautious estimate, it may therefore be anticipated that the degree of reaction of the detonation products of a mixture of emulsion matrix and gunpowder particles will be at least equal to that occurring upon detonation of a mixture of emulsion and microspheres. A more realistic estimate is the hypothesis of the thermodynamic ideality of the detonation of a mixture with gunpowder or nonideality caused by partial mixing or total nonmixing of the detonation products of the emulsion and gunpowder as a result of the dimensions of the latter's microparticles. In the latter case, the aforementioned scenario involving the formation of two chemical subsystems in the detonation products may serve as a model of nonideality of detonation. The results of calculations performed for the said scenario practically coincide with the results of calculations performed for ideal detonation.

Estimates of detonation parameters based on thermodynamic calculations and general discussions of the mechanism of the emulsion explosives' sensitivity thus make it possible to conclude that the strength characteristics of such explosives can realistically be increased by 10-

20 percent or more (depending on the reference values) by replacing the sensitivity-increasing hollow glass microspheres and gas-forming additives with disperse explosives, especially gunpowder, the problem of whose recycling in view of conversion of the defense complex still remains far from solved.

References

1. V.V. Odintsov, V.I. Pepekin, S.A. Gubin, B.L. Korsunskiy, *KHIMICHESKAYA FIZIKA*, Vol 13, No 8-9, 1994, p 179.
2. V.V. Odintsov, V.I. Pepekin, B.N. Kutuzov, *KHIMICHESKAYA FIZIKA*, Vol 13, No 11, 1994, p 79.
3. V.V. Odintsov, V.I. Pepekin, S.A. Gubin, *KHIMICHESKAYA FIZIKA*, Vol 12, No 10, 1993, p 1404.
4. J. Lee, F.W. Sandstrom, B.G. Craig, P.-A. Persson, *Proc. Ninth Symp. (Int.) on Detonation*, Res. Center for Energ. Mater., New Mexico, 1989, p 263.
5. S.A. Gubin, V.V. Odintsov, V.I. Pepekin, *Termodinamicheskiye raschety slozhnykh khimicheskikh sistem* (Thermodynamic Calculations of Complex Chemical Systems), MIFI, Moscow, 1987.
6. V.V. Odintsov, S.A. Gubin, V.I. Pepekin, L.N. Akimova, *KHIMICHESKAYA FIZIKA*, Vol 10, 1991, p 687.

New Hypothesis on the Role and Importance of the Electric Field in Oceans

964100070A Khabarovsk TIKHOOKEANSKAYA
GEOLOGIYA in Russian Vol 14 No 1, May-Jun 95
(manuscript received 10 May 94) pp 121-123

[Annotation and Article by E. A. Altan, commentary
by V. A. Akhmadulin, St. Petersburg; UDC 550.37]

[FBIS Translated Text]

Annotation

This article examines the reasons for the generation of a telluric electric current in oceans. It is shown that it flows not only in the water, but also to a significant extent below the ocean floor and continents. This explains the formation of uplifts and troughs on the surface of the oceans above those areas of the ocean floor which have a high electric conductivity. Even small shifts in the Earth's crust or the covering of underground channels of juvenile waters may lead to a drastic change in the vertical component of this current, which in a number of cases leads to the formation of tsunamis and earthquakes, the generation of infrasonic sound and, as a result of the latter, to catastrophes involving ships and aircraft.

The materials of the article also confirm and supplement the little known hypothesis of V. S. Borkhsenius on the oceanic origin of the earth's magnetic field.

[Text of article]

In many places, the surface of the ocean has smooth deflections of tens of meters, that is, unique uplifts and troughs. Usually they are explained by a hypothesis which presumes the presence of gravitational anomalies. These deflections of the ocean can be explained by the effect on the water of electrostatic fields in the depths of the ocean and below it. The existence of such fields is evidenced by the presence of electric telluric currents in oceans. Water, like other dielectrics, is attracted to a zone of greater electrostatic field strength. Consequently, if there are local regions in the ocean in which the vertical component of the electrostatic field reaches a significant value, the surface of the water should deflect downward or upward in these zones. Possible orders of magnitude of the electrostatic field are indicated in the calculations of V. S. Borkhsenius.¹ He showed that when water evaporates and condenses the configuration of molecules changes, as does their electric charge. Consequently, between heated and cooled zones of the ocean there occurs a difference of potentials and an electric current flows. Since during evaporation and condensation each molecule changes in charge by 1 eV, the total difference of potentials that is formed is

sufficient to explain not only the origin of telluric currents, but according to the hypothesis of V. S. Borkhsenius, the Earth's magnetic field as well

The meridional direction of the telluric current in the Atlantic confirms the presence of differences in potential between heated equatorial and cooled arctic regions of the oceans. A sample calculation using data presented in Ref. 4 shows that on average a current on the order of 1,000,000 A flows in a band of ocean 100 km wide.

According to the hypothesis of V. S. Borkhsenius the Earth's magnetic field is due to an electric current flowing in the oceans in a direction of parallels between the day side of the Earth heated by the sun and the cool night side. Actually, on planets which do not have oceans one observes only a weak magnetic field. The essential objection to Borkhsenius' hypothesis is that several continents lie in the path of the oceanic current in the equatorial direction. The path of the current around them in the ocean would significantly weaken it. Borkhsenius died without finishing and popularizing his hypothesis.

To solve our problem we seek the vertical component of the electrostatic field while at the same time refining and supplementing Borkhsenius' hypothesis. Actually, is it possible that the electric current which arises due to the differences in potential at the surface of the ocean flow only along the water? Obviously, it should branch and flow in the depths of the Earth under the ocean floor and under continents, where the electric resistance of the rock is significantly less than the electric resistance of ocean water. This is shown schematically in Fig. 1. Current I flows through the ocean from zone A of the heated ocean to zone B of the cooled ocean. The electric conductivity of ocean water is about $2.5 \text{ O}^{-1}\text{m}^{-1}$. In the Gutenberg layer² (under the substrate) the temperature rises to $1500\text{--}1800^\circ\text{C}$, that is, the melting point of minerals. Their electric conductivity reaches $1000 \text{ O}^{-1}\text{m}^{-1}$. In deeper layers of the mantle and in the Earth's core the electric conductivity rises by several orders of magnitude. The basalt rocks of the ocean floor are a good insulator. Thus, according to the notation in Fig. 1, the electric resistance of the lower mantle R_n and the core R_c is significantly less than the electric resistance of the ocean R_o , but between them are layers of greater electric resistance, R_{ks} , R_s , R_g . However, in those places where this layer is disrupted or very thin, a significant part of the electric current is directed from the ocean downward or from beneath the ocean floor upward. Consequently, a current flows along the lower mantle (current I_2) and the Earth's core (current I_1) from point A to point B parallel to current I in the ocean. Currents I_2 and I_1 obviously also flow beneath continents between the day and night sides of the Earth, participating in the formation of the Earth's magnetic field.

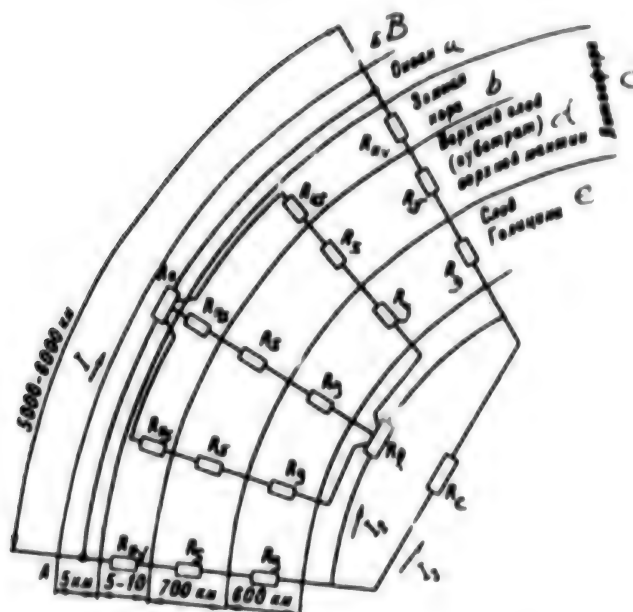


Figure 1. Schematic of electric resistances of a portion of the ocean and layers of the Earth beneath it.

Current I moves through the ocean from zone A of the heated ocean to zone B of the cooled part of the ocean. The electric resistance of the lower part of the mantle R_m and core R_c are significantly less than the resistance of the ocean R_0 , but between them are layers of large resistance R_k , R_s , and R_g . The calculations show that in zones where the integrity of the earth's crust is disrupted (the emergence of juvenile water, magma, etc.) the electric resistance R_{kv} is significantly less than R_k , and thus a substantial portion of current I is directed from the ocean into the depths and flows parallel to the current in the ocean from point A to point B along the lower mantle (current I_2) and the Earth's core (current I_1). Key: a. ocean; b. Earth's crust; c. lithosphere; d. upper layer (substrate) of the upper mantle; e. Golitsin layer.

In the Bermuda Triangle there are several zones of high electric conductivity. First, there is the Puerto Rican depression. Above it the surface of the ocean is depressed downward by 15-25 m. The juvenile waters have a high electric conductivity and their suboceanic bed links the ocean with the depths of the Earth. These waters probably emerge in the Sargasso Sea (the depression of the surface is about 60 m). An excellent conductor of electric current is the lava of underwater volcanoes, for example, at the Middle Atlantic fault.

Since, as noted above, a current on the order of 1,000,000 A flows through every 100 km band of ocean, and in regions where the integrity of the ocean floor is disrupted the current may be directed from zones with a width of several hundred kilometers, the value of the vertical component in the areas of these disruptions also may be on the order of millions of amperes. This type of current obviously, is associated with significant electrostatic fields.

Since the electric current in these zones is constant, or changes very slowly, deflections of the ocean surface retain their size and physical properties. The value of the electric current flowing under the ocean or from beneath the floor of the ocean may change drastically, for example, as a result of small shifts in the layers of rock under the ocean floor in a region of high electric conductivity. This may lead to the generation of infrasonic sound, to the formation of long waves (tsunamis) and earthquakes.

An electric current in the stream of juvenile waters helps to dissolve rock, eroding the underground channel. The separated chunks of rock may partially or completely cover its underground bed for some time. Partial coverage may lead to the formation of an infrasonic liquid or vapor gush below the ocean. If the frequency of the infrasonic sound coincides with the frequency of the alpha rhythm of the brain, then this may lead to insanity and death of people in the affected zone. The infra-

sonic sound may froth the water at a depth of tens or hundreds of meters. The frothed water is lighter than common water and a ship in this region will collapse under the water.

Moving from the ocean into the atmosphere and creating an alternating decrease and increase in air density, the infrasonic sound leads to an alternating (with the frequency of the infrasonic sound) decrease and increase in lift, affecting the (wing) planes of aircraft. This, obviously, is the reason for the known, but unexplained phenomenon which occurs when even in calm weather an aircraft over the ocean suddenly begins to shake, which sometimes leads to a catastrophe. The drastic change in the vertical component of the electric current due to the movement of rock or covering of an underground part of the beds of juvenile waters in itself may generate an infrasonic sound pulse, because the rock of the ocean floor has piezoproperties. This may lead to the aforementioned phenomena, as well as to earthquakes.

If the current-conducting channel below the ocean floor is covered for a long time, the deflection upward of the ocean surface begins to overflow, generating long waves (tsunamis). The nature of these tsunamis was unexplained because they arise in the absence of cyclones and other known causes.

Using the invention¹ of the author of this article, use of the laws described above makes it possible to determine the points of origin of these tsunamis and the moment of their formation. This makes it possible to promptly warn the population of the coastal zones of the ocean and save tens of thousands of lives.

References

1. E. A. Alftan, Copyright No 795221 "Method of Determining the Origin of Tsunamis" Priority 1 Mar 73.
2. BSE Vol 9, 1972 pp 481-482.
3. V. S. Borkhsenius, "On the Nature of Heat and Natural Magnetism" in *Materialy k Soveshchaniyu "Obshchive zakonomernosti geologicheskikh yavleniy"* [Materials for the Conference titled "General Laws of Geological Phenomena"] (10-15 Jan 1965) Issue 1, Leningrad, 1965.
4. V. V. Shuleykin, *Fizika morya* [Physics of the Sea] 4th ed. Moscow: Nauka, 1968 p 1014.

Discussion by V. A. Akhmadulin

The proposed hypothesis is based on the little known ideas of V. S. Borkhsenius on the origin of electric charges in the evaporation and condensation of water, which themselves require proof. The author of the article should have presented in more detail the essence of this hypothesis and presented quantitative calculations, as well as shown how such fantastic figures (1,000,000 amperes per 100 km or 10 A/m) may be obtained from the initial data in reality. In addition, it should be pointed out that the latitudinal currents of Borkhsenius, which flow from the heated day side to the cool night side, interact with meridional currents which arise due to differences in temperature between heated equatorial and cooled arctic regions of the ocean. In addition it was important to estimate the currents which are induced in conducting sea water by the Earth's external electromagnetic field. It is completely unclear what conducting branches in the depths of the Earth the author is talking about, because the conductivity of sea water is much higher than the conductivity of sedimentary rock, not to mention the magmatic and metamorphic rock comprising the upper part of the Earth's crust of oceans and continents. Practically, current conducting zones, in the opinion of the author, should penetrate to the lower mantle, but the arguments in support of this view are not presented, although the experience of geoelectricians in the study of conducting objects in the Earth's crust and upper mantle exclude the presence of such vertical channels. There is no basis to link this with the lava of underwater volcanos of the Middle Atlantic fault. The effect of these channels would undoubtedly have been recorded by geoelectricians. It is also unclear what stream of juvenile water the author is talking about, implying that under the ocean floor there may exist underground rivers of the type which are formed in karst cavities. All of this requires proof because it contradicts available data and existing ideas.

Shares Sold in Seven New Oil Companies

964D0121A Moscow KOMMERSANT DAILY
in Russian 2 Nov 95 p 5

[Article by Olga Gorokhova under the "Oil Company Stock Auctions" rubric: "Seven New Oil Holdings Sold"]

[FBIS Translated Text] **The lethargy of the financial market has finally been shaken by an event that investors could not even have dreamt of half a year ago. The sale of shares in seven new oil companies began straight off at the all-Russian financial auction conducted by the Federal Fund Corporation (FFK) on behalf of the Russian Federal Property Fund (RFFI). Because of a number of factors, these valuable pieces of paper may turn out to be an extremely profitable acquisition.**

At the beginning of August of this year, Goskomimushchestvo [Russian Federation State Committee on the Administration of State Property] issued a directive confirming the plan for selling shares designated state property. The list contained 136 enterprises, including the following newly formed holdings: Eastern Oil Company (VNK), Eastern Siberia Oil and Gas Company (Vostsibneftgaz), Siberia-Ural Petrochemical and Gas Chemistry Company (SIBUR), Orenburg Oil Joint-Stock Company (ONAKO), and Siberian-Far Eastern Oil Company (SIDANKO). The RFFI later added the Sibneft Oil Company, NORSI-Oyl Oil Company, and Tyumen Oil Company (TNK) to the list. The said enterprises' shares have not been circulated on the secondary market, which makes potential investors' task much more difficult inasmuch as investors generally use market prices as a guide when submitting orders.

At the same time, rather large blocks of shares—from 10 to 15 percent of each holding's authorized capital—have been put forward. As a result, shares worth more than 241 billion rubles [R] (a figure based on the shares' initial prices) have entered the market at the same time. Clearly, so large a "surge" of shares is inconsistent with the drop in demand that is currently evident in the market.

It should also be borne in mind that the auction results will not be tallied until after the elections, the outcome of which is unclear as of today. The political uncertainty is not very likely to inspire participation in trading even by Russian investors who are accustomed to everything, and nervous foreigners are most likely to be scared away

altogether. All of this would seem to indicate that the oil shares offered for sale may turn out to be underpriced. However, that is precisely what makes them a good way of investing capital.

True, investors should consider the fact that each of the companies (except for Vostsibneftgaz) has retained ownership of 34 percent of its shares (in addition to the government-owned block of shares) and that, in accordance with the privatization plan, no more shares will be offered through financial auctions but will instead only be able to be acquired at investment competitions planned for 1996. And that is generally more expensive and more troublesome than at auctions. As far as further privatization of the holdings is concerned, all the companies except for SIDANKO are still quite young, and the sale of those blocks that have been deemed federal property cannot begin until at least autumn 1998 (the state-owned block of SIDANKO may be offered for sale as early as spring 1997). It will therefore be difficult to form a rather large block of shares.

According to an unnamed source, large Russian banks and investment companies are now appearing. True, experience has demonstrated that most orders will probably be placed in the last few days of the order period in the second 10 days of November. The "Nashe otechestvo" [Our Fatherland] IPK [Advanced Training Institute], an agent of the Federal Fund Corporation, has proposed that rather large Russian structures take part in the trades. This includes both outside oil companies and possibly those companies that are issuing the shares, which will buy their own shares. Private individuals will hardly want to take part in such a game.

It is interesting that in accordance with the Chubays directive dated 21 July 1995, a new method of determining the initial price of a share is being used at the auctions. Previously the initial price simply could not exceed 20 times the face value. Now, however, book values are used to make the calculation. It is true that for all practical purposes these "fresh-out-of-the-oven" holdings have no such values, and data regarding their subsidiary structures are used. Thus the initial price of shares in SIDANKO is R120,000, and that of shares of ONAKO is R110,000. The initial prices of shares in the other companies are as follows: VNK, R80,000; SIBUR, R70,000; Sibneft, R115,000; TNK, R85,000, and NORSI-Oyl, R160,000. Only the initial price of a share of Vostsibneftgaz has remained at R20,000.

[Boxed item]

Companies Whose Shares Are Being Offered at Financial Auctions:

VNK: Authorized capital of approximately R3 billion. Owns controlling blocks of nine companies, including Tomskneft and the Tomsk NKF.

Vostsibneftegaz: Authorized capital of more than R342 million. The holding includes the Yeniseyneftegaz and Yeniseygeofizika.

SIBUR: Authorized capital of approximately R514 million. Owns controlling blocks of six companies, including the Scientific Research and Design Institute of Gas Refining (NIPI gazpererabotki) and Sorbent.

ONAKO: Authorized capital of approximately R2 billion. Owns controlling blocks of six companies, including Orenburgneft and Orenburggeolgiya.

SIDANKO: Authorized capital of approximately R9.3 billion. Owns controlling blocks of 26 joint-stock companies, including Udmurtneft and the Angara Petrochemical Company (Angarskaya Neftekhimicheskaya kompaniya).

Sibneft. Authorized capital of approximately R7.226 billion. Owns controlling blocks of the joint-stock companies (AOs) Noyabrskneftegaz AO and Omskiy NPZ [oil refinery] AO and a number of other companies.

TNK: Authorized capital of R790.882 million. Owns controlling blocks of the Tyumenneftegaz AO, Nizhnevartovskneftegaz, etc.

NORSI-Oyl: Authorized capital of R1.497 billion. Its authorized capital includes blocks of shares in six oil recovery and oil refining companies, including the Norli AO.

This is a U.S. Government publication produced by the Foreign Broadcast Information Service (FBIS). Its contents in no way represent the policies, views, or attitudes of the U.S. Government.

FBIS collects, translates, disseminates, and analyzes foreign open-source information on behalf of the U.S. Government. Its publications may contain copyrighted material. ***Copying and dissemination is prohibited without permission of the copyright owners.***

- Bracketed indicators before the first sentence of each item describe the way in which the material was processed by FBIS.
- Headlines and all bracketed explanatory notes are supplied by FBIS.
- Personal and place names are rendered in accordance with the decisions of the U.S. Board on Geographic Names as adapted by FBIS. Unverified names in radio and television material appear in parentheses and are spelled phonetically; words and phrases in parentheses preceded by a question mark are unclear in the original and deduced from context.

SUBSCRIPTION INFORMATION

U.S. Government Customers

For a list of FBIS products, to subscribe to an FBIS publication, or to indicate a change of address contact:

FBIS
P.O. Box 2604
Washington, DC 20013-2604
Telephone: (202) 338-6735
FAX: (703) 733-6042

Non-Government Customers

Subscriptions are available from the National Technical Information Service

NTIS
5285 Port Royal Road
Springfield, VA 22161
Telephone: (703) 487-4630
FAX: (703) 321-8547

New subscribers should expect a 30-day delay in receipt of the first issue.

END OF

FICHE

DATE FILMED

8 Feb 96